

Magnetic Resonance Imaging of the Brain

Paul M. Parizel, Luc van den Hauwe, Frank De Belder,
J. Van Goethem, Caroline Venstermans, Rodrigo Salgado,
Maurits Voormolen, and Wim Van Hecke

Contents

2.1 Coils and Positioning	108	2.6.3 Pituitary Adenoma	148
2.1.1 Coil Choice and Patient Installation	108	2.6.4 Other Intra-, Supra-, and Parasellar Lesions	149
2.1.2 Imaging Planes	108	2.7 Cerebrovascular Disease	151
2.1.3 Protocol for Routine MRI of the Brain	109	2.7.1 Stroke	151
2.1.4 Spatial Resolution	112	2.7.2 Subarachnoid Hemorrhage	162
2.1.5 Signal-to-Noise Ratio	112	2.7.3 Dural Sinus and Cerebral Vein Thrombosis	163
2.1.6 The Big Question: 1.5 or 3.0 T (or More)?	113	2.7.4 Vascular Malformations	165
2.2 Congenital Disorders and Hereditary Diseases	114	2.8 White Matter Lesions	169
2.2.1 Craniocervical Junction	114	2.8.1 Introduction	169
2.2.2 Posterior Fossa	116	2.8.2 Normal Development	169
2.2.3 Supratentorial Midline Structures	117	2.8.3 T2-W and FLAIR	170
2.2.4 Cerebral Hemispheres	119	2.8.4 T1-W Sequence	170
2.3 Mass Lesions	120	2.8.5 Delayed Myelination	170
2.3.1 Introduction	120	2.8.6 Leukodystrophy	170
2.3.2 Tumor or Not?	120	2.8.7 Multiple Sclerosis	171
2.3.3 Lesion Location	121	2.8.8 Toxic and Degenerative Demyelination	178
2.3.4 Edema and Mass Effect	123	2.9 Intracranial Infection	179
2.3.5 Lesion Characterization	124	2.9.1 Imaging Strategy	179
2.4 Supratentorial Brain Tumors	126	2.9.2 Meningitis	179
2.4.1 Introduction	126	2.9.3 Encephalitis	181
2.4.2 Basic Neuroradiological Features	126	2.9.4 Acute Disseminated Encephalomyelitis	185
2.4.3 Extra-Axial Supratentorial Tumors	128	2.9.5 Tuberculosis	185
2.4.4 Intra-Axial Supratentorial Tumors	128	2.10 Normal and Abnormal Aging of the Brain	187
2.5 Infratentorial Tumors	138	2.10.1 White Matter Changes in Aging	187
2.5.1 Anatomy and Technique	138	2.10.2 Age-Related Changes in the CSF Spaces and Cortical Gray Matter	188
2.5.2 Age-Related Frequency of Posterior Fossa Tumors	138	2.10.3 Age-Related Changes in Brain Iron	188
2.5.3 Extra-Axial Posterior Fossa Tumors	138	2.10.4 MRI in Abnormal Aging and Dementia	189
2.5.4 Intra-Axial Posterior Fossa Tumors	140	2.11 Craniocerebral Trauma	189
2.6 Sella Turcica and Hypophysis	146	2.11.1 MRI in Acute and Subacute Trauma	189
2.6.1 Introduction	146	2.11.2 MRI in Chronic Trauma	190
2.6.2 MRI Technique	146	2.12 Seizures	193
		2.12.1 Mesial Temporal Sclerosis	193
		2.12.2 MRI Strategy for Epilepsy	194
		Further Reading	194

P. M. Parizel (✉)
 Department of Radiology,
 Antwerp University Hospital
 and University of Antwerp,
 Wilrijkstraat 10, 2650 Edegem, Belgium

2.1 Coils and Positioning

2.1.1 Coil Choice and Patient Installation

Magnetic resonance imaging (MRI) examinations of the brain can be performed with several coil types, depending on the design of the MRI unit and the information required.

- Traditionally, MRI examinations of the brain are performed with quadrature (i.e., circularly polarized) head coils. These volume coils are closely shaped around the head of the patient and usually present a so-called “bird-cage” configuration. Many coils are split in half, for easier patient access and positioning.
- Recently, phased-array head coils have become the standard of practice for state-of-the-art high-resolution MRI of the brain. Phased-array head coils contain multiple small coil elements, which are arranged in an integrated design which surrounds the head (e.g., 8-, 12- or even 32-channel head coils). Data from the individual coils are integrated by special software to compensate for the nonuniform distribution of the signal-to-noise ratio (SNR) between the peripheral and central parts of the brain. The major advantage of a multichannel, phased-array head coil is that it allows the application of parallel acquisition techniques (PAT), which can be used to speed up MRI. The concept is to reduce the number of phase-encoding steps by switching a field gradient for each phase-encoding step. Skipping, for example, every second phase-encoding line accelerates the acquisition speed by a factor of two. This is called the acceleration or PAT factor. The trade-off for this increased imaging speed is a decrease in SNR. Image reconstruction with PAT techniques is more complicated, and several algorithms have been described, depending on whether image reconstruction takes place before (SMASH, GRAPPA (generalized autocalibrating partially parallel acquisition)) or after (SENSE) Fourier transform of the image data.
- In MRI systems where the direction of the B_0 field is oriented perpendicular to the long axis of the body, e.g., open-design resistive or permanent magnet systems, solenoid head coils can be used. By diagonally crossing two solenoid wire loops, a CP head coil can be created to improve SNR.

- Surface coils are rarely used for brain imaging and are usually reserved for “special” applications: high-resolution imaging of the orbits or the temporomandibular joints (double-doughnut surface coil). One should keep in mind that phased-array coils are, in fact, a combination of multiple small surface coils.

For MRI examinations of the brain, the patient is placed in a supine position. Before the table is entered into the magnet, the patient must be correctly positioned in the head coil. Most MRI systems provide laser cross-hairs to assist in patient positioning. The narrow nature of the head coil may induce anxiety. Therefore, it is important that the patient feels comfortable. A pillow placed under the shoulders may be helpful. A wide field-of-view (FoV) mirror, placed on top of the coil allows the patient to see outside the magnet and reduces anxiety and claustrophobia. For some patients, sedation may be required and should be individually tailored.

2.1.2 Imaging Planes

An MRI examination of the brain begins with one (or more) fast localizer scans (also known as scout or survey images). For this purpose, we use fast sequences (obtained in seconds), and ideally obtain slices in three orthogonal imaging planes. On the basis of the initial localizer images, additional localizer scans are performed, if needed, until the operator is satisfied that imaging sequences can be started in true sagittal, coronal, or axial planes. On the coronal localizer image, a fast mid-sagittal acquisition is positioned. We then position our first series of axial scans on this image. Modern MRI scanners provide software that allows the user to position slices simultaneously on three localizer images. This permits multiple oblique slice orientations and obviates the need to obtain several sequential localizer scans.

The positioning of sagittal images is obvious, due to the left-right symmetry of the brain. Sagittal images are placed on a coronal localizer image if the head is not rotated. An axial plane can also be used, provided there is no left-right tilt of the head. In clinical practice, the positioning of sagittal images is self-explanatory. Ideally, on the midsagittal image, the following anatomical landmarks should be identified: corpus callosum (over its entire length), Sylvian aqueduct, fourth ventricle, and cervical spinal cord.

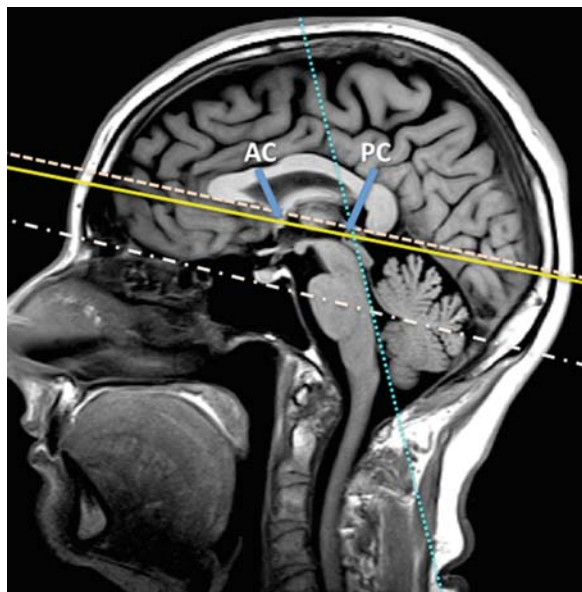


Fig. 2.1 Anatomic landmarks for positioning of axial slices. Axial slices should be positioned parallel to the bicommissural line, which links the anterior to the posterior commissure (*yellow line*). Alternatively, axial slices can be oriented parallel to a line linking the floor of the sella turcica to the fastigium of the fourth ventricle (*lower dotted line*). A third alternative solution is to position slices parallel to a line linking the inferior borders of the genu and splenium of the corpus callosum (*upper dotted line*). In most (adult) patients, these imaging planes differ by only a few degrees. For coronal scans, we prefer a plane parallel to the posterior surface of the brainstem (*blue dotted line*)

The plane of axial images should be parallel to the bicommissural line, which links the anterior to the posterior commissure (Fig. 2.1). Sometimes, this line may be difficult to identify on a low-resolution localizer image. There are two alternative solutions: (1) position the center of the slice group at the inferior borders of the genu and splenium of the corpus callosum or (2) use a plane parallel to a line linking the floor of the sella turcica to the fastigium (the highest point in the roof of the fourth ventricle). In most adults, these imaging planes differ only by a few degrees. It is important, however, to set a standard imaging plane, so that images obtained in follow-up examinations can be compared with the baseline study. Some vendors are nowadays implementing automatic alignment software, which provides reproducible slice positioning for the MRI of the head, without the need for manual adjustments. This maximizes standardization and comparability in follow-up MRI examinations of the same patient.

For coronal images, we typically choose a tilted plane, perpendicular to the long axis of the temporal lobes. This can be obtained by positioning the coronal slices on a midsagittal image, parallel to the posterior part of the brainstem (Fig. 2.1). For pituitary studies, the coronal images should be perpendicular to the sellar floor or tilted slightly backward (parallel to the pituitary stalk).

The choice of imaging planes should be determined by the clinical questions to be answered. For example, in a patient with optic neuritis, thin coronal fat-suppressed images through the orbits are useful for comparing the right and left optic nerves. To rule out hippocampal sclerosis in patients with intractable partial complex seizures, tilted coronal slices perpendicular to the long axis of the hippocampus are preferred; axial scans tilted parallel to the hippocampal axis may also be helpful. In a patient with multiple sclerosis (MS), subependymal white-matter lesions perpendicular to the ventricular surface (“Dawson’s fingers”) are particularly seen well on the sagittal images. Lesions within the corpus callosum are well depicted on the sagittal or coronal sections and may be difficult to see on axial scans.

2.1.3 Protocol for Routine MRI of the Brain

Imaging protocols for the brain should meet several criteria:

- They must address the clinical questions to be answered
- They must be complete and provide all the required information
- They must be as short as possible (to minimize the time the patient has to spend in the magnet and optimize patient throughput)
- They must be reproducible

Protocols should be standardized to ensure continuity over time. Frequent changes in imaging protocols should be avoided, since this may confuse the technologists operating the MRI equipment. Obviously, imaging protocols should be adapted to the equipment available.

As a general rule, MRI studies of the brain should include at least two imaging planes and two “weightings,” and preferably more. Table 2.1 provides an overview of (some) standard sequences for MRI of the brain,

Table 2.1 Overview of some commonly used MRI sequences

FLAIR	<ul style="list-style-type: none"> Standard sequence for lesion detection, especially in white matter Less sensitive in the posterior fossa Usually applied in axial and/or coronal imaging planes Sagittal FLAIR is indicated in demyelinating disease Often combined with fat saturation to avoid the “glare” of bright subcutaneous fat
FLAIR + Gd	<ul style="list-style-type: none"> Indicated for the detection of leptomeningeal disease
PD/T2	<ul style="list-style-type: none"> Proton density (first echo) can be used as an alternative to FLAIR, and is more sensitive for the detection of posterior fossa lesions T2-WI (second echo) are a staple sequence for detection of long T2 lesions
DWI/ADC	<ul style="list-style-type: none"> Is mandatory in all patients referred with a suspicion of stroke or cerebrovascular disease Is indicated in the evaluation of cystic lesions (e.g., to differentiate abscess from necrotic tumor, or epidermoid from arachnoid cyst) Is useful in trauma to detect diffuse axonal injury (DAI) and hemorrhagic lesions; findings on DWI are believed to correlate closely with outcome Is indicated in brain tumors to assess cell density The motto should be: “diffusion imaging for all patients”
SWI	<ul style="list-style-type: none"> Sequence which combines magnitude and phase information Useful for the detection of intracranial calcifications or hemosiderin deposits (cavernous malformations, hemosiderin deposits, DAI, ...) Is more sensitive for the detection of “microbleeds” than gradient echo T2*-WI
T2*	<ul style="list-style-type: none"> Gradient echo sequence provides information about hemoglobin breakdown products and calcifications Sensitivity to susceptibility effects is proportional to TE and field strength
T1±Gd	<ul style="list-style-type: none"> Part of most routine brain imaging protocols Usually applied in sagittal, axial or coronal imaging planes, depending on indication Same imaging plane should be used before and after gadolinium-chelate injection
MP-RAGE, 3D SPGR (\pm Gd)	<ul style="list-style-type: none"> Isotropic 3D T1-W sequence, allowing reformatting in other imaging planes Provides excellent differentiation between gray and white matter Indicated to detect migration disorders (e.g., gray matter heterotopia, etc.) Less sensitive to enhancement as compared to SE or TSE T1-W sequences
Fat-sat T2, STIR	<ul style="list-style-type: none"> Indicated to detect white matter-lesions in “difficult areas,” e.g., in the optic nerve (optic neuritis)
TOF MRA	<ul style="list-style-type: none"> Indicated to examine intracranial vessels and circle of Willis
Contrast-enhanced MRA	<ul style="list-style-type: none"> Indicated in follow-up after endovascular aneurysm coiling Allows for time-resolved angiography (separating afferent arteries and draining veins)

with their specific indications. The choice of the imaging sequence influences the look, signal intensity (SI), conspicuity, and even the size of a lesion. For example, vascular malformations or tumors can present a highly variable appearance, depending on the imaging parameters; this can be illustrated by applying different pulse sequences to a patient with a right parietal cavernous malformation (Fig. 2.2). Some clinically important lesions may remain undetected if the wrong imaging protocol is applied. Therefore, there is no such thing as an “ideal” imaging protocol, and there is not a single imaging protocol that befits all indications. The imaging strategy should be guided by the questions to be answered and the clinical information available. We use a set of standard imaging protocols for some of the most common indications (e.g., stroke, tumor, dementia,

epilepsy, ...). However, for difficult cases, or patients who do not fit into these broad categories, the imaging protocol should be individually tailored. Moreover, imaging protocols should be adapted to the available equipment (magnet, coils, sequences, software, etc.). Finally, there may be individual preferences.

A long repetition time (TR) sequence is still a standard part of most imaging protocols. This sequence can be obtained with either a spin-echo (SE) or turbo spin-echo (TSE) technique and provides proton-density weighted images (PD-WI) and T2-W images (T2-WI). They are used to detect intraparenchymal signal abnormalities. Most pathological processes in the brain result in increased water content (vasogenic edema, cytotoxic edema, necrosis, or cyst formation) and are therefore readily identified on T2-WI.

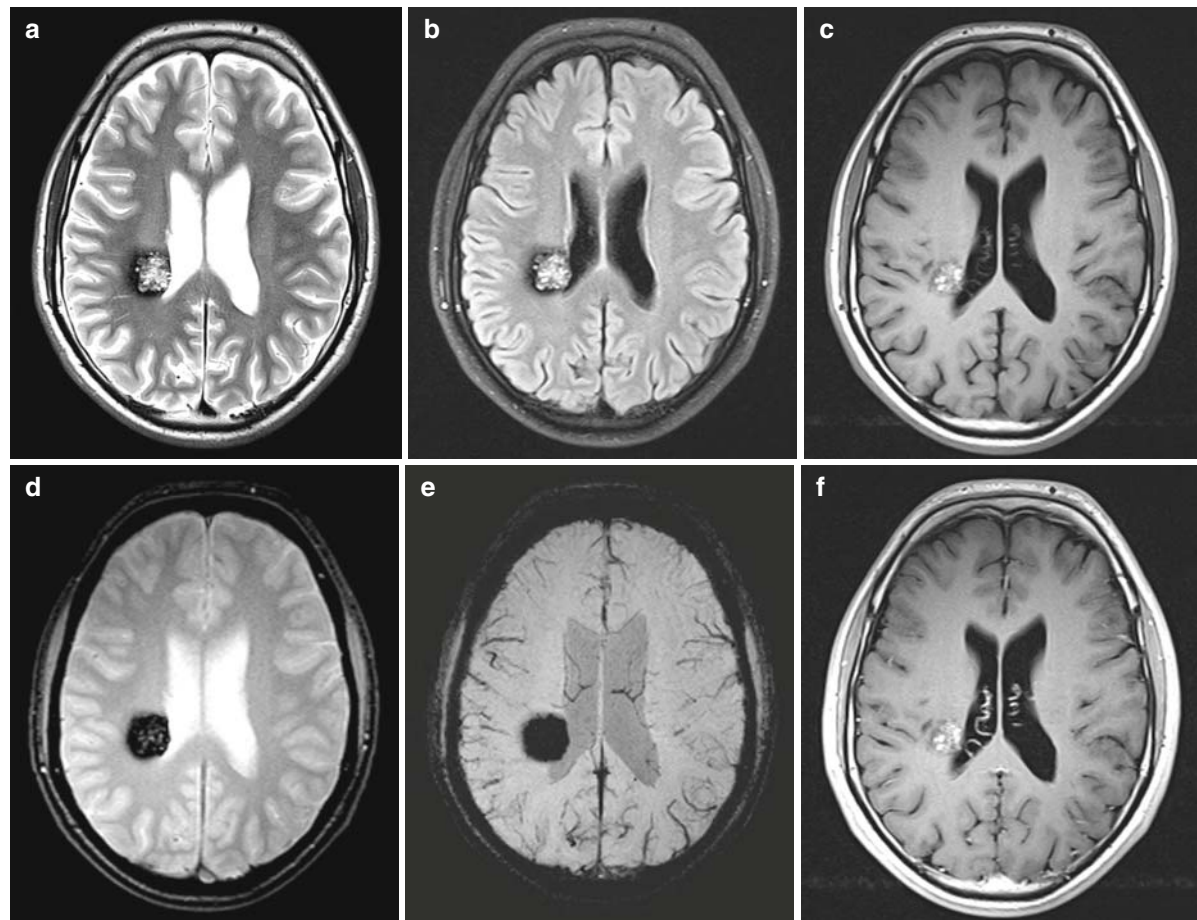


Fig. 2.2 Cavernous malformation: overview of imaging sequences. (a) Axial TSE T2-WI. (b) Axial fat-sat turbo FLAIR. (c) Axial TSE T1-WI. (d) Axial gradient echo FLASH T2*-WI. (e) Axial susceptibility-weighted image (SWI). (f) Gd-enhanced axial T1-WI. On T2 and FLAIR images, the cavernous malformation presents a characteristic “popcorn” appearance; the center of the lesion is inhomogeneous but predominantly hyperintense, and is surrounded by a hypointense halo, repre-

senting blood degradation products (hemosiderin). On TSE T1-WI, the cavernous malformation is predominantly hyperintense, and shows only minimal enhancement (compare (c) with (f)); the surrounding hypointense rim is not seen. On gradient echo T2*, and even more so on SWI, the lesion becomes almost completely hypointense; this is due to dephasing susceptibility effects caused by hemosiderin

Small high-SI lesions adjacent to the ventricles or subarachnoid spaces, e.g., periventricular white matter and cortical gray matter, may be missed on T2-WI, because they cannot be differentiated from the cerebrospinal fluid (CSF), which is also hyperintense. These lesions are better appreciated on PD-WI, where the lesions are hyperintense, but the SI from the CSF is diminished. An alternative is to use a T2-W sequence with dark CSF signal, such as fluid attenuated inversion recovery (FLAIR). In this T2-W sequence, the signal of CSF is attenuated by the use of a long inversion time, typically around 2,000 ms. FLAIR provides excellent contrast resolution at brain-CSF interfaces and improves the conspicuity of small white-matter

lesions. Thus, in most modern imaging protocols, FLAIR and TSE T2-W sequences are used instead of the dual-echo PD-W and T2-W sequence.

The short TR/short echo time (TE) or T1-W sequence is used to evaluate the gross anatomy and structure of the brain. Moreover, T1-WI are often better for the anatomical definition of an underlying lesion (the increased signal of an intraparenchymal area of edema on T2-WI may obscure the underlying lesion). Following the intravenous injection of a paramagnetic contrast agent, T1-WI in two orthogonal planes should be obtained. Alternatively, a three-dimensional (3D) volume acquisition can be used, which permits reconstructions in multiple planes. Unenhanced and gadolinium (Gd)-enhanced

images with the same thickness, positions, and parameters should be available for comparison in at least one imaging plane.

The effect of contrast agents can be potentiated using spectral fat-suppression techniques (e.g., in the orbit) or magnetization-transfer contrast techniques for background suppression (e.g., in MS). On most modern MRI equipment, magnetization transfer is a push-button option that is frequently used for most Gd-enhanced brain scans, except when thin slices are required, e.g., for the pituitary gland or internal auditory canal.

2.1.4 Spatial Resolution

Spatial resolution in an MR image is determined by slice thickness, FoV, and matrix size. These parameters define the size of a voxel (volume element). The slice thickness for routine MRI of the brain is usually between 3 and 5 mm, with an interslice distance of ≤ 1 mm. When imaging at 3 T, we routinely use 3 mm slices, whereas with a field strength of 1.5 T, a slice thickness of 5 mm is advocated to obtain sufficient SNR. Complete coverage of the brain, for example in the axial or sagittal plane, usually requires 25–35 slices. For a quantitative assessment of the number of lesions, as in MS trial protocols, a slice thickness of 3 mm or less is usually advocated. For a volumetric assessment of white-matter lesions or tumors, a 3D sequence should be employed.

In specific anatomic regions (pituitary gland, CP angle, and internal auditory canal), thin slices (0.5–3 mm) must be used. With 3D volume acquisitions, the dataset consists of a much larger number of thin slices (thickness ≤ 1.0 mm), e.g., magnetization-prepared rapid acquired gradient-echoes (MP-RAGE).

In-plane resolution is determined by FoV and matrix size. For routine adult MRI of the brain, we typically use an FoV of 230 mm (range 220–250 mm, depending on the size of the patient's head) and a matrix of 512 or 256, depending on sequence and equipment. Images with 512 matrix are preferable because they offer improved anatomic detail. More and more, for applications which require high spatial resolution, a matrix size of 1,024 is used. Images with higher in-plane spatial resolution can be obtained by increasing the matrix size (with constant FoV) or by

decreasing the FoV (with constant matrix); however, increasing the spatial resolution results in decreased SNR, due to the smaller pixel size.

Rectangular FoV is routinely used in cerebral MRI in the axial and coronal imaging planes (*not* in the sagittal plane). In axial images, phase encoding is chosen left to right, to avoid superimposition of phase artifacts from eye movement on the temporal and occipital regions. The exception to this rule is axial diffusion-weighted images, where the phase encoding is placed in anterior to posterior direction.

2.1.5 Signal-to-Noise Ratio

Intrinsic SNR scales linearly with static magnetic field strength: high-field-strength magnets provide a proportionally higher SNR. However, due to hardware limitations, the actual SNR that can be achieved is somewhat lower than the intrinsic SNR gain. For a given magnetic field strength, the SNR can be improved by using state-of-the-art hardware. Phased-array head coils provide a higher SNR than quadrature CP head coils. SNR is also dependent on sequence parameters. For example, SNR is also proportional to the pixel size (FoV/matrix), slice thickness, and a number of acquisitions (N_{acq}), and is inversely proportional to the receiver bandwidth.

The SNR can be improved by increasing N_{acq} . SNR increases with $\sqrt{N_{\text{acq}}}$, whereas acquisition time increases linearly with N_{acq} . Thus, after increasing to four N_{acq} , it becomes relatively inefficient in terms of improving the SNR. Moreover, the probability of patient motion increases with longer imaging times.

The SNR for a particular examination can be optimized using sequences with a narrow bandwidth. This is commonly done at lower field strengths, where chemical-shift artifacts are less of a problem. At higher field strengths, mixed bandwidth sequences are useful with multi-echo sequences. The bandwidth for the second echo of a long TR sequence (T2-WI) is lower than that for the first echo (PD-WI). This improves the SNR on the longer TE images, where it is most needed.

Spatial resolution can be traded in for improvements in SNR. The larger the voxels, the better SNR is obtained. Therefore, in MR examinations of the brain, there is a trade-off between spatial resolution (slice

thickness, FoV, matrix size) and SNR. The goal should be to find a voxel size that provides an adequate SNR for contrast resolution, yet is small enough to provide the necessary spatial resolution.

With phased-array head coils, the SNR is nonuniformly distributed throughout the volume examined, and a “normalization” process is required to compensate for SNR differences between the peripheral and central parts of the brain. When phased-array head coils are used in conjunction with PAT, the imaging speed increases, but SNR decreases by the square root of the acceleration factor. Furthermore, the image reconstruction process for a phased-array head coil with PAT may further reduce the SNR.

2.1.6 The Big Question: 1.5 or 3.0 T (or More)?

MRI of the brain at 3.0 T provides a higher signal-to-noise ratio and allows improved spatial resolution (thinner slices, higher matrix). A few years ago, when 3.0 T MRI of the brain was being assessed, there were some doubts whether the improvements in image quality had a clinically beneficial effect. These doubts have dissipated. MRI of the brain at 3 T is superior in detection and accurate characterization of structural brain lesions (Fig. 2.3). Compared with 1.5 T MR images, whole brain 3 T images are of better quality, can be performed with thinner slices, and offer superior SNR.

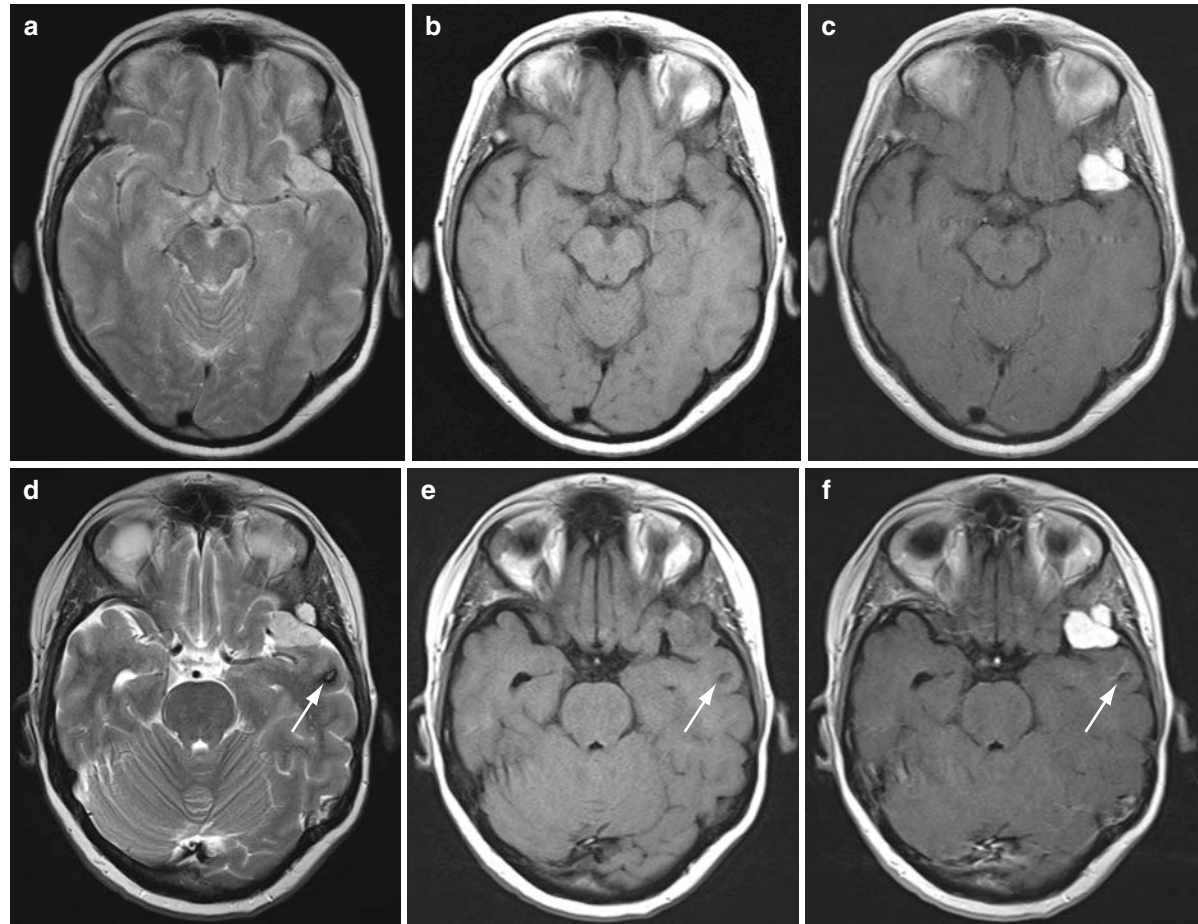


Fig. 2.3 Improved lesion detection on 3 T compared with 1.5 T MRI. (a–c) Imaging at 1.5 T. (a) Axial TSE T2-WI. (b) Axial TSE T1-WI. (c) Gd-enhanced axial T1-WI. (d–f) Imaging at 3.0 T. (d) Axial TSE T2-WI. (e) Axial TSE T1-WI. (f) Gd-enhanced axial T1-WI. The patient is a 50-year-old woman with a history of intractable focal epileptic seizures, originating in the left temporal lobe. MRI of the brain at 1.5 T, with a slice thickness of 5 mm,

shows a sharply marginated and intensely enhancing meningioma of the greater wing of the sphenoid on the left, with intra-osseous extension. MRI of the brain at 3 T, with a slice thickness of 3 mm, reveals a small hypointense, nonenhancing cavernous malformation in the left temporal lobe, which is much more conspicuous at 3 T than at 1.5 T (arrow)

2.2 Congenital Disorders and Hereditary Diseases

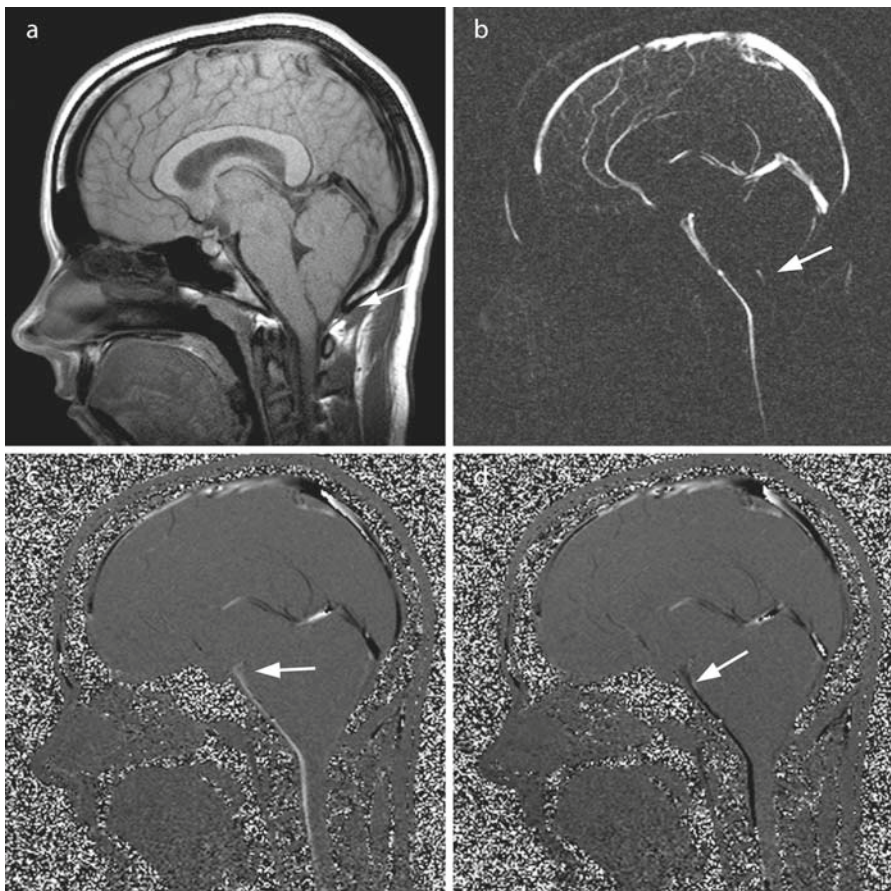
Clinical suspicion of a developmental anomaly of the central nervous system (CNS) is a frequent indication for performing an MRI examination of the brain. For a more complete discussion of developmental abnormalities, the reader should consult Chap. 13.3.3. In the following paragraphs, we shall focus on practical guidelines for interpreting MRI studies in adult or adolescent patients with suspected congenital disorders.

2.2.1 Craniocervical Junction

The craniocervical junction (CCJ) is best appraised on sagittal images. Sagittal (T)SE T1-WI constitute an essential part of the imaging protocol, although sagittal T2-WI are also acceptable. Coronal sections are very useful as a second imaging plane for the CCJ.

On a midsagittal image, the level of the foramen magnum can be identified by drawing a line from the *basion* (lowermost portion of the clivus, anterior border of the foramen magnum) to the *opisthion* (free margin of the occipital bone which constitutes the posterior margin of the foramen magnum). Normally, the inferior pole of the cerebellar tonsils lies above or not more than 3 mm below this line. *Chiari type I malformation* is defined as a downward displacement of the cerebellar tonsils through the foramen magnum into the upper cervical spinal canal. When the tonsillar herniation is 5 mm or less, this condition is described as “tonsillar ectopia.” In the true Chiari I malformation, tonsillar herniation exceeds 5 mm below the level of the foramen magnum. Sagittal MR images typically show a low position of the cerebellar tonsils with a wedge-like configuration of their most inferior aspect. The cisterna magna is obliterated. Cardiac-gated phase-contrast techniques are useful to assess the flow of CSF at the CCJ (Fig. 2.4). Chiari I malformation is commonly associated with syringohydromyelia (40–70%) and

Fig. 2.4 Chiari I malformation with phase-contrast CSF flow study. (a) Midsagittal SE T1-WI. (b) Midsagittal ECG-triggered magnitude image. (c, d) Midsagittal ECG-triggered phase-contrast images during systole and diastole, providing directional flow information. There is a downward herniation of the cerebellar tonsils into the foramen magnum (*long arrow*) (a). The cisterna magna is obliterated and the magnitude image shows absence of CSF flow posteriorly (*short arrow*) (b). In the prepontine cistern and anterior cervical subarachnoid spaces, there is downward flow during systole and upward flow during diastole (*arrowhead*), as evidenced on the phase-contrast CSF flow quantification study



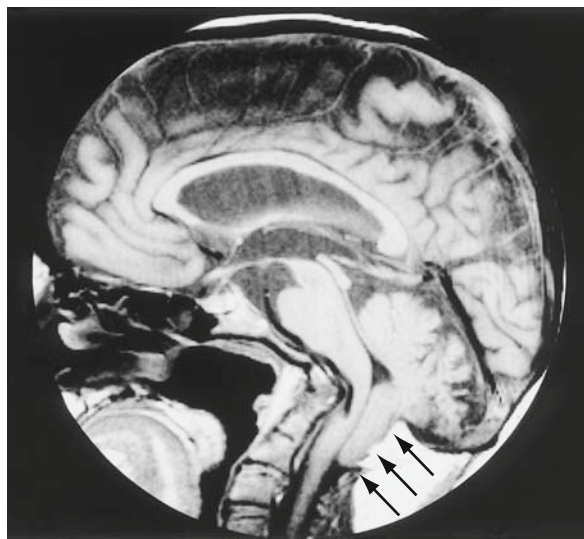


Fig. 2.5 Chiari I malformation with basilar invagination. This sagittal SE T1-WI shows downward displacement and peg-like configuration of the cerebellar tonsils (arrows). There is an associated osseous malformation of the skull base (platybasia). The tip of the odontoid is projected above the level of the foramen magnum

hydrocephalus (10–30%). The fourth ventricle is normal in size and position. In 20–30% of patients with Chiari I malformation, there is an associated osseous abnormality of the CCJ (platybasia or basilar invagination) (Fig. 2.5).

Chiari II malformation is a complex hindbrain-mesodermal malformation involving the entire neuraxis; it is most likely caused by a congenitally small posterior fossa (Fig. 2.6). The main imaging findings are: small posterior fossa with low tentorial attachment, compression of the hindbrain, indentation of the lower cerebellum by the foramen magnum or C1 and that of the upper cerebellum by the tentorium, and abnormality of the midbrain with tectal “beaking.” Chiari II malformation is almost invariably associated with myelomeningocele. Hydrocephalus and a variety of other intracranial abnormalities are common.

Osseous abnormalities of the CCJ can be congenital (basilar invagination) or acquired (basilar impression). Primary developmental craniocervical dysgenesis includes conditions such as basiocciput hypoplasia, occipital condyle hypoplasia, abnormalities of C1–C2,

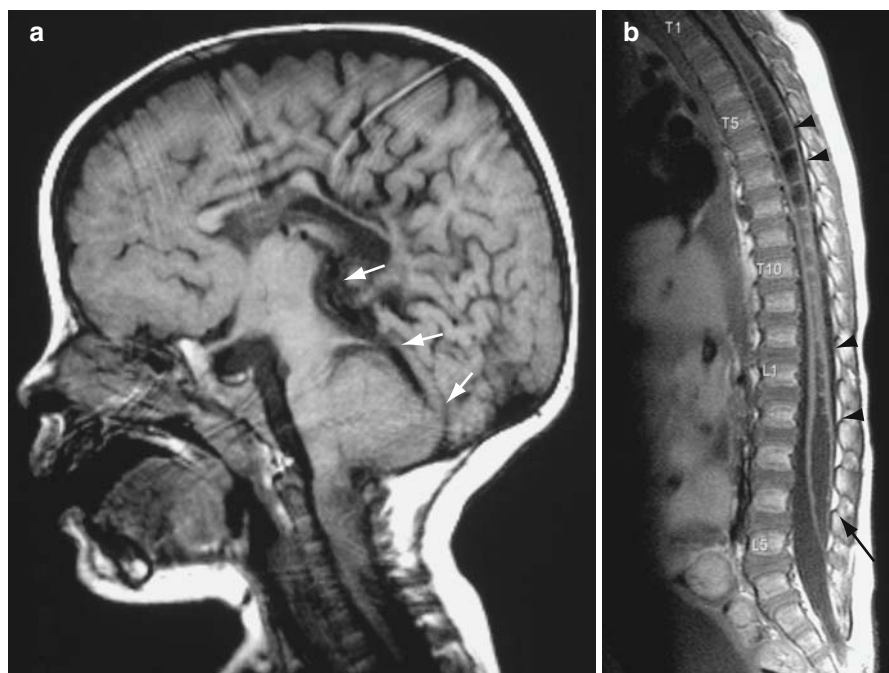
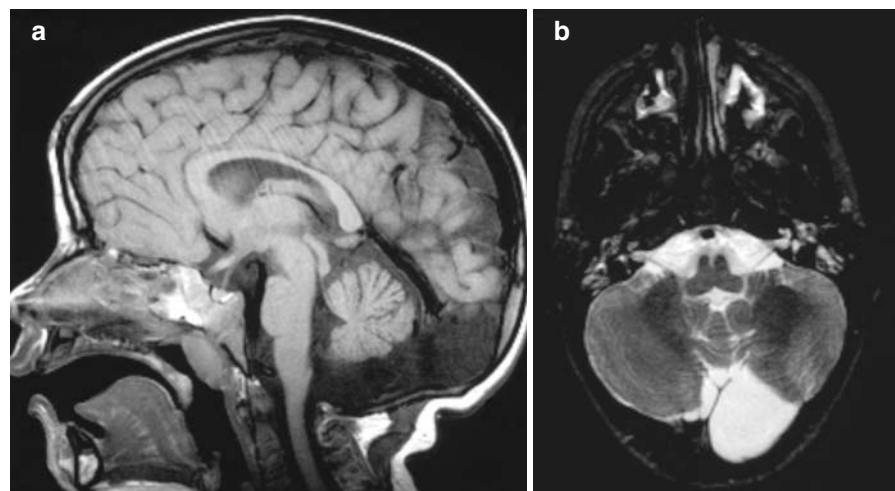


Fig. 2.6 Chiari II malformation. (a) Midsagittal SE T1-WI through the brain. (b) Midsagittal SE T1-WI through the thoraco-lumbar spine region. The patient is a 1-year-old boy after surgical repair of a myelomeningocele. At the level of the posterior fossa and craniocervical junction, the typical features of a Chiari II malformation are seen (arrows): beaking of the midbrain, small posterior fossa with low tentorial attachment,

inferior displacement and narrowing of the fourth ventricle, downward displacement of the pons and medulla, and peg-like protrusion of the vermis with cervicomedullary kinking. The spinal cord is tethered by scar tissue (*long arrow*), and is widened by a segmented syringohydromyelia extending down to the low-lying conus medullaris (*arrowheads*)

Fig. 2.7 Megacisterna magna or retrocerebellar arachnoid pouch. (a) Midsagittal SE T1-WI. (b) Axial SE T2-WI. The normally developed vermis and cerebellar hemispheres are associated with an enlarged cisterna magna, or retrocerebellar arachnoid pouch, which causes scalloping of the inner table of the occipital bone and mild enlargement of the posterior fossa. There is an incomplete and bifid falk cerebelli



Klippel-Feil syndrome, etc. Acquired basilar impression results from softening of the skull base, e.g., Paget's disease, osteomalacia, and rheumatoid arthritis. Achondroplasia is characterized by narrowing and deformation of the foramen magnum, short and vertical clivus, stenotic jugular foramina, hydrocephalus, and macrocephaly which occurs secondary to impaired venous outflow.

2.2.2 Posterior Fossa

The gross anatomic relationships of the posterior fossa contents are best evaluated on sagittal images. On a midsagittal image, the following anatomic landmarks should be recognized: mesencephalon, pons, medulla oblongata, fourth ventricle, cerebellar vermis, and foramen magnum, as defined by the line linking the basion to the opisthion.

Vermian-cerebellar hypoplasia is characterized by a small vermis and cerebellum with a prominent folial pattern, a large fourth ventricle, a large cisterna magna, and a wide vallecula. Vermian and/or cerebellar hypoplasia can be an isolated anomaly or occur in association with malformative syndromes.

Cystic malformations of the posterior fossa range from megacisterna magna, retrocerebellar arachnoid cyst, Dandy-Walker malformation, and Dandy-Walker variant. These entities may represent a continuum of

posterior fossa developmental anomalies. They are sometimes referred to as the Dandy-Walker complex.

Megacisterna magna is a large CSF space posterior and inferior to the cerebellum, which is normally developed. There is no mass effect. It cannot be differentiated from a retrocerebellar arachnoid cyst (Blake's pouch), which is a collection of CSF not communicating with the fourth ventricle (Fig. 2.7). It is most commonly situated in the midline, behind the vermis. The thin membrane surrounding the cyst is usually not seen on imaging. The cerebellar hemispheres and vermis are normally developed, but may be compressed from behind. The inner table of the occipital bone may be scalloped. The size of the posterior fossa, the position of the tentorium and straight sinus are normal. However, the cyst, when large, may show a diverticulum-like extension through the splayed tentorium. In most instances, a retrocerebellar arachnoid cyst is an incidental imaging finding. The condition is usually asymptomatic.

Dandy-Walker malformation (Fig. 2.8) is characterized by three key features: (1) dysgenesis or agenesis of the cerebellar vermis, (2) cystic dilatation of the fourth ventricle, which balloons posteriorly, and (3) enlargement of the posterior fossa, with high position of the tentorial insertion ("torcular-lambdoid inversion"). Additional imaging features include scalloping of the inner table of the occipital bone and hypoplasia of the cerebellar hemispheres. Associated findings are: hydrocephalus, corpus callosum dysgenesis, and heterotopic gray matter.

Fig. 2.8 Dandy-Walker malformation with agenesis of the corpus callosum. (a) Midsagittal TSE T1-WI. (b) Axial turbo IR T1-WI. (c, d) Coronal turbo IR T1-WI through the brainstem and posterior fossa. These images show the classic findings of a Dandy-Walker malformation: enlarged posterior fossa, high position of the tentorium, hypogenesis of the cerebellar vermis, and cystic dilatation of the fourth ventricle, extending below the cerebellum; which is pushed upward. Supratentorially, there is complete agenesis of the corpus callosum, with typical parallel orientation of the lateral ventricles, colpocephaly, and upward extension of the third ventricle into the interhemispheric fissure. The Dandy-Walker malformation is associated with 20–25% callosal agenesis



The term Dandy-Walker “variant” covers a heterogeneous group of atypical cystic posterior fossa malformations, for which common MRI findings include: cystic dilatation of the fourth ventricle, dysgenesis or hypoplasia of cerebellar hemisphere(s) and/or vermis. However, the posterior fossa is not enlarged, and the torcula is not elevated.

2.2.3 Supratentorial Midline Structures

On the midsagittal image, the corpus callosum constitutes an important anatomic landmark. It is the largest interhemispheric commissure and the most

concentrated bundle of axons in the brain. It contains myelinated fibers linking left and right cerebral hemispheres. The corpus callosum is a firm structure and helps the ventricles maintain their normal size and shape. Anatomically, on the midsagittal image, four elements constituting the corpus callosum can be identified (from anterior to posterior): rostrum, genu, body (or truncus), and splenium. Embryologically, the corpus develops in anterior to posterior fashion (genu first, then body, then splenium), with the exception of the rostrum which forms last.

Agenesis of the corpus callosum can be partial or complete (Fig. 2.9–2.11). Axons that would normally cross the midline instead run along the medial wall of the lateral ventricles, and thereby form the bundles of Probst.

Fig. 2.9 Agenesis of the corpus callosum. **(a)** Midsagittal SE T1-WI. **(b)** Axial SE T2-WI. **(c)** Coronal SE T2-WI. There is a complete absence of the corpus callosum. In the axial imaging plane, there is a parallel orientation of the widely spaced lateral ventricles. Note the widening of the posterior section of the lateral ventricles; this is termed “colpocephaly”. In the coronal plane, the high-riding third ventricle is in continuity with the interhemispheric fissure. The lateral ventricles are indented medially by Probst’s bundles

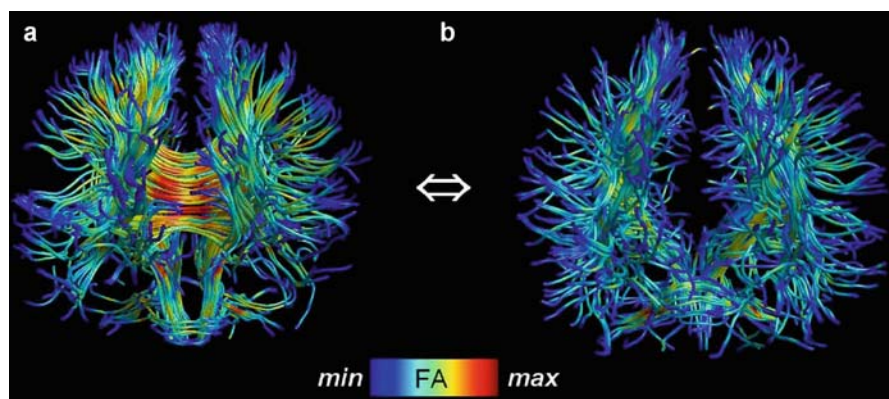
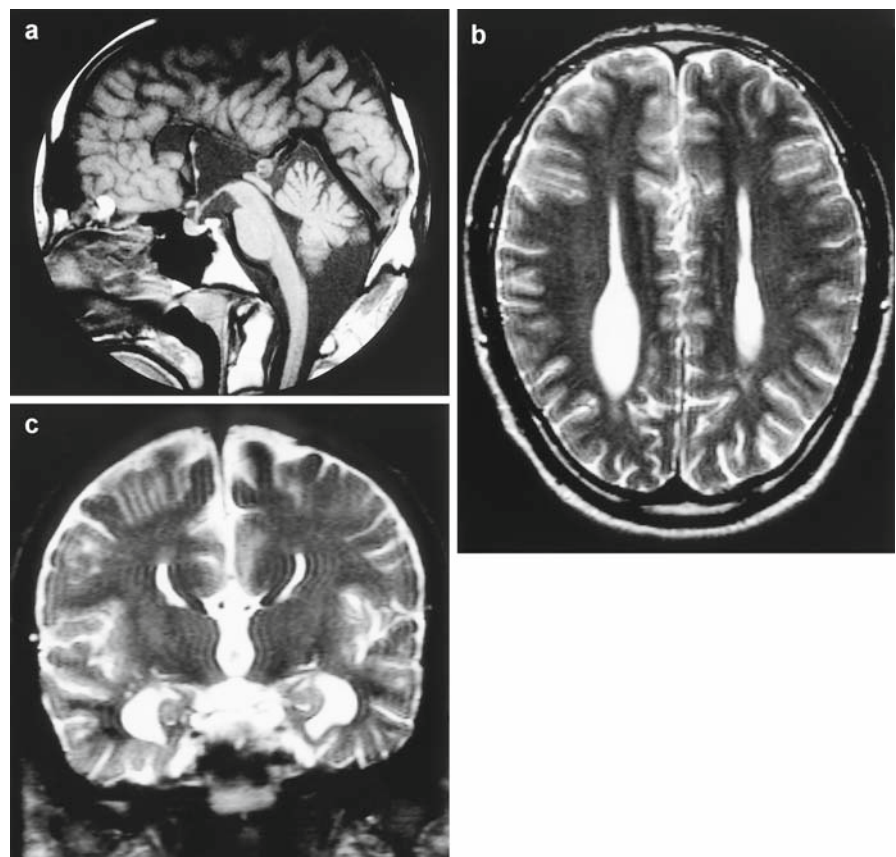


Fig. 2.10 A,B. Fiber tractography of cerebral white-matter tracts, AP views. **(a)** Normal brain (*left*). **(b)** Agenesis of the corpus callosum (*right*). The color coding indicates the degree of anisotropy; red denotes a high fractional anisotropy (FA) and blue a low FA. In the normal brain of a 26-year-old man (**a, left**),

the corpus callosum can be seen as a broad bundle of horizontal fibers, connecting both hemispheres. In the patient with complete agenesis of the corpus callosum (**b, right**), there is no connection between the right and left cerebral hemispheres

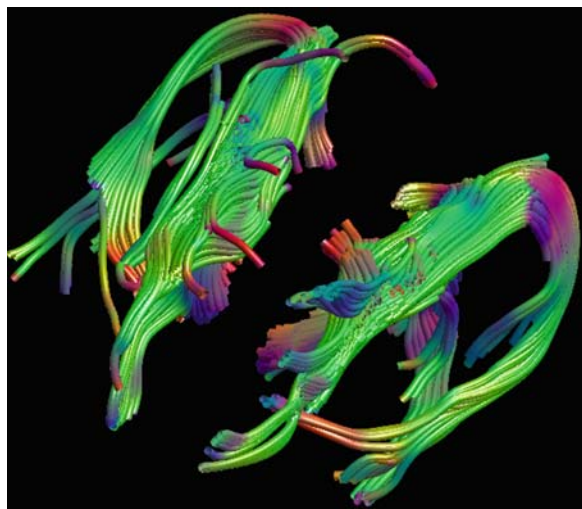


Fig. 2.11 Fiber tractography in complete agenesis of the corpus callosum (right), oblique superior view. In this graph, the color coding indicates the predominant diffusion direction. Green indicates anterior-posterior fibers, corresponding to the Probst and cingulate bundles, which course along the inner surface of the cerebral hemispheres. There is complete absence of the corpus callosum

- MRI findings of corpus callosum agenesis include:
- Partial or complete absence of the corpus callosum (midsagittal image)
 - Radial orientation of the gyri on the medial surface of the cerebral hemispheres (sagittal images) and eversion of the cingulate gyrus (coronal images)
 - Parallel orientation of the lateral ventricles (axial images)

- Longitudinal white-matter tracts (Probst bundles) indent the superomedial walls of the lateral ventricles (axial and coronal images)
- Colpocephaly, i.e., dilatation of the trigones and occipital horns (from the Greek word “kolpos” meaning a fold, cleft, or hollow)
- Upward extension of the third ventricle between the lateral ventricles (coronal images)
- Crescent-shaped (“bull’s horn”) frontal horns
- Hypoplastic or dysgenetic anterior commissure and hippocampal formation

Agenesis of the corpus callosum can occur as an isolated finding, but is frequently associated with other congenital anomalies of the brain, including Chiari II, Dandy-Walker, interhemispheric cysts, migration disorders, and lipoma. Other midline structures that should be identified on the midsagittal image include the anterior commissure, the posterior commissure, the pineal gland, the pituitary and pituitary stalk, the aqueduct, the quadrigeminal plate, and the floor of the anterior fossa.

2.2.4 Cerebral Hemispheres

The symmetry of the cerebral hemispheres is best appreciated on axial and/or coronal scans. A sequence providing high contrast between white and gray matter is preferred. Our choice is a “true” turbo inversion recovery (IR), heavily T1-W sequence (Fig. 2.12), or a 3D

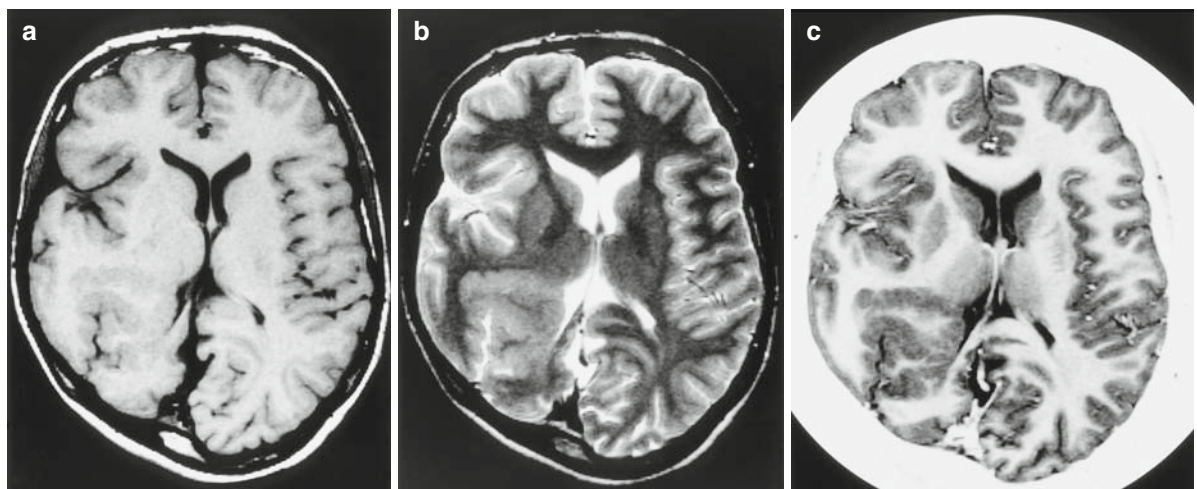


Fig. 2.12 Migrational disorder (gray matter heterotopia) in a patient with intractable seizures. (a) Axial SE T1-WI. (b) Axial TSE T2-WI. (c) Axial TIR T1-WI. The right occipital lobe contains dysplastic, disorganized gray matter. The heterotopic gray

matter indents the right lateral ventricle. On all sequences, the heterotopic gray matter is isointense to cortex. TIR images provide the best contrast between gray and white matter and can be very helpful in the characterization of migrational disorders

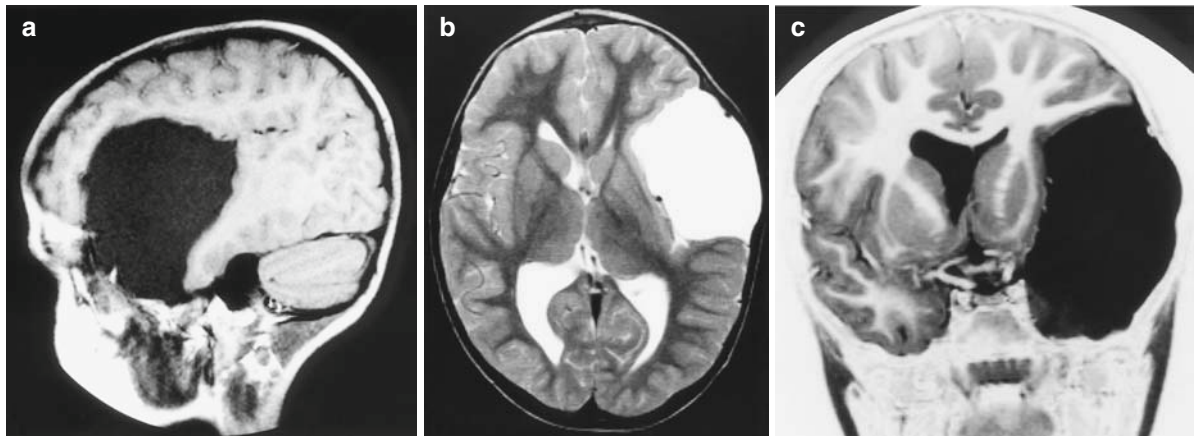


Fig. 2.13 Arachnoid cyst. (a) Sagittal SE T1-WI. (b) Axial TSE T2-WI. (c) Coronal TIR image. These images illustrate the typical appearance of a middle cranial fossa arachnoid cyst. Cyst contents are isointense to CSF. Branches of the middle cerebral artery, seen

as small areas of flow void, are displaced medially. Note that there is some outward bulging of the skull overlying the cyst (this 5-year-old boy presented with a growing “bump” on the head). The cyst is lined by displaced cortical gray matter (coronal image)

gradient echo sequence (GRE) with magnetization preparation, such as MP-RAGE, 3D-FSPGR, or 3D-TFE. On these MR scans, gray matter appears “gray” and white matter appears “white.” These images are well-suited for the detection of cortical lesions and neuronal migrational disorders. Embryologically, these conditions result from the abnormal migration of neurons from the germinal matrix to the brain surface. The spectrum of these disorders is wide and varied and includes lissencephaly, cortical dysplasias, heterotopias, schizencephaly, megalencephaly, etc.; these conditions are discussed in greater detail in Chap. 13.

When evaluating complex malformations of the brain or cystic lesions (Fig. 2.13), imaging should be performed in the three orthogonal planes to show the extent and anatomic relationships of the lesion accurately. Alternatively, a 3D sequence can be employed. IR images are also of value in following the process of myelination and in the diagnosis of myelin disorders. Fast FLAIR images are an alternative for the detection of white-matter diseases.

especially in patients presenting with focal neurological deficits (e.g., hemiparesis, hemianopia, etc.) and seizures. Clinical symptoms depend on the location of the lesion. Some of these patients have had a prior computed tomography (CT) scan of the brain. If the CT scan shows a mass lesion, MRI should be performed to look for additional lesions, to characterize the mass, and to plan the treatment. If the CT scan is negative but there is strong clinical suspicion of an intracranial mass, MRI should also be performed. Administration of contrast material is essential. MRI is the method of choice for virtually all types of intracranial mass lesions.

When confronted with an intracranial lesion, the radiologist should be able to answer the following questions:

1. Is the lesion a tumor?
2. What is the location of the lesion? (supra- or infratentorial? intra-axial or extra-axial?)
3. What is the amount of mass effect and edema?
4. What is the most likely diagnosis, keeping in mind the location of the lesion, the clinical history, and the patient’s age?

2.3 Mass Lesions

2.3.1 Introduction

One of the most common indications for MRI of the brain is to rule out an intracranial mass lesion,

2.3.2 Tumor or Not?

The clinical and MRI diagnosis of an intracranial mass lesion can be challenging. In most cases, the

initial clinical symptoms are nonspecific and result only from mass effect, local pressure, and distortion of adjacent structures. Not all mass lesions are tumors. Tumors are usually characterized by a gradual onset of symptoms, preferential involvement of white matter with sparing of cortical gray matter, round or infiltrating shape, and are not confined to a specific vascular distribution. Some of the major differential diagnostic considerations include: recent infarct, abscess, resolving hematoma, encephalitis, and developmental anomaly. The use of intravenously injected contrast agents does not always solve the issue. Some tumors do not enhance (e.g., low-grade astrocytoma), whereas intense enhancement is sometimes observed in nontumoral conditions (e.g., enhancement in recent stroke due to blood–brain barrier (BBB) breakdown, ring-like enhancement of an abscess). It is important to remember that in tumors, the amount of enhancement is not directly related to the degree of malignancy.

2.3.3 Lesion Location

Intracranial lesions can be classified as *supra-* or *infratentorial*, depending on their position relative to the tentorium cerebelli. Infratentorial tumors are more frequent in the pediatric age group. Some tumors occur in different topographical compartments, depending on the patient's age. A typical example are choroid plexus papillomas; in infants, they tend to occur supratentorially (lateral ventricles), whereas in adults they are more common infratentorially (fourth ventricle). Other tumors preferentially occur in one compartment, e.g., hemangioblastoma is almost exclusively an infratentorial tumor.

Perhaps, even more important for the differential diagnosis is to determine whether the site of origin of the lesion is *intra-axial* or *extra-axial*, depending on whether the neoplasm originates in the brain parenchyma or from the coverings of the brain. The prognosis and surgical approach for the two types differ. **Extra-axial tumors** can be of meningeal origin (meningioma, leptomeningeal seeding, lymphoma), nerve-sheath origin (schwannoma of N. VIII, V, VII), or osseous origin (chordoma, eosinophilic granuloma). In the broad sense of the definition, extra-axial tumors

also include maldevelopmental cysts and tumors (arachnoid cyst, (epi)dermoid cyst, lipoma). The cardinal feature of extra-axial tumors is that they are separated from the brain surface. The diagnosis depends primarily on the identification of anatomical boundary layers, which are interposed between the brain surface and the extra-axial tumor, e.g., CSF cleft, vascular cleft, and dural cleft. Most extra-axial tumors are benign. Because they are located outside of the brain, they do not possess a BBB. When an extra-axial tumor enhances after intravenous injection of a contrast agent, it is because of its intrinsic tumor vascularity. Enhancement often helps to define the anatomic compartmentalization of extra-axial tumors. Contrast enhancement is highly characteristic of some extra-axial tumors (meningioma, schwannoma), whereas others almost never enhance (epidermoid, dermoid).

The most common supratentorial extra-axial tumors are meningiomas and metastases. Meningioma is the most common primary nonglial intracranial tumor (13–19% of all operated brain tumors). Small meningiomas may be difficult to detect because they are almost isointense to cortical gray matter on T1- and T2-WI, and may be overlooked on noncontrast imaging studies (Fig. 2.14). Since meningioma capillaries lack a BBB, these tumors enhance strongly with Gd. Invasion of the skull bones is common (Fig. 2.3); another typical finding is the so-called “enostotic spur” (Fig. 2.15). Some meningiomas are intraventricular. Extra-axial metastases are most commonly caused by breast carcinoma (most common primary tumor). Metastases may involve the skull, pachymeninges (dura mater), and leptomeninges (arachnoid-subarachnoid metastases, pial metastases). Other supratentorial extra-axial tumors include lymphoma, sarcoidosis, and chordoma.

Infratentorially, extra-axial tumors occur predominantly in the cerebellopontine angle (CPA). In decreasing order of frequency, they include acoustic schwannoma (80%), meningioma (13–18%), epidermoid tumor (5%), and other lesions (schwannoma of N. V, VII, foramen jugulare tumors, chordoma, arachnoid cyst, aneurysm of basilar artery, and exophytic glioma).

Intra-axial tumors originate within the substance of the brain. They can be subdivided into primary and secondary tumors. The most common primary brain tumors are of glial cell origin. Gliomas account for 40–50% of

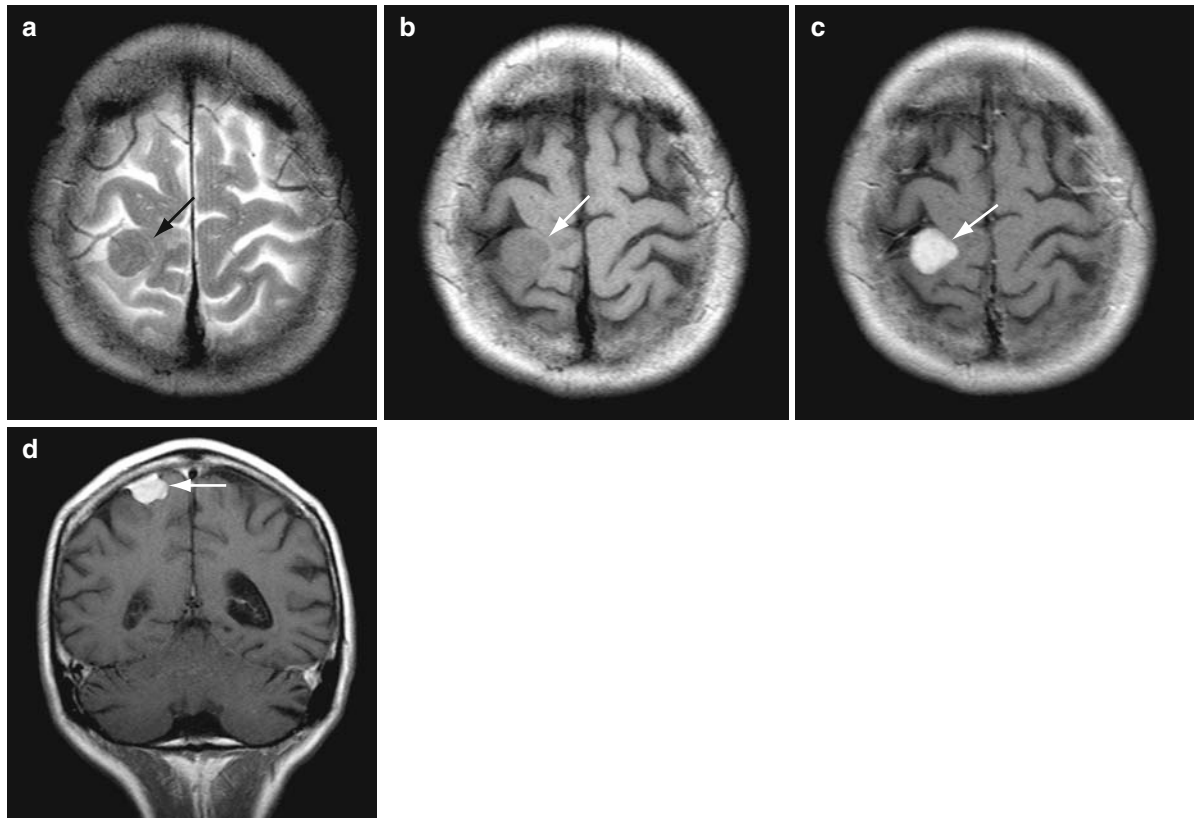


Fig. 2.14 Right parietal convexity meningioma (in a 65-year-old woman). (a) Axial TSE T2-WI. (b) Axial TSE T1-WI. Gd-enhanced axial (c) and coronal (d) TSE T1-WI. On T2- and T1-WI, this meningioma is almost isointense to hypointense compared to the

adjacent cortical gray matter in the central sulcus. Small meningiomas can be easily overlooked on precontrast images. After Gd injection, there is homogeneous enhancement, and the broad dural base of the lesion is well seen on the coronal scan (*arrows*)

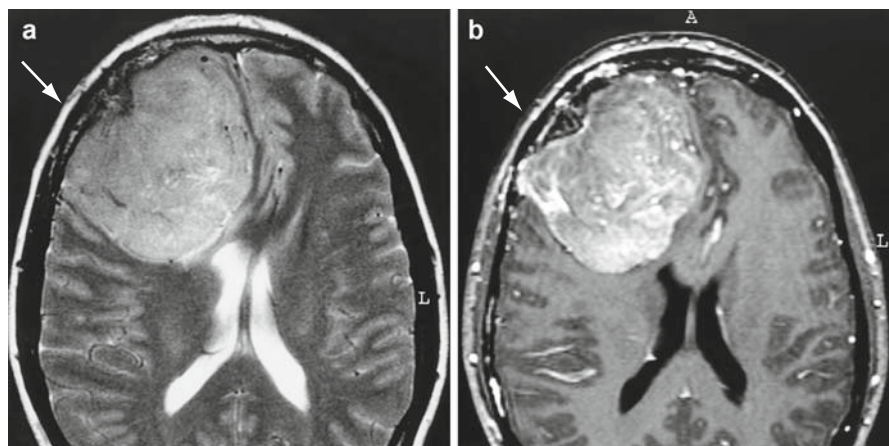


Fig. 2.15 Frontal convexity meningioma. (a) Axial TSE T2-WI. (b) Axial gadolinium-enhanced gradient-echo 3D FT T1-WI. The T2-WI reveals a large tumor which is isointense to cortical gray matter. The lesion is well demarcated. Displaced vessels and CSF clefts are visible in the brain-tumor interface, indicat-

ing the extra-axial nature of the tumor. There is no perifocal edema. The tumor enhances inhomogeneously. Numerous intratumoral vessels are present. Note the pathognomonic enostic spur and the accordion sign at the posterior margin of the lesion (*arrows*)

Table 2.2 Topography of intracranial tumors

	Intra-axial	Extra-axial
Supratentorial	Primary: glioma (astrocytoma, GBM, oligodendrogioma, ependymoma, DNET/ PNET, lymphoma)	Primary: meningioma, pituitary adenoma, epidermoid, dermoid, bone tumors
	Secondary: intraparenchymal metastases	Secondary: leptomeningeal metastases
Infratentorial	Primary: astrocytoma, medulloblastoma(PNET), ependymoma, brainstem glioma, hemangioblastoma	Primary: schwannoma, meningioma, (epi)dermoid, chordoma
	Secondary: intraparenchymal metastases	Secondary: leptomeningeal metastases

all primary intracranial tumors. Examples of intra-axial tumors include astrocytoma (low-grade, anaplastic, glioblastoma multiforme (GBM)), oligodendrogioma, ependymoma, dysembryoplastic neuroectodermal tumor (DNET), and lymphoma. However, metastases are still the most frequent intra-axial tumors in the supratentorial compartment. Intra-axial tumors can enhance because of the BBB breakdown (e.g., high-grade astrocytoma) or because of their intrinsic tumor vascularity (hemangioblastoma). The degree of enhancement may play a role in differentiating high-grade from low-grade gliomas. Table 2.2 provides an overview of intracranial tumors depending on their location.

Some tumors are located in the ventricles. Table 2.3 provides a differential diagnostic list for intraventricular mass lesions.

2.3.4 Edema and Mass Effect

MRI is more sensitive than CT in detecting intracranial mass lesions because of the intrinsically higher soft tissue contrast resolution and because the associated edema is easily observed on FLAIR and T2-WI. In many instances, peritumoral edema is more conspicuous than the tumor itself. Three types of edema can be discerned.

Table 2.3 Intraventricular tumors (listed alphabetically)

Astrocytoma, Glioblastoma
Choroid plexus papilloma/carcinoma
Colloid cyst (third ventricle) Craniopharyngioma
Ependymoma
Epidermoid/dermoid Medulloblastoma (PNET)
Meningioma Metastases (CSF seeding)
Neurocytoma (or neuroepithelioma, usually centered around the septum pellucidum)

Vasogenic edema is caused by a breakdown of the BBB, which allows excessive fluid to pass from the capillaries into the extracellular space. Vasogenic edema extends along white-matter tracts and generally spares the cortical gray matter (Fig. 2.16). Vasogenic edema is associated with primary and metastatic tumors, contusion, inflammation, hemorrhage, and the subacute stage of cerebral infarcts.

Cytotoxic edema is most often due to ischemia. When the blood supply to brain cells is decreased below a certain threshold (approximately 15 mL/min/100 g of tissue), the production of adenosine triphosphate (ATP) is reduced, and the Na/K pump fails. This results in cellular swelling and a decrease in the volume of the extracellular spaces. Cytotoxic edema is typically seen in (hyper)acute ischemic arterial infarction (Fig. 2.17) and can involve both gray and white matter. If damage to the BBB follows, vasogenic edema may ensue in addition to the cytotoxic edema.

Interstitial edema occurs around the ventricles and is induced by acute hydrocephalus. It results from transepidual migration of CSF into the periventricular white matter, due to a pressure gradient.

All types of edema result in an increased water content of the tissues and are therefore hyperintense on FLAIR and T2-WI. Interstitial edema results in diffuse periventricular hyperintensity along the lateral ventricles. Diffusion-weighted MRI is the technique of choice for early detection of cytotoxic edema, which may be detected within minutes after an acute cerebral infarct.

Intracranial mass effect is determined not only by the tumor volume, but also by the amount of edema that is present. Mass effect can lead to displacement of brain tissue, a process that is known as “cerebral herniation.” This is important to recognize, because it can lead to severe neurological dysfunction and is more commonly the cause of death than the tumor itself. Four types of internal *brain herniation* are distinguishable.

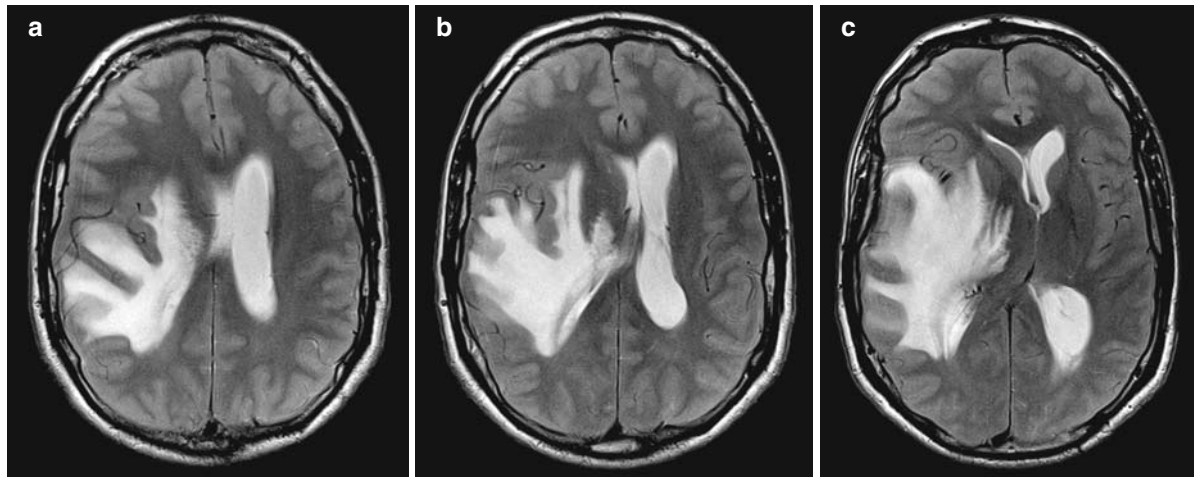


Fig. 2.16 Vasogenic edema, associated with anaplastic astrocytoma (WHO grade III). (a–c) Axial TSE T2-WI. “Fingers of edema” extend along white-matter tracts, into the subcortical white matter (a). The claustrum is outlined by vasogenic edema in the capsula externa and extrema (b). Edema also extends into

the posterior limb of the internal capsule and surrounds the different layers of the lentiform nucleus. Vasogenic edema is due to increased vascular permeability with accumulation of fluid in the intercellular spaces

1. Subfalcine herniation: Brain tissue is displaced horizontally from left to right or vice versa, and the cingulate gyrus is pushed under the falx. This process is best seen on coronal MR images, though it should also be recognized on axial scans.
2. Descending transtentorial herniation (uncal herniation, hippocampal herniation): The uncus and/or hippocampal gyrus of the temporal lobe are pushed medially and downward into the tentorial incisura, thereby compressing the mesencephalon and upper pons. Displacement of the medial temporal lobe is best seen on coronal images, but the compression of the brainstem is best observed on axial T2-WI.
3. Ascending transtentorial herniation: Upward displacement of the vermis and cerebellum through the incisura due to an infratentorial mass. The sagittal imaging plane is preferred.
4. Cerebellar tonsillar herniation: Downward displacement of the cerebellar tonsils and hemispheres through the foramen magnum behind the cervical spinal cord. Sagittal and coronal imaging planes are preferred.

2.3.5 Lesion Characterization

2.3.5.1 Signal Intensity

Most tumors appear hyperintense on FLAIR and T2-WI, and are iso- to hypointense on precontrast

T1-WI. These MR findings are not helpful in characterizing the lesion. Some mass lesions display unusual signal features, which may narrow the differential diagnosis. Table 2.4 lists a differential diagnosis for lesions that are hypointense on T2-WI. Table 2.5 provides a differential diagnostic list for lesions that are hyperintense on T1-WI. Cystic lesions are relatively rare, and their differential diagnosis is listed in Table 2.6.

Enhancement Pattern and Perfusion

Presence of contrast enhancement does not necessarily differentiate a tumor from a nontumoral lesion, since many nonneoplastic conditions also enhance. Moreover, the boundary of the enhancing area does not always delimit the tumor extent. This is especially true for gliomatous tumors, which project areas of infiltrating tumor cells beyond the margin of enhancement. Moreover, the intensity of contrast enhancement is not always correlated with the degree of malignancy of the lesion (e.g., pilocytic astrocytomas demonstrate marked enhancement, despite their relatively benign nature). Some specific types of enhancement provide interesting diagnostic gamuts, e.g., ring-like enhancement which may be encountered in a wide variety of lesions including GBM, metastasis, abscess, areas of demyelination, and others (Table 2.7).

The use of perfusion imaging has opened up new horizons in tumor imaging (see below).

Fig. 2.17 Cytotoxic edema in hyperacute infarction (arrows). (a) Axial TSE T2-WI. (b) Axial fat-sat turbo FLAIR. (c) Axial EPI diffusion-weighted “trace” image (DWI). (d) Apparent diffusion coefficient (ADC) map. The patient is a previously healthy 38-year-old man who presented with sudden onset of left hemiparesis, left hemianesthesia, left homonymous quadruplopia. No signal abnormality is seen on T2 (a) or FLAIR (b) images. Conversely, diffusion-weighted trace images show a focal area of high signal intensity (c) with lowered ADC values (d) in the posterior limb of the right internal capsule. These findings are consistent with a hyperacute infarction of the right anterior choroidal artery. This case illustrates the importance of DWI and ADC maps for early detection of cytotoxic edema, at a time when other imaging sequences are negative.

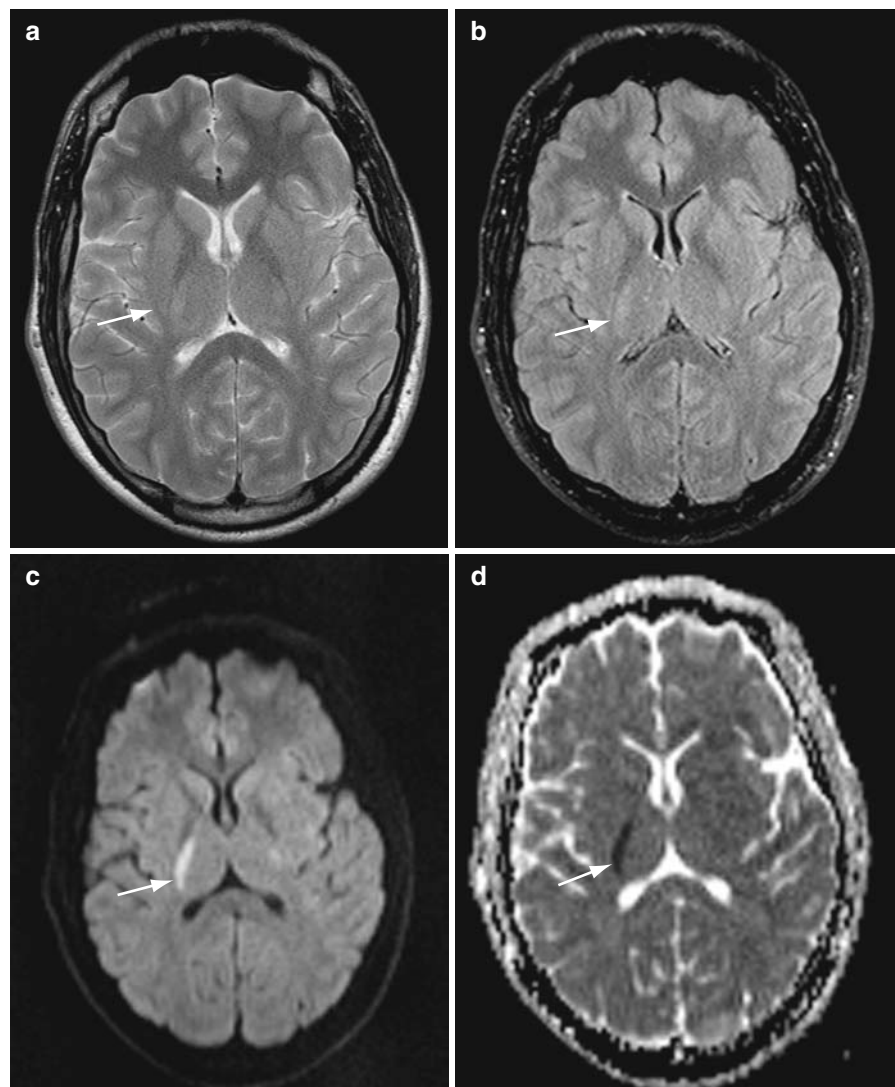


Table 2.4 Differential diagnosis of lesions with low signal intensity on T2-W images

Paramagnetic effects	<ul style="list-style-type: none"> Iron in dystrophic calcification Old hemorrhage (ferritin, hemosiderin) Acute hemorrhage (deoxyHb) Subacute hemorrhage (intracellular metHb) Melanin (free radicals)
Low proton density	<ul style="list-style-type: none"> Calcification High nucleus/cytoplasm ratio Dense cellularity
Macromolecule content	<ul style="list-style-type: none"> Very high protein concentration Fibrocollagenous stroma Caseating granuloma (e.g., tuberculoma)
Intratumoral vessels	<ul style="list-style-type: none"> Rapid blood flow (flow voids)

Table 2.5 Differential diagnosis of lesions with high signal intensity on T1-W images

Paramagnetic effects from hemorrhage	<ul style="list-style-type: none"> Subacute-chronic blood, e.g., methemoglobin
Paramagnetic effects without hemorrhage	<ul style="list-style-type: none"> Melanin Ions associated with necrosis or calcification: Mn, Fe, Cu
Nonparamagnetic effects	<ul style="list-style-type: none"> Very high protein concentration Fat Flow-related enhancement in vessels

Table 2.6 Differential diagnosis of cystic lesions

True cyst	<ul style="list-style-type: none"> Sharply demarcated, ovoid or round
Signal intensity	<ul style="list-style-type: none"> Isointense with CSF on all pulse sequences (e.g., arachnoid cyst, cysts associated with extra-axial masses) Slightly higher SI than CSF on T1-WI and PD-WI (proteinaceous debris and/or small concentrations of paramagnetic substances)
Diffusion	<ul style="list-style-type: none"> No diffusion restriction (e.g., arachnoid cyst, necrotic tumor, ...) Diffusion restriction (e.g., bacterial abscess, epidermoid, mucinous metastasis, ...)
Enhancement	<ul style="list-style-type: none"> Ring enhancement Mural nodule (e.g., hemangioblastoma)

Table 2.7 Differential diagnosis of ring-enhancing brain lesions

Neoplasm	<ul style="list-style-type: none"> Primary neoplasm (high-grade glioma, meningioma, lymphoma, acoustic schwannoma, crano-pharyngioma) Metastatic tumor
Abscess	<ul style="list-style-type: none"> Bacterial, fungal, parasitic abscess Empyema (epidural, subdural, or intraventricular)
Hemorrhagic-ischemic lesion	<ul style="list-style-type: none"> Resolving infarction Aging hematoma Operative bed following resection
Demyelinating disorder	
Radiation necrosis	

2.4 Supratentorial Brain Tumors

2.4.1 Introduction

Traditionally, MR examinations for supratentorial brain tumors have provided anatomic and structural data: location and margins of the tumor in various imaging planes, SI behavior, pattern of contrast enhancement, etc. Recently, MR has evolved toward a “multimodal” or “multi-parametric imaging platform” which incorporates perfusion and diffusion imaging, spectroscopy, tensor imaging, etc.

The axial plane is the plane of first choice for the supratentorial compartment; the coronal plane is the second best. In cases of midline lesions, such as pineal region tumors, the sagittal plane must be used.

Intravenous (i.v.) contrast agents, such as Gd-chelates are frequently necessary for the detection and improved delineation and characterization of the tumor. Without i.v. contrast, it is not possible to differentiate nonspecific high-intensity foci attributed to aging or ischemia from metastasis or lymphoma. Small lesions, such as metastases can be invisible without Gd. The pattern of contrast enhancement yields important information about the differential diagnosis and the degree of malignancy.

The questions to be answered are: what is the exact location of the tumor, and what is the probable histologic type and degree of malignancy? The radiologist must be aware of other factors of clinical importance: the mechanical effects such as obstructive hydrocephalus and descending transtentorial herniation.

Although intrinsically superior to CT, MRI also has its limitations! Neuroradiological examinations do not show the true neuropathological extent of many intra-axial brain tumors. MRI is a highly sensitive technique, but there is still a lack of specificity. On T2-WI, high SI lesions from a MS plaque and a metastasis can be very similar. MRI is not as sensitive for intratumoral calcifications as CT. Necrosis, a prognostically important factor in brain tumor diagnosis is not reliably detected by MRI.

2.4.2 Basic Neuroradiological Features

2.4.2.1 Description of the Lesion

In an MRI report, the following basic neuroradiological characteristics of an intracranial tumor should appear: location (intra-axial or extra-axial, supratentorial or infratentorial, frontal or temporal, etc.), SI, degree of perifocal edema, space-occupying characteristics, what happens after i.v. contrast, solitary or multiple lesions. Together with other factors, such as the clinical information, the speed of evolution, the age of the patient, and the relative frequency of certain tumors in certain locations, these neuroradiological features should lead to a probable neuropathological diagnosis or differential diagnosis.

2.4.2.2 Intra-Axial or Extra-Axial Location

The most important question for the radiologist when confronted with an intracranial mass lesion is whether

it is located in the intra-axial or extra-axial compartment. This is of great clinical importance. The location affects the operative planning and prognosis. Extra-axial tumors are located outside the brain parenchyma and are mostly benign. There are several signs of an extra-axial location (Table 2.8).

2.4.2.3 Signal Intensity

Because of their high water content, most brain tumors are hypointense on T1-WI and hyperintense on T2-WI images. However, there are many exceptions to this rule. The signal behavior of a tumor can be homogeneous or heterogeneous. There are many causes of heterogeneous SI (Table 2.9).

Tumors with a dense cellularity have a relatively low SI on T2-WI. This is a characteristic MR feature of medulloblastoma, pinealoblastoma, neuroblastoma, lymphoma, and mucinous adenocarcinoma metastasis (Table 2.4).

Some tumors exhibit high SI on T1-WI. This characteristic is mainly found in tumors containing fat (lipoma, dermoid), melanin (metastatic melanoma),

Table 2.8 MR signs of extra-axial tumor location

Difference in signal intensity between the tumor surface and the cortex	Arterial encasement; dural sinus invasion
Elements of a brain-tumor interface	Dural-tail sign
White-matter buckling	Gyrаль compression: the accordion sign
Osseous changes	Paradoxical cisternal widening
Vascular pedicle	Broad-based dural contact

Table 2.9 Causes of heterogeneous signal intensity

Hemorrhage
Necrosis
Calcification
Cyst
Blood vessels
Inhomogeneous enhancement
Fat
Melanin

methemoglobin (hemorrhagic tumors), or high protein concentrations (craniopharyngioma) (Table 2.5).

2.4.2.4 Patterns of Contrast Enhancement in Brain Tumors

The pattern of contrast enhancement supplies important information about the possible histological type of the tumor (Tables 2.7, 2.10, and 2.11).

2.4.2.5 MR Perfusion Imaging of Brain Tumors

Brain tumors are known for their capacity to induce the formation of new blood vessels, a process which is known as angiogenesis. When a brain tumor starts to outgrow its blood supply, it produces angiogenic cytokines, which are the driving force behind angiogenesis. The blood vessels which are produced in this way are histologically abnormal, tortuous, irregular, and disorganized. They do not possess a BBB and are more permeable than normal capillaries. When tumors enhance after injection of a gadolinium-chelate, it is because the contrast agent leaks out of the abnormal blood vessels, and through these fenestrations, enters the interstitial space. The vascular abnormalities and changed flow dynamics in tumor blood vessels can be used in MR perfusion imaging. The most frequently used parameter in neuro-oncology is regional cerebral blood volume (rCBV). It is expressed in mL/100 g of brain tissue, and is a good indicator of the blood passing through the tumor or

Table 2.10 Superficial tumor with homogeneous enhancement

Meningioma
Lymphoma
Anaplastic astrocytoma
Metastasis

Table 2.11 Cyst with enhancing mural nodule

Pilocytic astrocytoma
Hemangioblastoma
Pleomorphic xanthoastrocytoma
Ganglioglioma

normal brain tissue. High-grade glial brain tumors have greater rCBV than their low-grade counterparts, reflecting their greater angiogenetic activity. In patients with brain tumors, MR perfusion imaging is helpful:

- To identify high-grade tumor components, and thus to guide stereotactic biopsy (and avoid areas of necrosis)
- To better delineate and define the true extent of glial tumors (since the hyperintense areas on FLAIR or T2-WI do not always correspond to the true tumor margins)
- To assist in surgical planning or radiation therapy, by outlining the tumor boundaries
- To differentiate tumor recurrence (increased rCBV) from radiation-induced necrosis (diminished rCBV)

2.4.3 Extra-Axial Supratentorial Tumors

Extra-axial tumors, are by definition, located outside the brain parenchyma. Meningioma is the most common tumor in this category. Other extra-axial tumors include schwannoma, arachnoid cyst, epidermoid-dermoid, lipoma, extra-axial metastasis, etc.

Meningiomas arise from meningotheelial (arachnoidal) cells along the inner surface of the dura mater. They have a distinct predilection for specific locations: convexity (Fig. 2.15), parasagittal, sphenoidal ridge (Fig. 2.3), anterior skull base, cavernous sinus, CPA, etc. Most meningiomas demonstrate a heterogeneous SI pattern. They are typically isointense with gray matter on most sequences and may, therefore, be missed unless contrast is administered (Fig. 2.14). On T1-WI, meningiomas are almost always hypo- to isointense compared with brain tissue. On PD-WI and T2-WI, meningiomas tend to be iso- to hyperintense compared with the adjacent brain parenchyma. The identification of an anatomic brain-tumor interface is pathognomonic for the extra-axial localization. Three different anatomic interfaces may be identified with MRI: pial vascular structures, CSF clefts, and dural margins.

Following Gd administration, meningiomas generally display intense and homogeneous enhancement. Even heavily calcified meningiomas tend to enhance. Multiplanar imaging is useful for the preoperative delineation of the extent of the meningioma. Dural enhancement adjacent to the tumor is a striking finding

in contrast-enhanced MRI. It is referred to as the “dural-tail sign.” It is not specific for meningiomas; it indicates dural involvement by an adjacent mass.

2.4.4 Intra-Axial Supratentorial Tumors

2.4.4.1 Neuroepithelial Tumors

Tumors of neuroepithelial tissue, also known as glial tumors or “gliomas,” account for 40–45% of all primary intracranial tumors. They arise from the glial cells, which have a great propensity to malignant transformation. The three most common groups of gliomas, which correspond to the three histologic subgroups of glial cells, are: astrocytoma, oligodendrogioma, and ependymoma. Neoplasms arising from the choroid plexus can also be considered as neuroepithelial tissue tumors, because the choroid plexus contains modified ependymal cells. Gliomas occur predominantly in the cerebral hemispheres, but the brain stem and cerebellum are frequent locations in children, and they can also be found in the spinal cord. In 2007, the World Health Organization (WHO) published a new classification of tumors of the CNS, which lists several new entities.

Astrocytic Tumors

Astrocytic brain tumors can be divided into two major groups: the fibrillary (also known as infiltrative or diffuse) astrocytoma and the circumscribed (localized or noninfiltrative) astrocytoma (Table 2.12).

Well-differentiated (diffuse) low-grade *astrocytomas* (WHO grade II) are the low-grade member of the fibrillary or diffuse astrocytomas (Fig. 2.18). Well-differentiated low-grade astrocytomas are relatively rare, affect younger patients, and have a better prognosis than their more aggressive counterparts. On MRI, a low-grade astrocytoma is seen as a homogeneous mass lesion, involving gray and white matter. The lesion is typically hypo- or isointense on T1-WI and hyperintense on FLAIR and T2-WI. The tumor causes local mass effect with gyral swelling, though perifocal edema is usually absent or slight. MRI misleadingly displays these lesions as clearly defined, especially on T2-WI. However, it should be remembered that they belong to the group of diffuse astrocytoma, and tumor cells extend beyond the MRI

Table 2.12 Classification of astrocytic brain tumors

Name	Fibrillary (diffuse or infiltrative) astrocytoma	Circumscribed (localized or noninfiltrative) astrocytoma	Glioblastoma multiforme	Pilocytic astrocytoma	Giant-cell astrocytoma	Pleomorphic xanthoastrocytoma
Common locations	Cerebral hemispheres, pons (in children)	Cerebral hemispheres, brainstem	Cerebral hemispheres	Cerebellum, diencephalon	Subependymal in lateral ventricle (at the foramen of Monro)	Cerebral hemispheres, superficially located, often temporal lobe
Demographics	4th and 5th decades	Variable	Peak 50–65 years	5–15 years (peak around 10 years)	Children, young adults	Young adults with a history of seizures
Imaging findings	Expansion, no enhancement (intact BBB), follows white matter tracts	Variable appearance, no enhancement, no necrosis or cyst formation	Grossly heterogeneous (necrosis, ring enhancement, vasogenic edema, hemorrhage)	Cyst with enhancing nodule	Variable enhancement associated with other features of tuberous sclerosis	Heterogeneous (cyst with enhancing mural nodule, dural tail due to superficial location)
Malignancy grading (WHO)	Grade II	Grade III	Grade IV	Grade I	Benign	Benign (10% may have malignant degeneration)
Enhancement	Enhancement with Gd-chelates increases with degree of malignancy (breakdown of blood-brain barrier)	Enhancement is not related to degree of malignancy				

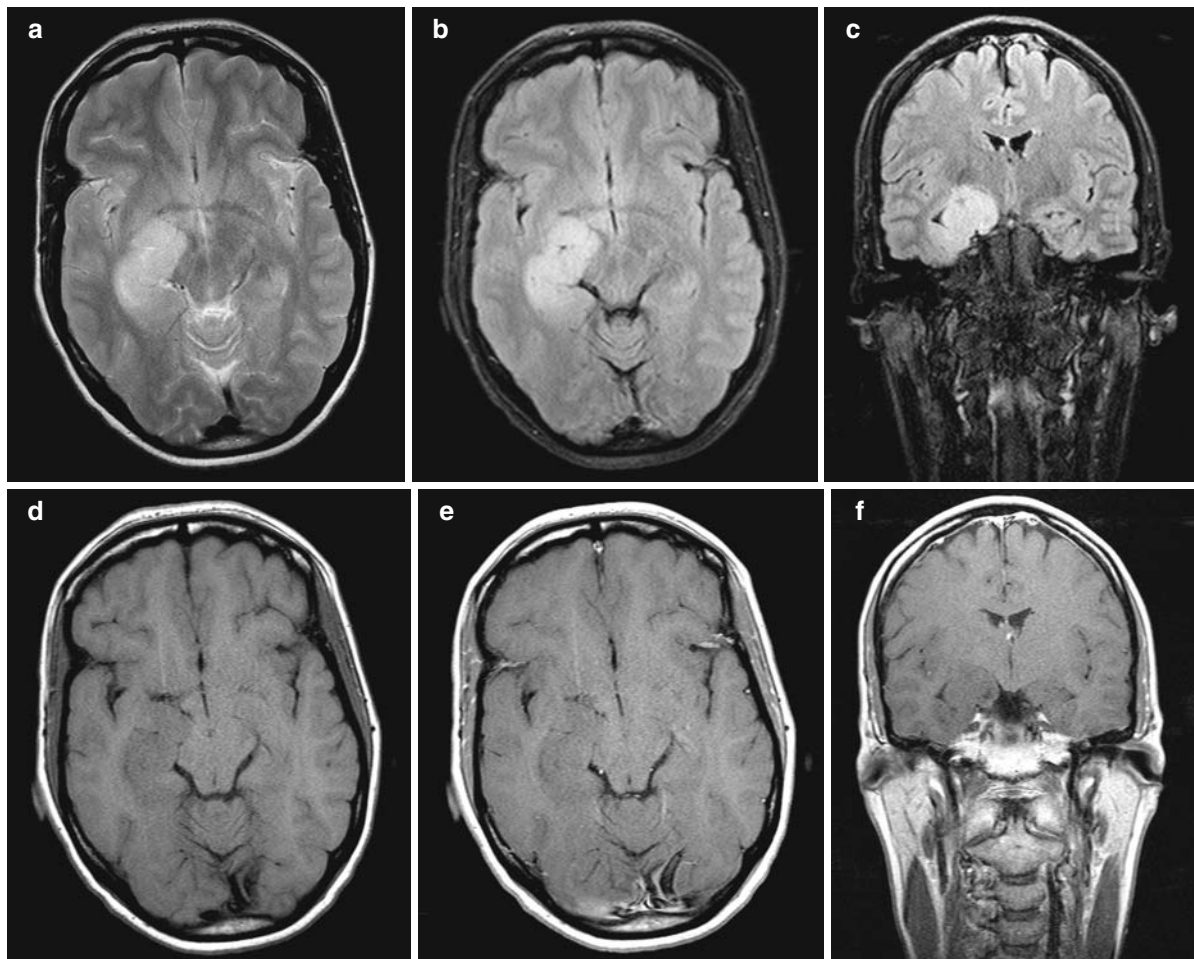


Fig. 2.18 Low-grade diffuse astrocytoma (WHO grade II). **(a)** Axial TSE T2-WI. **(b)** Axial fat-sat turbo FLAIR. **(c)** Coronal fat-sat turbo FLAIR. **(d)** Axial TSE T1-WI. **(e)** Gd-enhanced axial T1-WI. **(f)** Gd-enhanced coronal T1-WI. This 44-year-old woman presented with an epileptic seizure. MRI of the brain

reveals a tumor in the medial part of the right temporal lobe. The tumor is hyperintense on T2 and FLAIR images (**a–c**) and hypointense on T1 images (**d**). There is no enhancement (**e, f**). Stereotactic biopsy revealed a low-grade diffuse astrocytoma (WHO grade II)

visible margins of the tumor! Typically, a low-grade astrocytoma shows no contrast enhancement. Moreover, though initially benign, a low-grade astrocytoma can evolve into a higher grade tumor over time. Different parts of the tumor can exhibit varying degrees of malignancy; this makes histological grading from biopsies difficult. MRI perfusion imaging and/or magnetic resonance spectroscopy (MRS) may be helpful in identifying a suitable stereotactic biopsy site.

Anaplastic astrocytomas (WHO grade III) are more common than their low-grade counterparts. These malignant, aggressive tumors infiltrate adjacent brain structures, and have a poor prognosis. On MRI, anaplastic astrocytomas present a more heterogeneous appearance, both on T1-WI and FLAIR or T2-WI.

They exhibit marked mass effect and perifocal vasogenic edema, which spreads with fingerlike projections along white-matter tracts. The tumor may contain hemorrhagic foci. Marked but irregular enhancement is usually present, indicating breakdown of the BBB (Fig. 2.19). MRS shows increased choline (Cho), decreased N-acetyl-aspartate (NAA), and may show lactate (indicating necrosis, even though the tumor does not contain macroscopically visible cysts or areas of necrosis) (Fig. 2.20). MRS can be useful to differentiate recurrent tumor from radiation necrosis.

Glioblastoma multiforme (GBM) is the most malignant neuroglial tumor (WHO grade IV). In the older adult (>45 years), high-grade GBM is the most common primary intra-axial supratentorial neoplasm. The imaging

Fig. 2.19 Anaplastic astrocytoma. (a) Axial TSE T1-WI. (b) Axial TSE T2 WI. (c) Axial FLAIR TSE. (d) Gd-enhanced axial T1-WI. This 17-year-old young woman presented with a right frontal headache. MRI of the brain reveals a large tumor in the frontal right lobe with partial extension to the left side. The tumor consists of solid and cystic components extending from the right frontal lobe to the contralateral side with some vasogenic edema. The solid component shows mixed and inhomogeneous contrast enhancement. Stereotactic biopsy followed by tumor resection revealed an anaplastic pilocytic astrocytoma

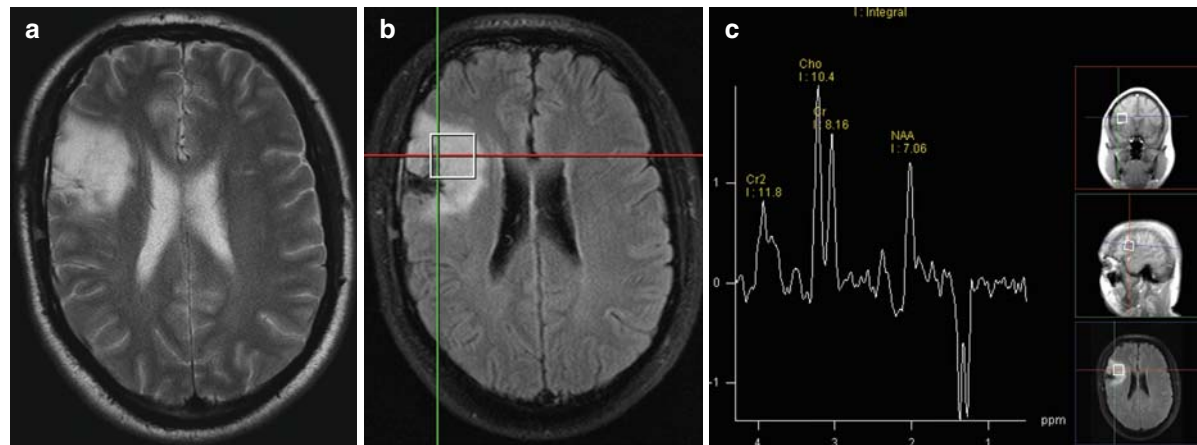
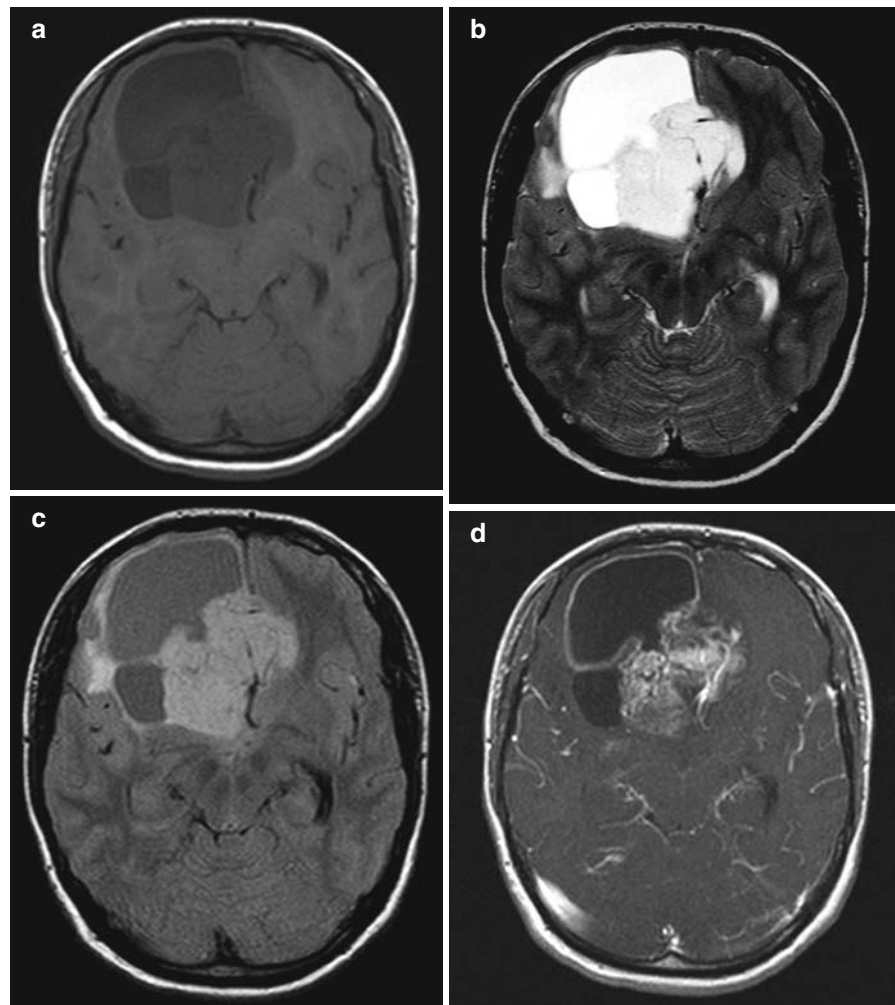


Fig. 2.20 Recurrent anaplastic astrocytoma (WHO grade III) in a 36-year-old man. (a) Axial TSE T2-WI. (b) Axial fat-sat turbo FLAIR. (c) Single voxel proton MR spectroscopy (MRS) ($TE = 135$ ms). The tumor recurrence is located in the right operculo-frontal region, and is hyperintense both on T2 and FLAIR

images. Single voxel proton MRS shows moderate increase in choline (Cho), decrease in *N*-acetyl-aspartate (NAA), and an inverted doublet of lactate (indicating necrosis, even though the tumor does not contain macroscopically visible cysts or areas of necrosis)

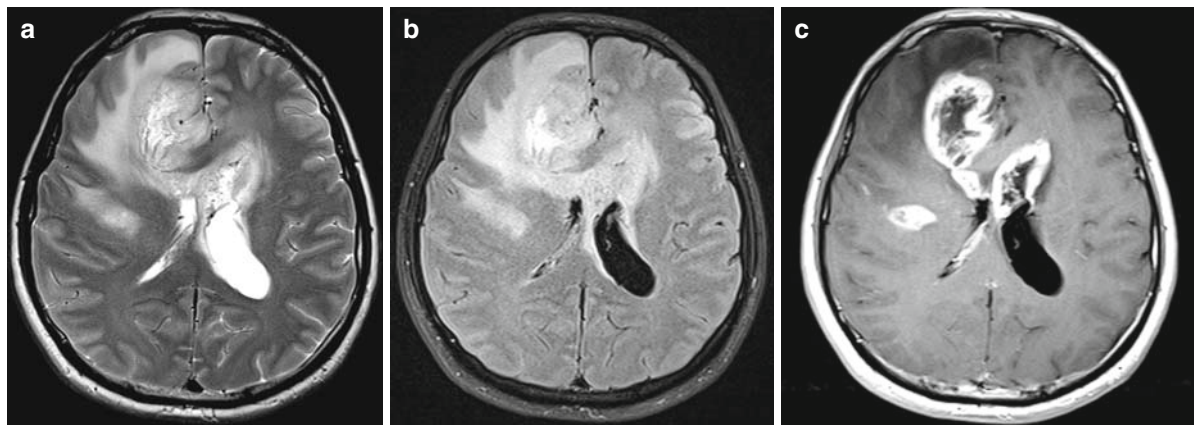


Fig. 2.21 Glioblastoma multiforme. **(a)** Axial TSE T2-WI. **(b)** Axial fat-sat turbo FLAIR. **(c)** Gd-enhanced axial T1-WI. Glioblastoma is an aggressive tumor, surrounded by vasogenic edema, with strong contrast enhancement (reflecting tumor

angiogenesis), and areas of necrosis or cyst formation. The tumor has spread from the right frontal lobe across the corpus callosum to the left hemisphere, along the ventricular surface, and there is a satellite nodule in the right fronto-parietal region

findings can be predicted from the neuropathologic key features: cell heterogeneity, vascular cell proliferation (angiogenesis), necrosis, and infiltration. On MR images, these properties are translated into: heterogeneous signal intensities, cystic or necrotic areas, perifocal edema (with tumor inside and outside), intratumoral signal void of vessels, extensive mass effect, and inhomogeneous contrast enhancement (Fig. 2.21). Sometimes, these highly vascular tumors can even mimic arteriovenous malformations (AVMs). They often contain intratumoral hemorrhages. Enhancement with contrast is intense and heterogeneous.

Gliomatosis cerebri is an unusual condition in which multiple lobes of the brain are diffusely invaded by contiguous extension of glial tumor cells. It may represent the extreme form of diffusely infiltrating glioma.

The group of circumscribed (localized or noninfiltrative) astrocytomas includes pilocytic astrocytoma, pleomorphic xanthoastrocytoma (PXA), and subependymal giant cell astrocytoma (SCGA).

Pilocytic astrocytomas occur predominantly in children and adolescents. They are also known as “juvenile pilocytic astrocytomas” (JPA). The most common location for pilocytic astrocytomas is infratentorial (Fig. 13.46), but the tumor can be encountered supratentorially in the optic chiasm or hypothalamus or, less commonly, in the cerebral hemispheres (Fig. 2.22). Optochiasmatic-hypothalamic pilocytic astrocytomas are usually solid tumors, with moderate or even strong enhancement. When large, these tumors may

contain cysts or trapped CSF, and should be differentiated from craniopharyngioma. There is an association with neurofibromatosis type 1.

Subependymal giant cell astrocytoma (SGCA) is a slow-growing, indolent, benign tumor, and is typically found in a subependymal location at the foramen of Monro. It occurs most commonly in children and young adults. Symptoms are usually secondary to obstructive hydrocephalus. SCGA shows intense and heterogeneous enhancement. The tumor occurs with tuberous sclerosis.

Pleiomorphic xanthoastrocytoma (PXA) is a rare and generally benign tumor. It is found predominantly in young adults, who often present with a history of seizures. PXA occurs in the cerebral hemispheres and is often located superficially, with the temporal lobes most commonly affected. On MRI, PXA presents as a superficial, partially cystic mass, with an enhancing mural nodule.

In the revised and updated WHO classification of tumors of the CNS, many other tumors are listed. A full discussion of these entities, many of which are very rare, is beyond the scope of this chapter.

Oligodendroglial and Oligoastrocytic Tumors

Oligodendrogliomas arise from oligodendrocytes. They are less common than astrocytic tumors, and constitute 2–5% of all primary brain tumors. They tend to occur in adults between the ages of 25 and 50 years, with a peak

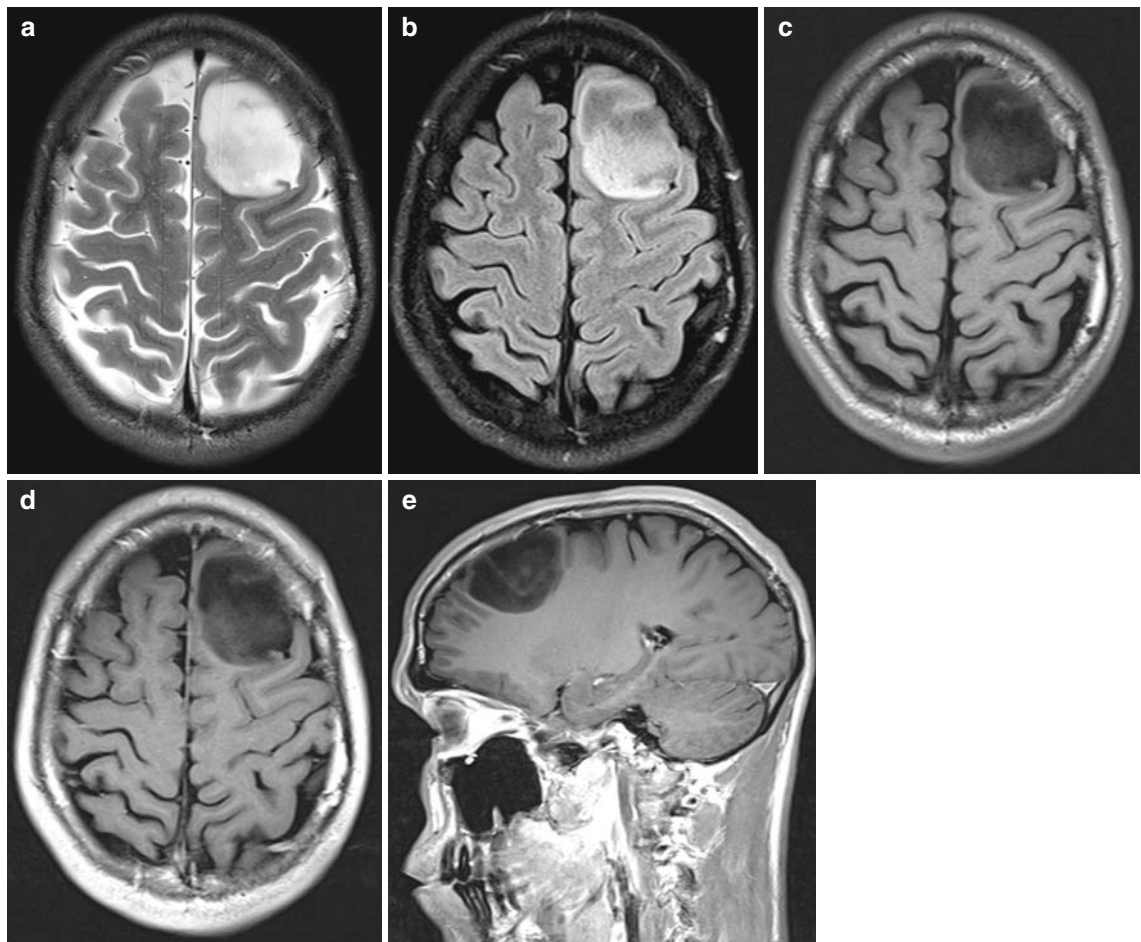


Fig. 2.22 Low grade astrocytoma (WHO grade I). (a) Axial TSE T2-WI. (b) Axial fat-sat turbo FLAIR. (c) Axial TSE T1-WI. (d) Gd-enhanced axial T1-WI. (e) Gd-enhanced sagittal T1-WI. This 26-year-old man presented with an epileptic seizure. The tumor in the left frontal lobe is inhomogeneously hyperintense on T2 and FLAIR, hypointense on T1, and does

not enhance (no signs of angiogenesis, no blood-brain barrier breakdown). The tumor was surgically resected and neuropathological examination revealed pilocytic astrocytoma. Differential diagnosis for such a lesion should include low grade astrocytoma (WHO grade II), dysembryoplastic neuroepithelial tumor (DNET), ganglioglioma or oligodendrogioma

incidence around 35–45 years. Oligodendrogiomas are the most benign of the gliomas. They are slow-growing and are found predominantly in the frontal lobes and tend to infiltrate the cortex. MRI is less sensitive than CT in detecting calcifications, which occur in >70% of cases.

Oligoastrocytomas are brain tumors of mixed glial cell origin, containing elements from both astrocytoma and oligodendrogloma. They are also known as “mixed gliomas,” and represent approximately 2% of all primary brain tumors. Oligoastrocytomas can be further subdivided into low-grade and anaplastic types.

Ependymal Tumors

Ependymomas are slow-growing neoplasms arising from cells of the ependymal lineage. They comprise 4–8% of primary brain tumors and are most commonly found in children. Two-thirds of ependymomas occur infratentorially (especially in the fourth ventricle), and one-third are found supratentorially. Of supratentorial ependymomas, more than half are extraventricular, presumably arising from ependymal cell nests in the cerebral parenchyma. On MRI, ependymomas present as a heterogeneous tumor of mixed signal intensities.

Calcifications, present in 50% of cases, may be difficult to detect on routine MRI sequences, and the use of a gradient-echo T2*-weighted sequence or susceptibility-weighted imaging (SWI) sequence can be helpful. After contrast injection, the enhancement is moderate to intense, depending on the vascularization of the tumor.

2.4.4.2 Intracranial Lymphoma

Intracranial lymphoma may be primary or secondary. Primary CNS lymphoma is usually non-Hodgkin's lymphoma (NHL), B-cell type and there is a strong association with Epstein-Barr virus. It is an aggressive brain tumor with a poor prognosis. Typically, primary CNS lymphoma shows multicentric involvement of the deepest parts of the hemispheres, around the ventricles and in the corpus callosum. The tumor tends to disappear rapidly with corticosteroids and/or radiation therapy; hence the name "ghost tumor." The risk of primary CNS lymphoma dramatically increases in immunocompromised patients (AIDS, after renal transplantation, immunoglobulin deficiency syndromes, etc.). Secondary CNS lymphoma is a complication of systemic lymphoma. It shows a tendency to invade the dura mater and leptomeninges; common clinical presentations include cranial nerve palsies and hydrocephalus.

Imaging studies reveal a well-demarcated mass lesion (Fig. 2.23), which is typically found supratentorially in the paramedian structures, including the deep white matter and corpus callosum, as well as the deep central gray matter (basal ganglia, thalamus, hypothalamus). Contact with an ependymal surface is a characteristic feature. Involvement of the posterior fossa occurs, but is not as common as in the supratentorial compartment. Up to half of all cases are multicentric.

On noncontrast CT, lymphoma is hyperdense relative to the surrounding brain tissue, because of the cell density. On MRI, primary CNS lymphoma tends to be iso- to hypointense to brain on both T1-WI and FLAIR or T2-WI (in contradistinction to glioma). The diminished signal on FLAIR and T2-WI may reflect the dense cellularity and relatively decreased water content (high nucleus-to-cytoplasmic ratio) of these tumors. The SI is of course altered in the presence of necrosis, which is a feature frequently found in AIDS patients. There is relatively little mass effect for the size of the tumor. After intravenous injection of Gd-chelates, CNS lymphoma

typically enhances intensely (Fig. 2.23), but the pattern of enhancement is variable. Solid homogeneous enhancement is usually observed in immunocompetent patients. Conversely, in immunocompromised patients, the enhancement pattern tends to be irregular, heterogeneous, or ring-like. Periventricular enhancement is highly specific (though not pathognomonic) for CNS lymphoma.

The differential diagnosis of CNS lymphoma includes tumors (glioma, metastases, primitive neuroectodermal tumor (PNET), ...), infectious diseases (toxoplasmosis, tuberculosis, ependymitis,...), and demyelinating disorders (MS, PML).

2.4.4.3 Intracranial Metastasis

Intracranial metastases are the most common intracranial neoplasms. They account for 15–40% of all clinically detected brain tumors. Metastases can be located in the skull, epidural space, meninges, and subarachnoid space (meningeal carcinomatosis), but they occur most frequently in the brain parenchyma. The most common primary tumors to metastasize to the adult brain are, in order of decreasing frequency, bronchial carcinoma, breast carcinoma, gastrointestinal tract tumors (colon, rectum), renal cell carcinoma, melanoma, and choriocarcinoma. Together, these six primary tumors account for 95% of all brain metastases in adults. In children, the most common primary tumors are leukemia, lymphoma, and neuroblastoma.

Cerebral metastases can occur anywhere in the brain, but they occur most frequently in the cortex or at the corticomedullary junction (hematogenous spread). Intraparenchymal metastases are most common in the cerebral hemispheres, but they also occur in the cerebellum and brainstem. At the time of diagnosis, multiple lesions are found in 2/3 of cases, and a single metastasis is found in 1/3. Metastatic cells can also spread via the CSF, a condition known as carcinomatous meningitis. Subependymal spread is encountered, for example, in metastatic breast carcinoma. Nodular metastatic deposits in the dura mater are not uncommon, and this is known as dural carcinomatosis.

On MRI, cerebral metastases are hypointense on T1-WI and present a variable SI on FLAIR and T2-WI (due to hemorrhage, melanin, necrosis, cyst formation, etc.). They are generally round and better circumscribed than primary tumors. Cerebral metastases from a "mucinous" adenocarcinoma may appear hypointense on

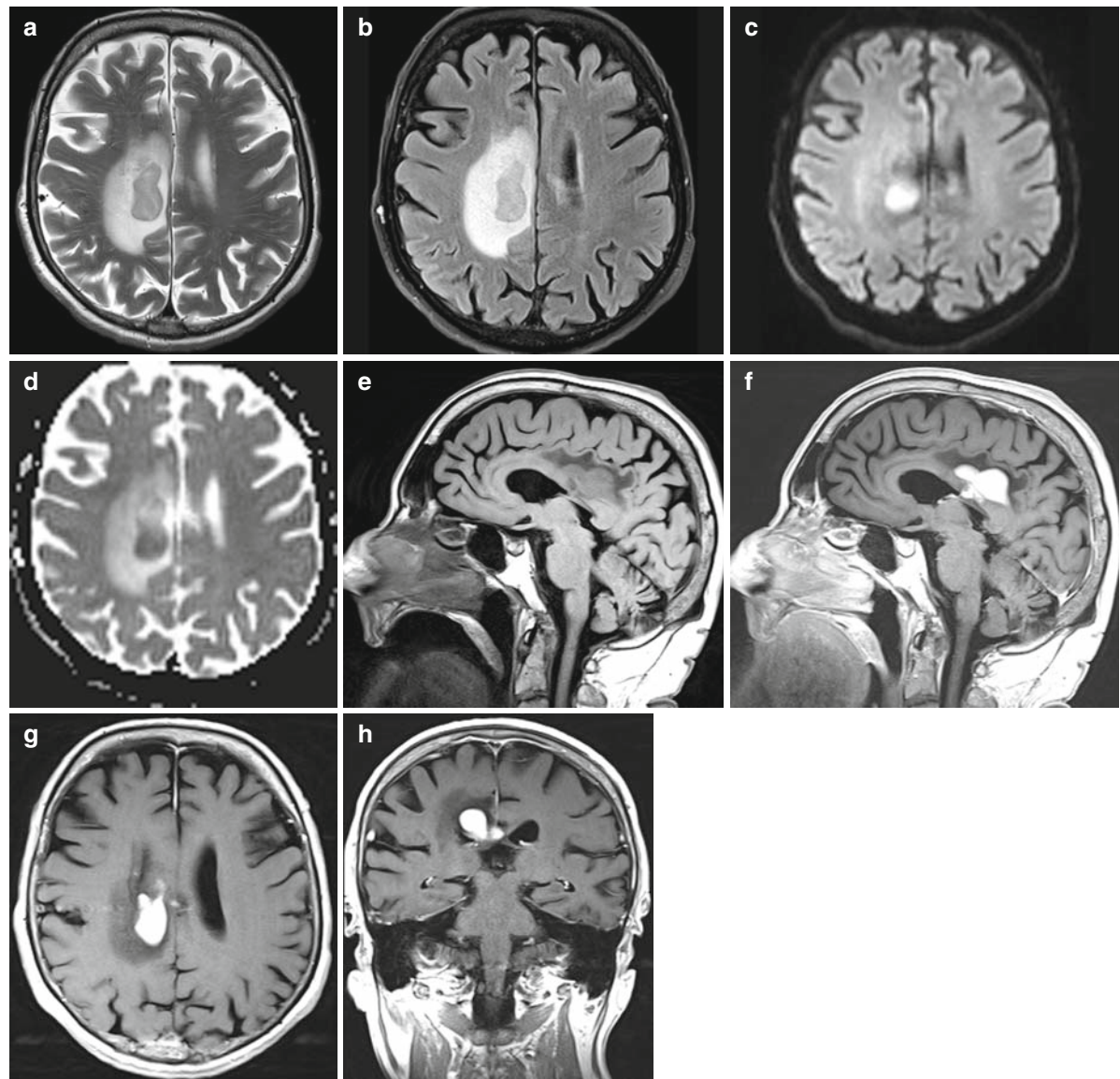


Fig. 2.23 Non-Hodgkin's lymphoma. (a) Axial TSE T2-WI. (b) Axial fat-sat turbo FLAIR. (c) Axial EPI diffusion-weighted 'trace' image. (d) Apparent diffusion coefficient (ADC) map. (e) Sagittal TSE T1-WI. (f–h) Gd-enhanced sagittal (f), axial (g) and coronal (h) TSE T1-WI. This 73-year-old man has a history of Wegener's disease, and was treated with steroids and cyclophosphamide. He presented with sudden onset of gait instability and falling to the left side. The tumor is located

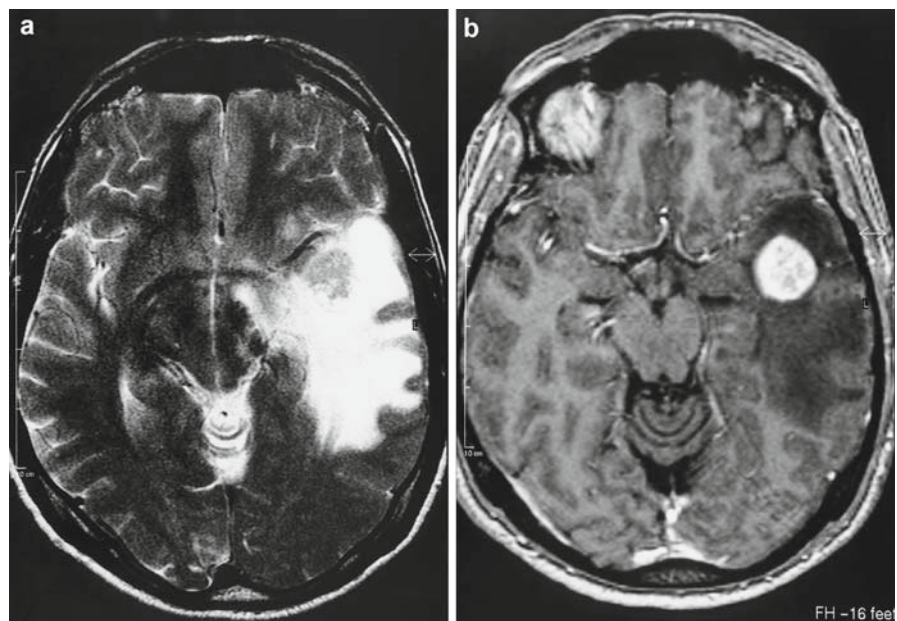
above the right lateral ventricle, extends into the corpus callosum, and is surrounded by a large rim of vasogenic edema. The tumor is relatively hypointense on T2-WI (a), hyperintense on diffusion-weighted trace images (b), with lowered ADC values (c); these findings reflect a high cell density and/or high nucleus/cytoplasm ratio, with little mobile water. After Gd injection, there is intense and homogeneous enhancement of the tumor

T2-WI and show diffusion restriction (their viscous content lowers apparent diffusion coefficient (ADC) values). When metastases are hyperintense on T1-WI, this can be due to the presence of hemorrhage or melanin (paramagnetic effect). The amount of peritumoral edema is variable. In small cortical lesions, edema may be absent, but

in general, the degree of edema is greater with metastatic lesions than with primary neoplasms (Fig. 2.24).

By far, the most sensitive examination for the detection of intracerebral metastases is gadolinium-enhanced MRI, especially for detecting small metastatic lesions. Gd-enhanced MRI is far superior to contrast-enhanced

Fig. 2.24 Solitary brain metastasis. (a) Axial TSE T2-WI. (b) Axial Gd-enhanced GRE 3D FT T1-WI. A nodular mass lesion is observed in the anterior part of the left temporal lobe. On T2-WI, the tumor is isointense with gray matter. Relative to the size of the tumor, there is a disproportionately large amount of perilesional vasogenic edema. After Gd injection, there is intense enhancement. The enhancing tumor can be sharply separated from the surrounding vasogenic edema



CT in the detection of cerebral metastases. On postcontrast T1-WI, cerebral metastases present strong enhancement, which can either be homogeneous, nodular, inhomogeneous, or ring-like (see Table 2.7) (Figs. 2.25 and 2.26). Some authors have shown that a high-dose

(0.3 mmol/kg) immediate study is superior to a normal-dose or delayed study in detecting small lesions. With the arrival of newer contrast agents with higher relaxivity there is less need for high-dose imaging. The use of magnetization transfer improves the contrast between

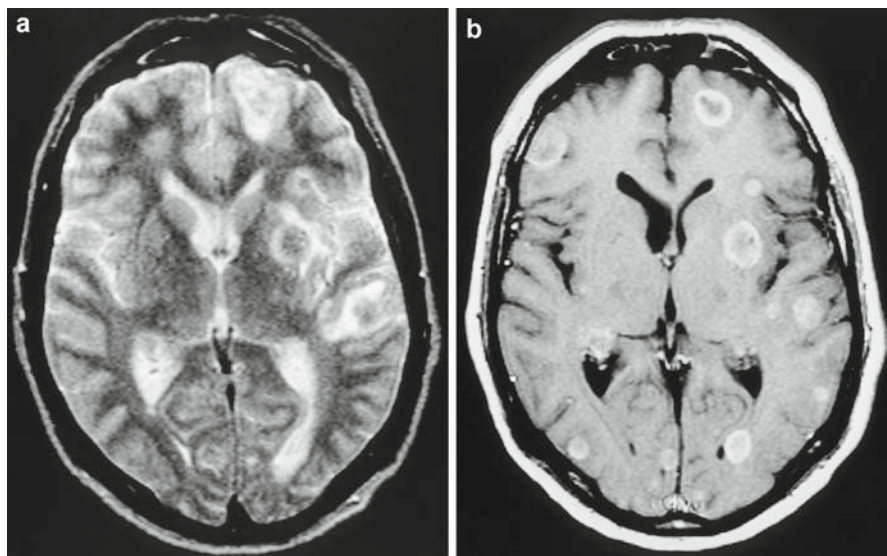


Fig. 2.25 Multiple metastases. (a) Axial TSE T2-WI. (b) Axial gadolinium-enhanced SE T1-WI. The precontrast T2-WI shows only a few lesions compared with the postcontrast T1-WI. The enhancement characteristics of the different metastatic tumors are not uniform; some enhance homogeneously, while other

lesions display a ring-shaped enhancement pattern. Also the amount of perilesional edema is variable. Notice the characteristic location of many of the metastatic lesions at the corticomedullary junction

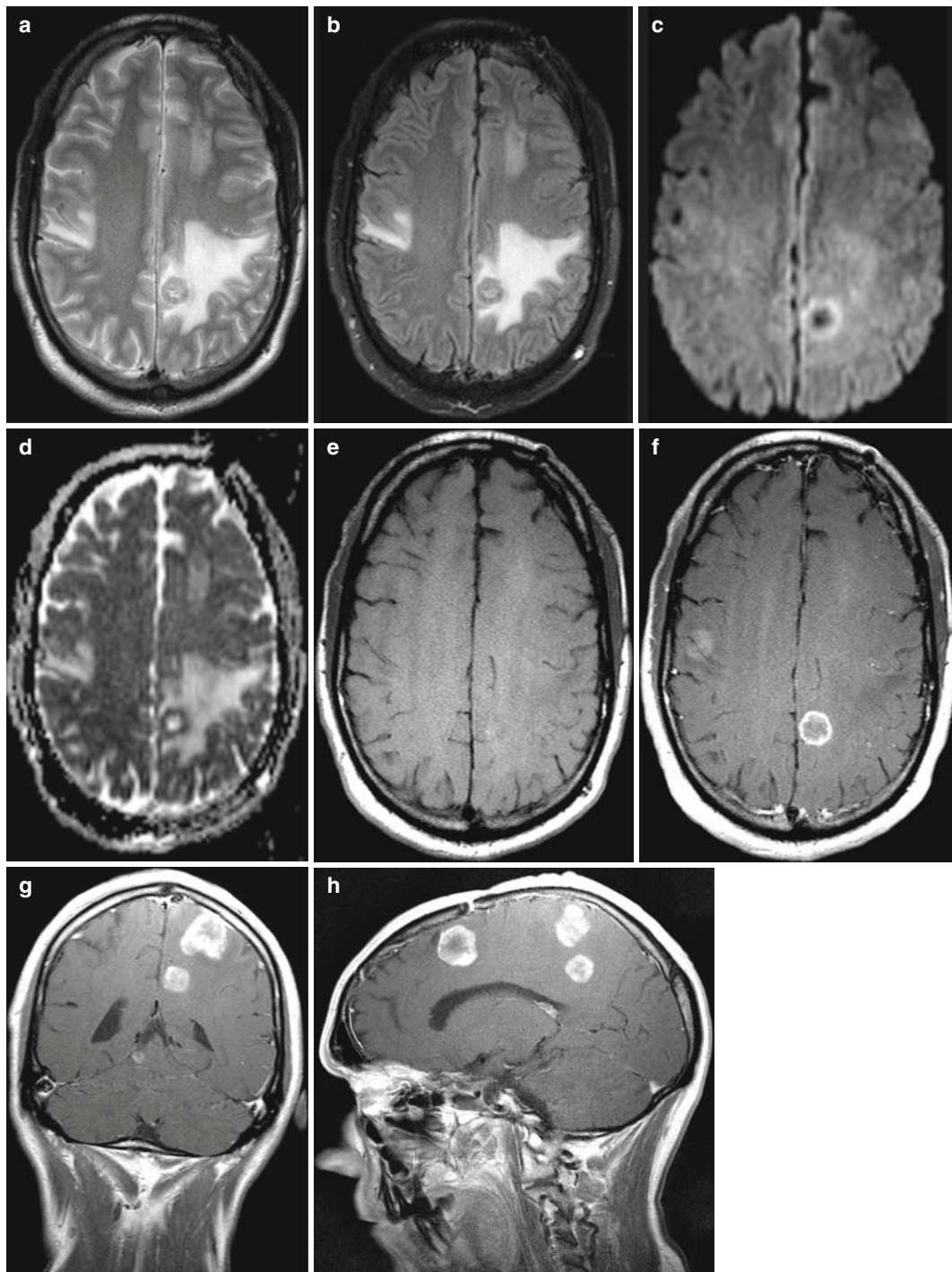


Fig. 2.26 Multiple cerebral metastases. (a) Axial TSE T2-WI. (b) Axial fat-sat turbo FLAIR. (c) Axial EPI diffusion-weighted “trace” image. (d) Apparent diffusion coefficient (ADC) map. (e) Axial TSE T1-WI. (f-h) Gd-enhanced axial (f), coronal (g) and sagittal (h) TSE T1-WI. The primary tumor of this 43-year-old man is a poorly differentiated pulmonary adenocarcinoma. A solitary left frontal lobe metastasis had been resected the pre-

vious year. He now presents with multiple metastases, with solid or ring-like enhancement pattern. The metastasis in the medial part of the left parietal lobe has a thick hypointense wall with a hyperintense center, consistent with necrosis. Dense ring enhancement is noted on the Gd-enhanced T1-WI. The diffusion-weighted image (c) and the ADC map (d) do not show restricted diffusion (DDx with cerebral abscess)

the enhancing lesion and the background. Enhancement and thickening (often asymmetric) of the dura mater suggests dural carcinomatosis (but beware of dural enhancement after recent lumbar puncture or intracranial hypotension syndrome). Leptomeningeal enhancement indicates carcinomatous meningitis.

Although there are no pathognomonic MRI features of cerebral metastases, the following findings are highly suggestive:

- One or more intracranial, enhancing tumor(s) in a patient with a known primary extracranial neoplasm
- A small lesion with a disproportionate amount of peritumoral edema
- Multiple enhancing lesions (Figs. 2.25 and 2.26)
- A solitary, thick-walled, ring-enhancing lesion (Ddx abscess)

2.5 Infratentorial Tumors

2.5.1 Anatomy and Technique

The posterior fossa is bordered anteriorly in the midline by the dorsum sellae and the clivus (body of sphenoid bone, basilar part of occipital bone, separated by the sphenooctipital synchondrosis). The posterior aspect of the petrous bone constitutes the anterior lateral border, while the lateral and posterior borders are formed by the occipital bone, parietal bone, sigmoid, and transverse sinus. The tentorium cerebelli and straight sinus compose the roof of the posterior fossa; the foramen magnum and jugular foramen are found in the floor of the posterior fossa.

The posterior fossa contains the brainstem (mesencephalon, pons, and medulla oblongata), cranial nerves III–XII, cerebellum (vermis, hemispheres, and tonsils), CSF spaces (fourth ventricle, cisterna magna, prepontine cistern, and CPA cisterns), arteries [vertebrobasilar artery and branches: posterior-inferior cerebellar artery (PICA), anterior-inferior cerebellar artery (AICA), superior cerebellar artery (SCA)], veins, and dural sinuses.

For the evaluation of posterior fossa lesions, axial and coronal imaging planes are preferred. Sagittal imaging is useful in fourth-ventricle mass lesions and CCJ abnormalities. When studying cranial nerve lesions, thin slices (<1 mm) should be obtained. T2-WI

are useful for demonstrating edema, cysts, areas of necrosis, and the presence of a CSF cleft in extra-axial tumors. Ultra-thin T2-WI (3D TSE with flip back pulse, e.g., RESTORE, FRFSE or DRIVE sequences) or T2*-WI constructive interference in the steady state (CISS, FIESTA, FFE) are useful for visualizing the CSF within the internal auditory canal and the fluid within the inner ear structures (cochlea, vestibule, and semicircular canals). When a tumor is suspected clinically, pre- and postcontrast T1-WI must be obtained.

2.5.2 Age-Related Frequency of Posterior Fossa Tumors

In children, posterior fossa tumors constitute the largest group of solid neoplasms. Posterior fossa tumors are second only to leukemia in overall frequency during childhood. They remain associated with a high mortality rate, despite recent therapeutic advances. In children over the age of 1 year, 50% of brain tumors occur infratentorially. Conversely, in infants (<1 year old), supratentorial tumors are more frequent [PNET, low-grade gliomas, and choroid plexus tumors]. Topographically, posterior fossa tumors can be subdivided into extra- and intra-axial tumors. The latter group can be further split into brainstem, cerebellar, and fourth-ventricle tumors.

2.5.3 Extra-Axial Posterior Fossa Tumors

In adults, the most common posterior fossa tumors are extra-axial in nature. The site of predilection is the CPA cistern, which is located between the anterolateral surface of the pons and cerebellum and the posterior surface of the petrous temporal bone. The following imaging signs may be helpful to determine the extra-axial nature of a mass lesion:

- Widening of the ipsilateral CPA cistern
- Presence of a CSF cleft between the tumor and the cerebellum
- Rotation of the brainstem away from the lesion
- Displacement of the gray matter–white matter interface around the mass

Mass lesions in the CPA in decreasing order of frequency are: acoustic schwannoma (80%), meningioma

Table 2.13 Mass lesions in the cerebellopontine angle cistern

Common	<ul style="list-style-type: none"> • Acoustic schwannoma (80%) • Meningioma (13–18%) • Epidermoid (5%)
Less common	<ul style="list-style-type: none"> • Other schwannomas: facial nerve, trigeminal nerve • Vascular: vertebrobasilar dolichoectasia, aneurysm of basilar artery, AVM • Metastases • Paraganglioma • Arachnoid cyst • Lipoma • Foramen jugulare tumors • Chordoma

(15%), epidermoid (5%), other schwannomas (facial nerve, trigeminal nerve), vascular lesions (vertebrobasilar dolicho-ectasia, aneurysm of basilar artery, AVM), metastases, paraganglioma, arachnoid cyst, lipoma, foramen jugulare tumors, and chordoma (Table 2.13). Some intra-axial tumors may secondarily extend into the CPA cistern, e.g., exophytic glioma, metastasis, hemangioblastoma, and ependymoma.

Acoustic nerve schwannoma is the most common CPA tumor (80%). Clinically, this tumor presents with sensorineural hearing loss, dizziness, and gait disturbance. Many acoustic schwannomas have both an intracanalicular and a CPA component. They may be solid or cystic (in large tumors necrosis occurs secondary to hemorrhage) (Fig. 2.27). In less than 5% of

cases, there is an associated CPA arachnoid cyst. The hallmark of acoustic schwannomas on MRI, except for their typical location, is the intense, often heterogeneous, enhancement. Small, purely intracanalicular schwannomas can be detected with thin (submillimeter), heavily T2-WI (e.g., 3D CISS), and their presence can be confirmed on Gd-enhanced T1-WI (Fig. 2.28). On these thin-section T2-W scans, there is often a decreased SI of the labyrinthine fluid on the affected side. This finding should be mentioned in the report, since it is associated with poor outcome.

Bilateral acoustic schwannomas occur in the setting of neurofibromatosis type 2 (Fig. 2.29). This is a neurocutaneous disorder with autosomal dominant inheritance (with high penetrance, linkage to chromosome 22). The occurrence frequency is $\pm 1/40,000$. The condition is characterized by bilateral acoustic schwannomas, intracranial meningiomas (convexity, falx), schwannomas of cranial nerves V, VII, IX, and X, spinal cord ependymoma, and astrocytoma. Neurofibromatosis type 2 is sometimes described by the acronym “MISME” (multiple inherited schwannomas, meningiomas, and ependymomas). Cutaneous lesions are less frequent than in neurofibromatosis type 1. Symptoms usually develop in the second decade (adolescents and young adults).

Meningioma is the second most common CPA tumor (<10%). Meningiomas show a broad-based dural attachment at the posterior surface of the petrous pyramid. A “dural-tail” sign is a frequent finding and is an important element in the differential diagnosis

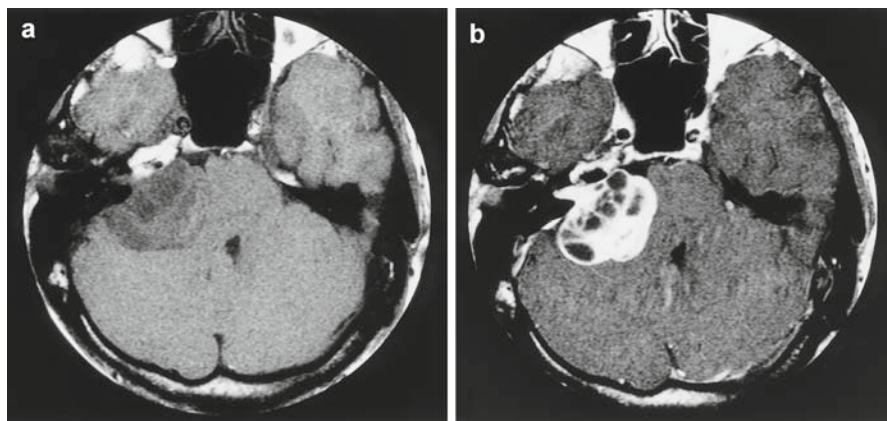


Fig. 2.27 Acoustic schwannoma. (a) Axial SE T1-WI. (b) Gd-enhanced axial SE T1-WI. A large tumor extends from the right internal auditory canal to the cerebellopontine angle cistern. The enhancement pattern is inhomogeneous. The tumor

contains numerous cystic areas. The brainstem is displaced, and the fourth ventricle is flattened, due to mass effect. Note that there is some enhancement of the meninges lining the posterior surface of the petrous bone

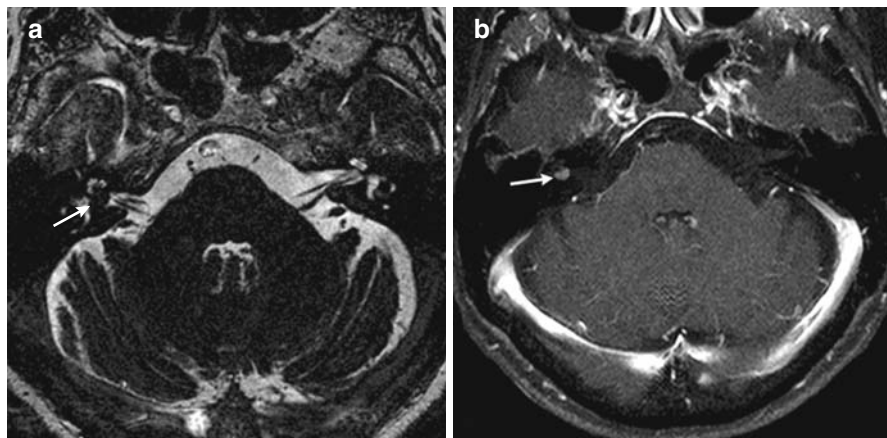


Fig. 2.28 Intracanalicular acoustic schwannoma. (a) Axial CISS T2-WI. (b) Gadolinium-enhanced axial SE T1-WI with fat saturation. On the heavily T2-WI CISS image, the intracanalicular acoustic schwannoma appears as a “filling defect,” outlined

by bright CSF (arrow). Enhancement is intense and homogeneous (arrow). Fat saturation can be of use to distinguish the enhancing tumor from the bright fatty bone marrow signal of the petrous apex or the walls of the IAC

with acoustic schwannomas. Meningiomas tend to be eccentric from the internal auditory canal. These tumors may contain (extensive) calcifications, which may be overlooked on MRI. After Gd-injection, enhancement can be heterogeneous or homogeneous, depending on the composition and size of the tumor.

Epidermoid tumor is the third most common CPA tumor. This benign, slow-growing cystic lesion results from an “inclusion” of epithelium during neural tube closure (third to fifth week of gestation). The wall of an epidermoid is composed of a connective tissue capsule (stratified squamous epithelium); the cyst contains desquamative epithelial debris (keratin products) and cholesterol crystals. On MRI, SI can be highly variable, but most often the cyst is isointense to CSF and the lesion is hyperintense on T2-WI and heterogeneously hypointense on T1-WI; this appearance is sometimes referred to as a “black epidermoid,” and is due to the presence of cholesterol crystals, keratin, and CSF in the interstices of the tumor. Conversely, a “white epidermoid” is hyperintense on T1-WI due to the presence of triglycerides and polyunsaturated fatty acids which cause shortening of the T1 relaxation time. Epidermoids do not enhance; they are avascular in nature. Diffusion-weighted imaging (DWI) typically shows diffusion restriction (high SI on diffusion trace images, and lowered ADC values). This is an important differential diagnostic feature, since arachnoid cysts and other cystic/necrotic tumors show no diffusion restriction. Though the CPA cistern is the site of predilection,

epidermoids can also occur in the middle cranial fossa in the parasellar-paracavernous region. Moreover, epidermoids can also be extradural, located within the calvarium, producing well-defined bone erosion.

Other schwannomas include facial nerve schwannoma, trigeminal nerve schwannoma (also known as gasserian ganglion schwannoma), and jugular fossa schwannomas arising from the glossopharyngeal (IX), vagus (X), accessory (XI) nerves. Less common CPA lesions are listed in Table 2.13.

2.5.4 Intra-Axial Posterior Fossa Tumors

2.5.4.1 Brainstem

Brainstem gliomas represent 25% of intracranial gliomas in children and young adults compared with only 2.5% in adults. Patients usually present with cranial nerve symptoms; hydrocephalus is uncommon at the time of initial presentation. The fourth ventricle is displaced backwards, and its width may be increased (stretching). The cardinal imaging feature is the characteristic location of the tumor (Fig. 2.30). Brainstem gliomas can present two different growth patterns: diffusely infiltrating growth with symmetric expansion, or focally exophytic growth in the adjacent cisterns. Regardless of their growth pattern, brainstem gliomas are not resectable. On MRI, they

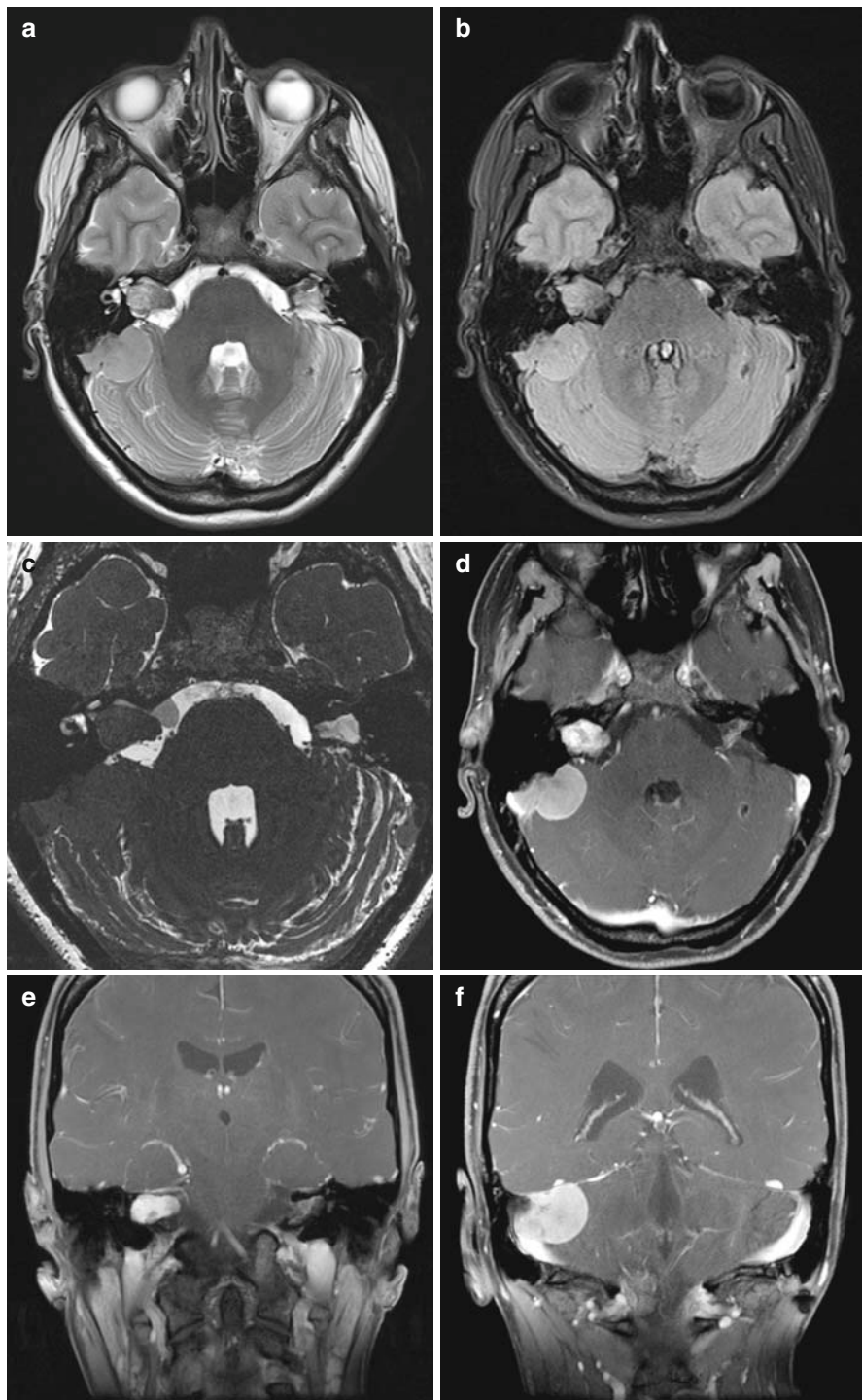


Fig. 2.29 Neurofibromatosis type II. (a) Axial TSE T2-WI. (b) Axial fat-sat turbo FLAIR. (c) Axial high-resolution CISS image. (d) Gd-enhanced fat-saturated axial TSE T1-WI. (e, f) Gd-enhanced coronal fat-saturated TSE T1-WI. There is an acoustic schwannoma on the *right*, which expands the internal auditory canal and extends into the right cerebellopontine angle

cistern. On the *left*, there is a postoperative status after resection of an acoustic schwannoma, with enhancing scar tissue (d). There is a large meningioma on the posterior wall of the right petrous bone (a, b, d), growing into the sigmoid sinus (e). A smaller meningioma sits on the anterior lip of the right internal auditory meatus (c)

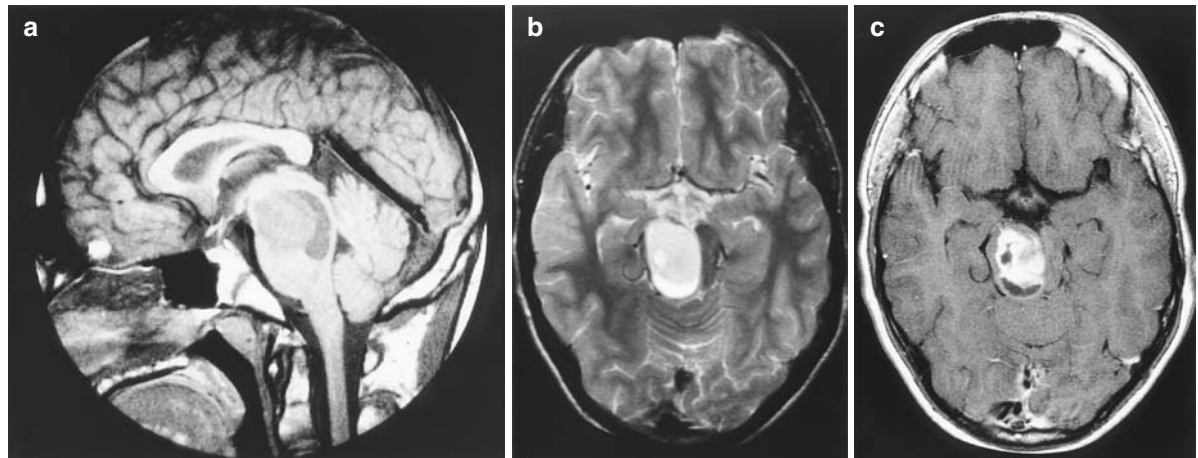


Fig. 2.30 Brainstem glioma. (a) Sagittal SE T1-WI. (b) Axial TSE T2-WI. (c) Gd-enhanced axial SE T1-WI. In this 16-year-old boy with a brainstem glioma, the tumor consists of an anterior solid component and a posterior cystic component. The signal intensity within the cyst is higher than that of CSF,

are hypointense on T1-WI and hyperintense on T2-WI, and may exhibit subtle enhancement indicating BBB breakdown. The expanding tumor enlarges the brainstem (usually the pons) and may engulf the basilar artery, which becomes trapped between the tumor and the clivus. MRS provides information regarding the biochemical signature of the tumor; high concentration of choline indicates increased cell membrane turnover, and is consistent with a more malignant tumor (Fig. 2.31).

Although 90% of cavernous malformations (syn. cavernous angioma) occur supratentorially, they can also be encountered in the brainstem. Clinical symptoms of brain-stem cavernous malformations include focal motor or sensory changes and are related to the exact location of the lesion. Imaging characteristics are discussed in Chap. 2.7.4.4.

2.5.4.2 Tumors in or Around the Fourth Ventricle

PNET constitute the second most common group of CNS tumors in children. *Medulloblastoma* is the most common representative of this group in the posterior fossa. The peak age range is 5–10 years, with a second, lesser peak between 20 and 30 years. In children, medulloblastoma typically arises in the midline

reflecting a higher protein content. Within the solid portion of the tumor, a necrotic area can be discerned. The necrotic portion does not enhance. There is linear enhancement along the walls of the cyst, confirming that this is an intrinsic part of the tumor

in the posterior vermis (Fig. 13.45). Due to its origin in the roof of the fourth ventricle, obstructive hydrocephalus is common. The presenting symptoms are related to increased intracranial pressure (headache, vomiting). On MRI examinations, these tumors are hypointense on T1-WI and hyperintense on T2-WI. They enhance with Gd-chelates. They have a propensity to leptomeningeal dissemination (metastatic seeding in the subarachnoid space). Therefore, during follow-up examinations, not only the posterior fossa, but the entire neuraxis should be examined. In adults, medulloblastoma typically arises in a cerebellar hemisphere.

Ependymoma represents 10% of childhood brain tumors. There appears to be a bimodal age peak at the age of 5 and 34 years. Two-thirds of intracranial ependymomas are located in the infratentorial compartment, especially in children. Ependymomas are often situated in the floor of the fourth ventricle (Fig. 13.47). They have a propensity to extend through the foramina of Magendie or Luschka, and grow into the CPA cistern or cisterna magna. As in medulloblastomas, the presenting symptoms are related to increased intracranial pressure (obstructive hydrocephalus). On noncontrast CT images, calcifications are present in 50% of cases. The MRI appearance of ependymomas is markedly inhomogeneous, due to the presence of calcifications, necrosis, and hemorrhage (hemosiderin deposits). Ependymomas

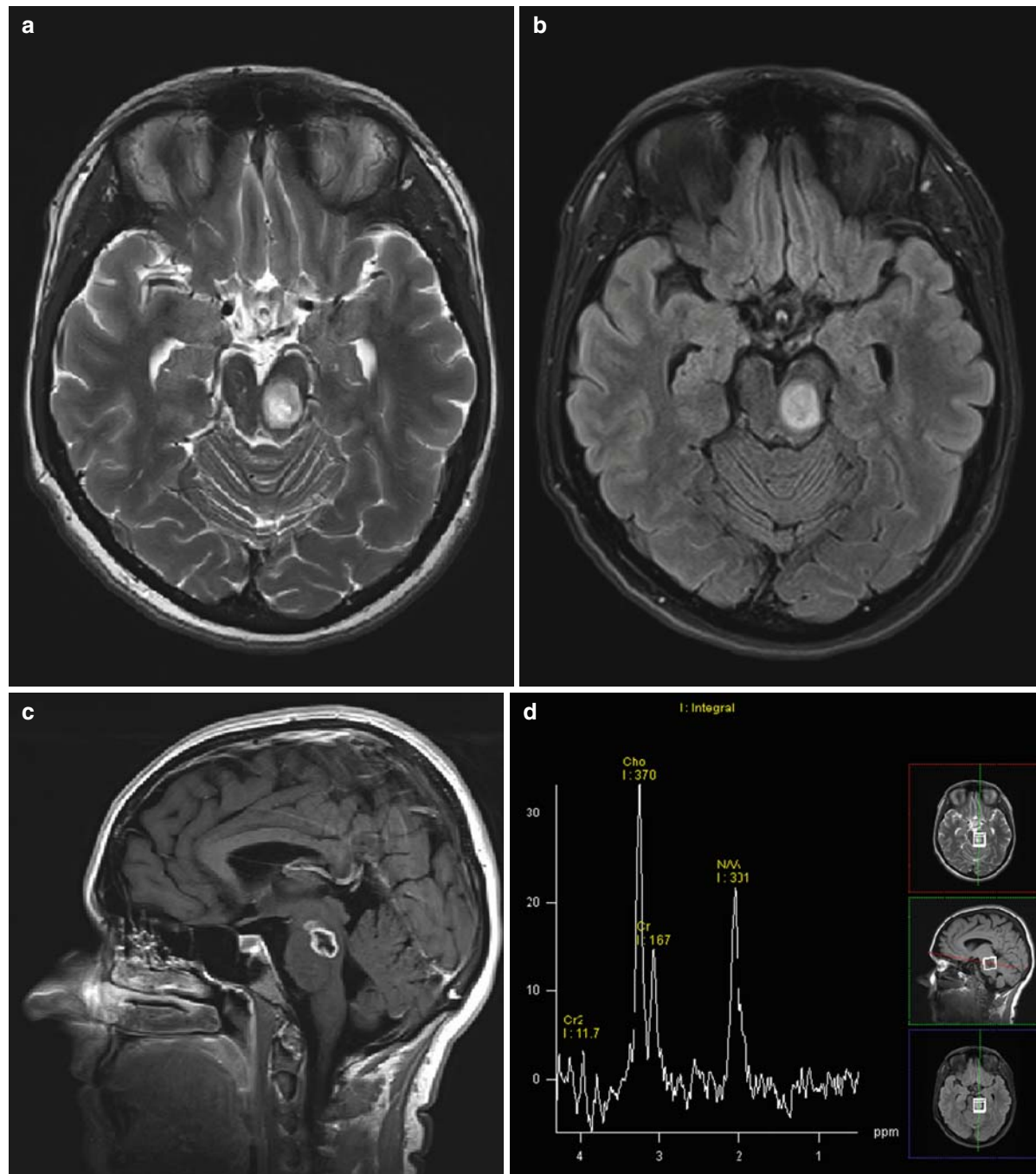


Fig. 2.31 Brainstem glioma in a 40-year-old woman. (a) Axial T2-WI. (b) Axial fat-sat turbo FLAIR. (c) Gd-enhanced sagittal TSE T1. (d) Single voxel proton MR spectroscopy (MRS). The tumor extends from the left side of the pons to the mesencephalon and left cerebral peduncle. The mass appears

homogeneously hyperintense on T2 and FLAIR, but after Gd administration, there is ring-enhancement, with a central nonenhancing area. MRS shows a markedly increased choline peak, indicating high cell-membrane turnover. Stereotactic biopsy of the lesion revealed astrocytoma grade III

are vascular in nature and enhance moderately or intensely with Gd.

Lesions of the choroid plexus can be cysts, papillomas, or carcinomas. *Choroid plexus cysts* are most often discovered in the lateral ventricles and are infrequent in the fourth ventricle. The MRI appearance is that of a small cystic lesion that is hypointense on T1-WI; there is no enhancement of the cyst contents. On DWI, plexus cysts may show restricted diffusion because of the high viscosity of their gelatinous content. The location of *choroid plexus papilloma* is age-related. In adults, choroid plexus papilloma is found in the fourth ventricle and CPA. In infants, it is found in the trigone of the lateral ventricle. On MRI, choroid plexus papilloma is iso-hypointense on T1-WI and slightly hypointense on T2-WI. The papilloma enhances markedly with Gd. Ventricular dilatation is a frequently associated finding; this can be due to overproduction of CSF by the papilloma and also due to the obstruction of CSF pathways by tumor and by repeated episodes of occult hemorrhage.

2.5.4.3 Primary Cerebellar Tumors

Cerebellar astrocytoma is the most common CNS tumor in children and the second most common

posterior fossa tumor (PNET is slightly more frequent) (Chap. 13.2.6.1); it is much less frequent in adults. Histologically, most cerebellar astrocytomas are low-grade and slow growing. They are typically large at diagnosis. Cerebellar astrocytomas arise in the cerebellar hemisphere or vermis. The fourth ventricle is displaced forward and often obliterated; obstructive hydrocephalus is common. The prepontine cistern is narrowed, due to mass effect. Many cerebellar astrocytomas are cystic, often with an enhancing mural nodule (Fig. 2.32). They can be indistinguishable from hemangioblastoma on MRI.

A special type of astrocytoma is the *juvenile pilocytic astrocytoma* (Fig. 13.46). It is the most benign histologic subtype of astrocytoma and predominantly affects children and young adults (Table 2.12). The typical appearance on the MRI is that of a cyst with an enhancing mural nodule (Table 2.11). The SI of the cyst is higher than CSF on T1-WI and T2-WI due to an increased protein content. However, solid forms are not unusual. On the MRI, they are characterized by a heterogeneously increased SI on early Gd-enhanced T1-WI, representing an enhancing matrix; homogeneous enhancement is observed on delayed images.

Hemangioblastoma is the most common primary intra-axial tumor of the adult posterior fossa. It is a benign tumor arising along a pial surface of the

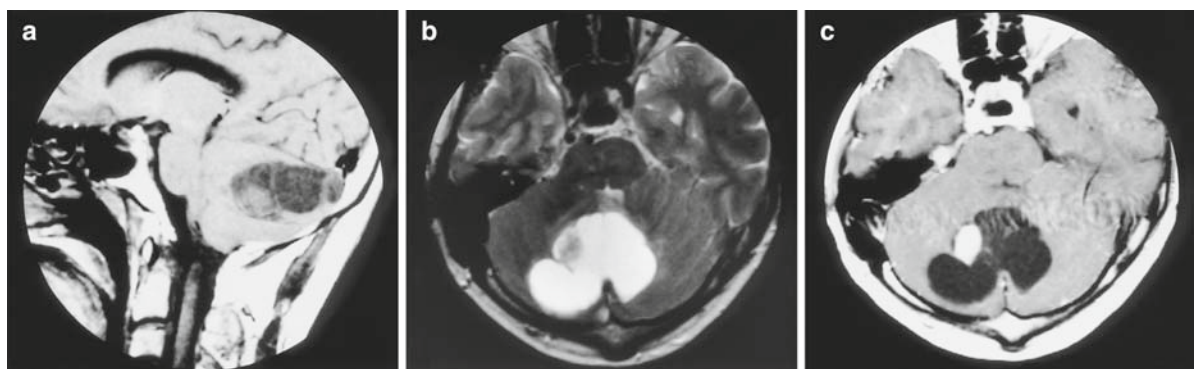


Fig. 2.32 Cystic cerebellar astrocytoma. (a) Sagittal SE T1-WI. (b) Axial TSE T2-WI. (c) Gd-enhanced axial SE T1-WI. There is a cystic-appearing cerebellar mass with a mural nodule. The fourth ventricle is flattened and displaced anteriorly. The cyst contents are of higher signal intensity than CSF, both on the

T1-WI and T2-WI, presumably indicating higher protein content. After contrast injection, the mural nodule enhances strongly and uniformly. The principal differential diagnosis involves hemangioblastoma, a tumor which can exhibit similar imaging characteristics

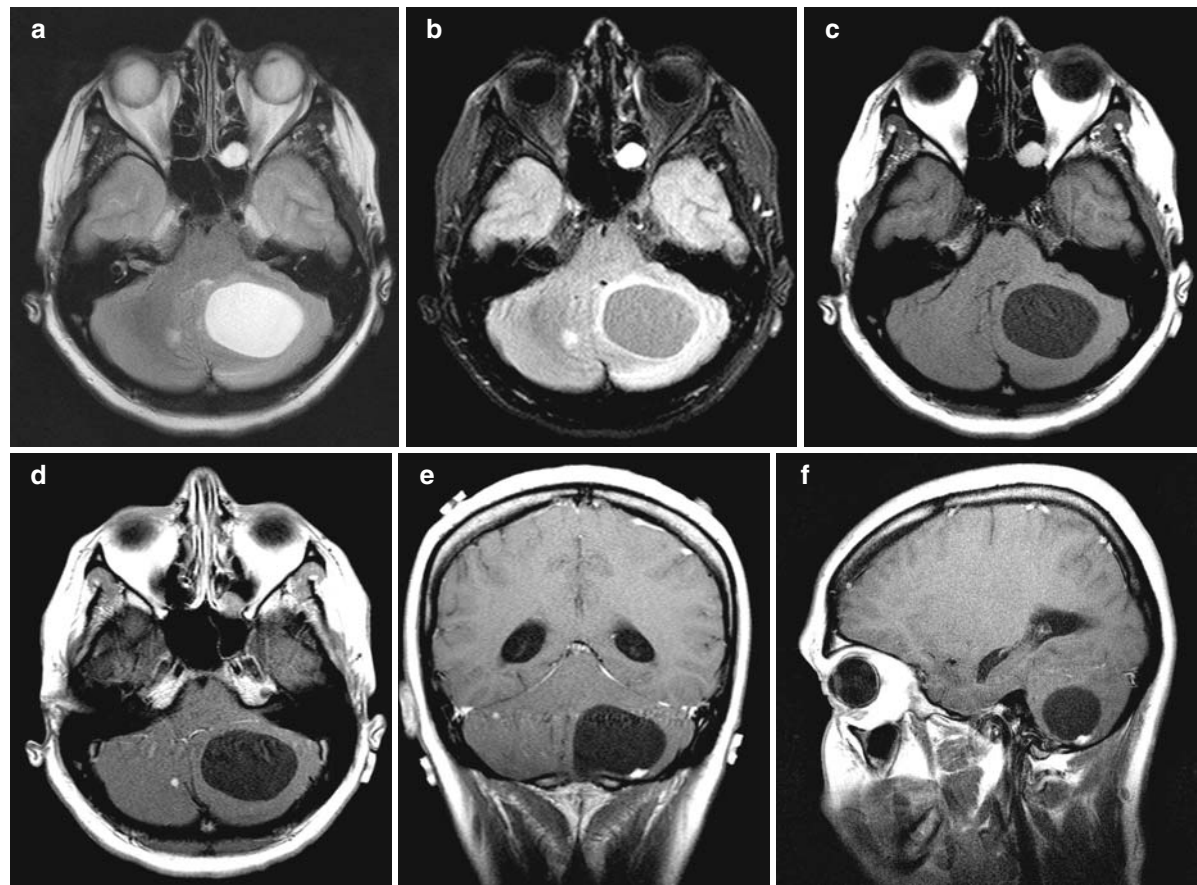


Fig. 2.33 Multiple cerebellar hemangioblastomas. (a) Axial TSE T2-WI. (b) Axial fat-sat turbo FLAIR. (c) Axial TSE T1-WI. Gd-enhanced axial (d), coronal (e) and sagittal (f) TSE T1-WI. The patient is a 25-year-old woman with von Hippel-Lindau syndrome, who presented with headaches, nausea, and

cerebellum, brainstem, or spinal cord. The MRI appearance is characterized by a combination of cysts containing proteinaceous fluid and solid mass lesions (Fig. 2.33). A typical appearance is that of a sharply demarcated cyst with an enhancing mural nodule (Table 2.11). Hemangioblastomas can be sporadic or inherited, solitary or multiple (von Hippel-Lindau). Between 4 and 40% of patients with hemangioblastoma match criteria for *von Hippel-Lindau syndrome*. This syndrome is a neurocutaneous disorder. It is defined by the association of two or more CNS hemangioblastomas (cerebellar hemangioblastoma, retinal angiomas, spinal cord, cauda equina hemangioblastoma) with multiple visceral organ cysts or neoplasms (kidney, liver, pancreas,

vomiting. The largest tumor in the left cerebellar hemisphere presents the classic appearance of a cystic mass, with a small enhancing mural nodule inferiorly. In addition, there are several other small, solidly enhancing hemangioblastomas in the right cerebellar hemisphere

epididymis, pheochromocytoma) and a family history of von Hippel-Lindau disease.

2.5.4.4 Secondary Tumors (Metastasis)

Although 85% of metastatic lesions are supratentorial, metastasis is still the most common intra-axial neoplasm of the adult posterior fossa; 15–20% of all intracranial metastases occur in the posterior fossa. Multiple lesions are the hallmark, but in the posterior fossa, there is a relatively high incidence of solitary lesions (25–50%). Metastases typically are found at gray-white matter interfaces; presumably because tumoral micro-emboli become stuck in the small capillaries. The MR SI of

metastases can be altered by the presence of hemorrhage (methemoglobin, hemosiderin), mucin content (hypointense appearance on T2), melanin (paramagnetic effect), and necrosis (high SI on T2-WI, no enhancement in the necrotic areas). Diffusion restriction occurs in metastases from mucinous tumors; conversely there is no diffusion restriction in necrotic areas of cystic metastatic lesions. Abscess, primary glial tumor, and radiation necrosis should be considered in the differential diagnosis. The origin of metastases is in decreasing order of frequency: lung > breast > skin (melanoma) > GIT & GUT. Lung cancer remains the most common source of brain metastases; 50% of lung tumor patients have CNS metastases. Breast carcinoma is the second most common source of intracranial tumors; 30% of breast carcinomas have associated CNS metastases. Malignant melanoma is the third most common tumor to involve the brain secondarily. Other primary tumors arise from the GIT and GUT.

2.6 Sella Turcica and Hypophysis

2.6.1 Introduction

The pituitary gland consists of two lobes that are physiologically and anatomically distinct: the anterior lobe (adenohypophysis) and the posterior lobe (neurohypophysis). Both are contained within the sella turcica.

The appearance of the pituitary gland depends on the age and the gender of the subject. In neonates (up to 2 months of age), the pituitary gland is normally very hyperintense on T1-WI (Fig. 2.34). It also appears larger than later in life. In adults, the adenohypophysis is isointense to cerebral white matter, whereas the neurohypophysis is hyperintense on sagittal T1-WI. The higher signal of the posterior lobe is believed to be caused by the presence of neurosecretory granules containing vasopressin. Absence of high signal can be associated with diabetes insipidus, but can also occur as a normal finding.

In men, the hypophysis is generally smaller than in women, with a maximum height of 6–8 mm. The pituitary gland decreases in size with aging. In pregnant women, the pituitary gland is spherical or upwardly convex. The anterior pituitary is enlarged, and the height may reach up to 12 mm. It may be hyperintense on precontrast T1-WI. Pituitary lesions

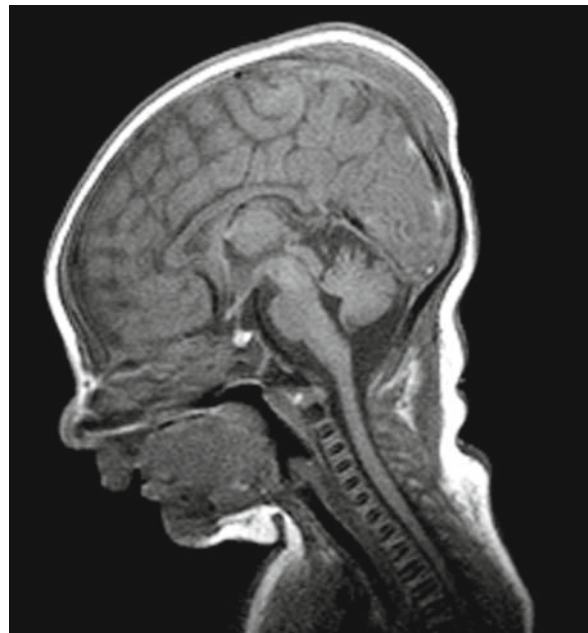


Fig. 2.34 In newborns, the pituitary gland is hyperintense on sagittal T1-WI. This is a normal finding up to the age of 2 months. The subcutaneous swelling in the parietal region represents a caput succedaneum

associated with pregnancy are lymphocytic adenohypophysitis and Sheehan's syndrome.

2.6.2 MRI Technique

The examination of the sella turcica and hypophysis places high demands on the MRI equipment and sequences. Because of the small volume of the pituitary gland, thin slices must be obtained (1–3 mm). In order to improve in-plane spatial resolution, a small FoV (<20 cm) and appropriate matrix (256 or higher) are recommended.

The close proximity of the air-filled sphenoid sinus constitutes an additional difficulty, because susceptibility artifacts may occur. Therefore, SE sequences are preferred; GRE sequences are generally avoided, except when operating at lower field strengths.

Presaturation pulses can be applied to eliminate phase-shift artifacts from the pulsatile arterial flow in the internal carotid arteries or venous flow in the superior sagittal sinus. For sagittal postgadolinium T1-WI, we routinely place an oblique coronal presaturation pulse

on the superior sagittal sinus to eliminate flow artifacts, which are more pronounced after contrast administration due to T1 shortening of the venous blood.

To improve the intrinsically lower SNR in mid- and low-field MRI units, SE sequences with a narrow bandwidth are often used. These sequences have a longer minimal TE value, and therefore, the number of slices (coverage) is lower. However, this is not a problem in pituitary imaging, since only a limited number of slices are needed to cover the area of interest. Another disadvantage is that sequences with narrow bandwidth increase chemical-shift artifacts. This may cause the fatty marrow of the dorsum sellae to overlap the high signal of the posterior pituitary on sagittal T1-WI; this artifact can be avoided by setting the read-out gradient in the anteroposterior direction, so that fat is shifted posteriorly. Similarly, on coronal images, the read-out gradient should be adjusted so that the fatty marrow of the sellar floor is shifted inferiorly. This technique ensures adequate visualization of the inferior part of the pituitary gland. Our standard imaging protocol is given in Table 2.14.

Following i.v. injection of Gd contrast agents, there is an immediate and intense enhancement of the pituitary stalk, adenohypophysis, and cavernous sinus. Enhancement is maximal after 1–3 min. The dynamic process of progressive enhancement of the pituitary gland can be visualized by using sequential T1-WI. In many institutions, dynamic imaging in the coronal plane has become part of the standard imaging protocol for pituitary adenoma. It is generally performed with a TSE T1-sequence, which is repeated every 20 s. Ideally, multiple slice locations should be imaged to completely cover the anterior pituitary lobe. GRE sequences are to be avoided because of the magnetic susceptibility artifacts caused by the air-containing sphenoid sinus.

Literature data suggest that for dynamic postcontrast pituitary imaging, a half dose of Gd may be sufficient (0.05 mmol/kg body weight). Moreover, a half dose of Gd improves contrast between the pituitary gland and the cavernous sinuses. However, when performing MRI of the pituitary at lower field strengths, we recommend a standard dose of Gd (0.1 mmol/kg body weight), because the T1-shortening effect of Gd is less pronounced.

For postcontrast images, magnetization transfer should not be used, because it further reduces the SNR of the thin-section, small-FoV images.

The protocol, as suggested in Table 2.14, should be adapted to the clinical demand. In children with

Table 2.14 Protocol for MRI of the pituitary gland

Sequence	Rationale
Coronal T1-WI	Baseline sequence
Sagittal T1-WI	Look for the signal intensity difference between adenohypophysis (isointense to white matter) and neurohypophysis (hyperintense)
Coronal T2-WI	Look for high signal abnormalities in the pituitary gland or adjacent structures (cavernous sinus, sphenoid sinus, ...)
Coronal DWI (trace images and ADC maps) (optional)	Useful in the preoperative evaluation of macroadenomas to assess the viscosity of the lesion
Intravenous contrast injection (half dose)	
Dynamic coronal T1-WI sequence	To assess the progressive enhancement which starts at the pituitary tuft and moves outward to the pituitary lobes
Coronal T1-WI	Look for adenomas, which in the early phase, enhance less intensely than normal pituitary tissue
Sagittal T1-WI	Look for thickening of the pituitary stalk, extension of lesion into the suprasellar cistern or sphenoid sinus

For pituitary gland imaging, high spatial resolution is required. This implies use of a small FoV (≤ 200 mm) with a 256 matrix. Alternatively, when a 512 matrix is used, the FoV can be somewhat larger. The key issue is pixel size. For the dynamic sequence, the FoV may need to be increased some what, to improve SNR. A limited number of slices is sufficient for a non-enlarged pituitary gland. In cases of pituitary macroadenoma, more slices should be obtained to cover the tumor. Slice thickness for the dynamic study may need to be increased to cover the whole mass. For the dynamic TSE coronal T1-W images, a high ETL increases the speed of the sequence, but also increases T2-W of the image, which is an unwanted effect. Therefore, a balance must be found between a short acquisition time (which requires a high ETL) and a sufficient number of T1-W images (which requires a shorter ETL)

growth-hormone-deficient dwarfism, the imaging protocol can be limited to precontrast sagittal and coronal SE T1-W sequences, which show an ectopic posterior pituitary lobe and absence of the stalk (Fig. 2.35). In patients with central diabetes insipidus, precontrast T1-WI demonstrates the absence of the posterior pituitary lobe high signal.

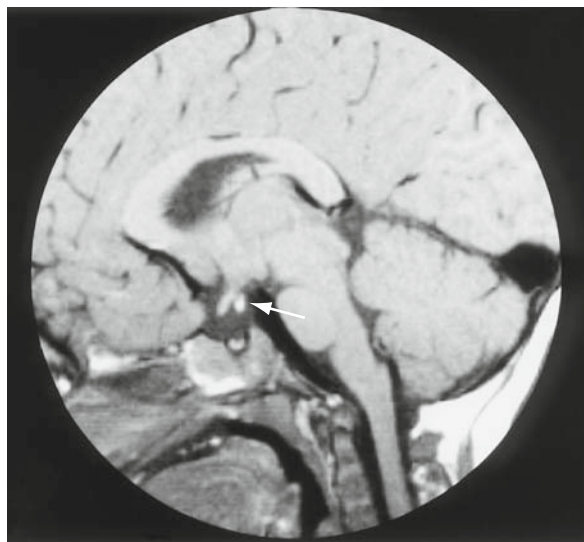


Fig. 2.35 Growth-hormone-deficient dwarfism. In this 3-year-old child with growth-hormone-deficient dwarfism, the sagittal SE T1-WI shows the ectopic posterior pituitary lobe as a focal area of high signal intensity at the proximal infundibulum (arrow). The pituitary stalk is absent. This example illustrates that precontrast sagittal SE T1-WI constitute an important part of the examination, especially in children and patients with diabetes insipidus

2.6.3 Pituitary Adenoma

Pituitary adenomas are benign, slow-growing neoplasms arising from the adenohypophysis. They represent 10–15% of all intracranial neoplasms and are the most frequent indication for pituitary MRI. On the basis of histology, pituitary adenomas are subdivided into

chromophobe (80%), acidophilic or eosinophilic (15%), and basophilic (5%) types. Alternatively, pituitary adenomas can be classified into functioning (prolactinoma, corticotrophic, and somatotrophic adenoma) or non-functioning lesions. An “incidentaloma” is defined as a nonfunctioning pituitary adenoma or pituitary cyst. However, there are no imaging features to distinguish between different types of adenomas. For medical imaging purposes, the most useful classification is to categorize pituitary adenomas by size into microadenoma (≤ 10 mm) or macroadenoma (>10 mm).

Microadenomas are by definition no larger than 10 mm in diameter. In many cases, MRI provides direct visualization of the adenoma. Typically, on precontrast or (early) postcontrast scans, the adenoma is seen as a small lesion of low SI relative to the normally enhancing pituitary gland (Fig. 2.36). This is due to the greater relative enhancement of normal pituitary tissue vs. adenoma. Adenomas display a later peak of enhancement, with slower washout. This implies that early postcontrast scans are required for lesion identification. On later postcontrast T1-WI, the adenoma may become isointense to normal pituitary tissue and may even become slightly hyperintense. Indirect signs of the presence of a pituitary adenoma include: focal depression or erosion of the sellar floor, displacement of the pituitary stalk, asymmetrical, focal upward convexity of the hypophysis, and invasion of the cavernous sinus.

By definition, *macroadenomas* are 10 mm or greater in size. Frequently, macroadenomas are nonsecretory. Clinical symptoms are caused by pressure on adjacent structures, especially the optic chiasm (Fig. 2.37). This

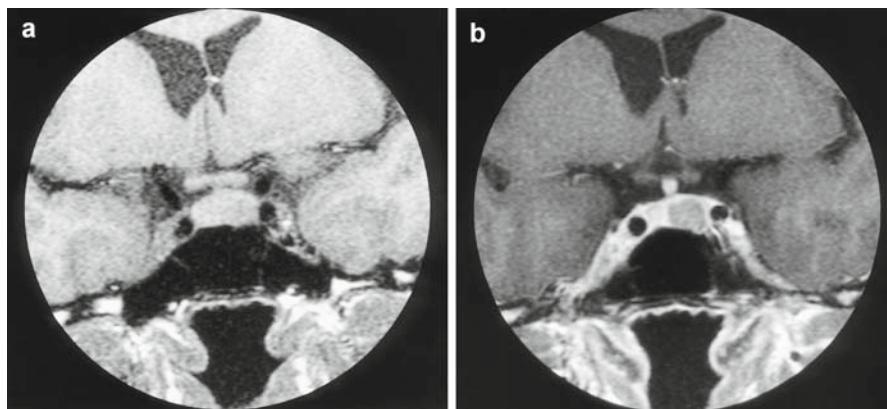
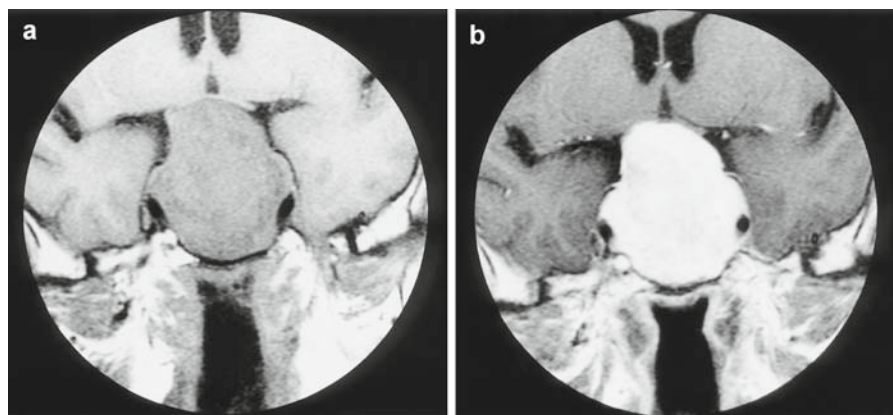


Fig. 2.36 Pituitary microadenoma. (a) Coronal SE T1-WI. (b) Coronal Gd-enhanced SE T1-WI. This 38-year-old woman had elevated serum prolactin levels. The precontrast image shows an asymmetry between the right and left pituitary lobes.

On the postcontrast image, the adenoma in the left pituitary lobe is outlined by the normally enhancing pituitary tissue. Thin slices with high spatial resolution are required

Fig. 2.37 Pituitary macroadenoma. (a) Coronal SE T1-WI. (b) Coronal Gd-enhanced SE T1-WI. This 45-year-old woman presented with progressive visual loss. The images show a typical pituitary macroadenoma. Note the upward displacement of the optic chiasm, which is draped over the top of the tumor. After Gd, the tumor enhances strongly but inhomogeneously



may lead to visual loss, most commonly bitemporal hemianopia. Compression of normal pituitary tissue may lead to hypopituitarism. The MRI technique is essentially the same, although more (or thicker) slices should be obtained to cover the tumor completely. On T1-WI and T2-WI, macroadenomas are usually iso-intense to brain tissue. They enhance with contrast; intratumoral cysts or areas of necrosis do not enhance and are hypointense on T1-WI and hyperintense on T2-WI. The use of Gd improves delineation of the mass, especially from the cavernous sinus. Many macroadenomas display enlargement and erosion of the sella, as well as extension into the suprasellar cistern, cavernous sinus, sphenoid sinus, and even the nasopharynx. On sagittal and coronal images, macroadenomas often display a dumbbell configuration, the “waistline” being caused by a constriction of the diaphragma sellae. Cavernous sinus invasion is common but difficult to ascertain on MRI. The most reliable sign is encasement of the internal carotid artery. The differential diagnosis includes suprasellar meningioma, pituitary metastasis, and craniopharyngioma. MRI allows reliable differentiation from an aneurysm. A recent development is the use of DWI in the preoperative assessment of macroadenomas. Signal intensities on DWI and ADC values provide an idea of the consistency of macroadenomas and are correlated with the percentage of collagen content at histologic examination. This is an important information for the neurosurgeon, when planning a transsphenoidal resection, to decide whether the tumor is “suckable” or not.

The appearance of a pituitary adenoma changes after treatment. Imaging findings after medical treatment (bromocriptine, cabergoline) include a decrease in the size of the adenoma, hemorrhage, and low SI on T2-WI. After transsphenoidal surgery, the following

can be observed: a defect in the anterior floor of the sella, fat and/or muscle plug, secondary empty sella, and herniation of the optic chiasm. After surgery via craniotomy, the FoV should be enlarged to study potential brain damage along the surgical approach route.

2.6.4 Other Intra-, Supra-, and Parasellar Lesions

Empty sella is defined as an extension of the subarachnoid space into the sella turcica. *Primary empty sella* can be due to a defect in the diaphragma sellae, involution of a pituitary tumor, or regression of the pituitary gland after pregnancy. *Secondary empty sella* is post-surgical in origin, presumably secondary to disruption of the diaphragma sellae. MRI shows an enlarged sella turcica, filled with CSF. The position of the optic chiasm is important to note; visual symptoms may occur if there is downward herniation of the optic chiasm.

Empty sella should be differentiated from a *suprasellar arachnoid cyst*, which is developmental in origin, due to an imperforate membrane of Lillequist. On MRI, a suprasellar arachnoid cyst appears as a well-margined, homogeneous lesion, which is iso-intense to CSF on all pulse sequences. In the differential diagnosis, epidermoid and craniopharyngioma should be considered.

Enlargement of the pituitary stalk, best seen on the coronal and sagittal postcontrast T1-WI, is a nonspecific finding. The differential diagnosis includes histiocytosis X, leptomeningeal carcinomatosis, metastasis, and granulomatous disorders (sarcoidosis, giant cell granuloma, tuberculosis, syphilis).

Craniopharyngiomas are slowly growing, benign tumors arising from epithelial remnants of Rathke's pouch. They represent 3–4% of all intracranial neoplasms and are the most common suprasellar mass lesions; 70% are both intra- and suprasellar, whereas 20% are entirely suprasellar. The age distribution is bimodal: the *adamantinomatous type* is encountered in children (first and second decades), whereas the *papillary type* occurs in adults (fourth and fifth decades). The pediatric craniopharyngioma (adamantinomatous type) is the most frequently occurring form. It typically contains cystic and solid components, and calcifications are frequent. It often invades the adjacent brain, leading to dense gliosis. Recurrence after surgery is common. The adult variety (papillary craniopharyngioma) is generally solid and often extends into the third ventricle.

Clinical symptoms are related to compression of the optic chiasm (bitemporal hemianopsia), hypothalamus, and pituitary gland (hypopituitarism, diabetes insipidus, and growth failure in children). Headaches may be secondary to hydrocephalus and increased intracranial pressure.

MRI typically shows a heterogeneous tumor with cystic and solid components. The cysts display variable SI on T1-WI, depending on their contents (cholesterol, protein, hemorrhage). Most frequently, the cysts are of higher SI than CSF on both T1-WI and T2-WI (Fig. 13.52). The solid components and the rim of cysts display enhancement with Gd. This is helpful in defining the extent of the lesion. Though essentially benign in nature, craniopharyngiomas have a tendency to recur after surgery, and Gd is useful in defining recurrent or residual tumor in the postoperative patient.

Calcifications, which occur in up to 80% of craniopharyngiomas in children (30–40% in adults) and are the hallmark of the lesion on plain skull films and CT, are difficult to detect on MR images. In theory, it would be useful to add a spoiled GRE T2*-WI sequence [fast low-angle shot sequence (FLASH), spoiled gradient recalled acquisition into steady state (GRASS), and fast-field echo sequence (FFE)] to the imaging protocol, to detect susceptibility effects from calcifications. Unfortunately, this sequence also brings out susceptibility artifacts due to air in the sphenoid sinus, and therefore, is of limited use.

Meningiomas occur in the suprasellar and parasellar region (sphenoid wing and cavernous sinus meningioma). They are usually slow growing but may compress vital structures. Meningiomas are isointense relative to gray

matter on T1-WI. On precontrast T1-WI, the sole clue to the diagnosis may be the presence of a dural or CSF cleft. Therefore, postGd images should always be obtained: meningiomas enhance intensely and homogeneously with Gd. A dural-tail sign is frequent: extension along the anterior margin/floor of the middle cranial fossa or along the tentorium. A meningioma arising from the planum sphenoidale may cause progressive expansion of the sphenoid sinus, a condition known as pneumosinus dilatans.

Optochiasmatic and hypothalamic gliomas are discussed together because the point of origin is often undeterminable. They account for 10–15% of all supratentorial tumors in childhood, with 75% occurring in the first decade (peak age 2–4 years). Histologically, most optochiasmatic-hypothalamic astrocytomas are of the pilocytic type. There is a strong association with neurofibromatosis type 1 in 20–50% of cases. Symptoms include vision loss, diencephalic syndrome, obesity, sexual precocity, and diabetes insipidus. MRI shows a suprasellar, lobulated mass with intense, but heterogeneous contrast enhancement. The presence of intratumoral cysts and areas of necrosis, as well as calcifications render the tumor inhomogeneous. Hydrocephalus is common, due to obstruction of the foramen of Monro by large tumors.

Germinoma is a highly malignant tumor with a predilection for the suprasellar and pineal region. If, in a child, an enhancing suprasellar lesion is discovered in conjunction with a pineal tumor, germinoma should be the primary diagnosis (Fig. 13.51). Germinoma is histologically similar to seminoma and is characterized by a rapid clinical evolution. It is also called "ectopic pinealoma." Germinoma enhances strongly with Gd, because of its highly vascular nature. CSF spread is common, and therefore, the entire neuraxis should be examined for staging and follow-up.

Tuber cinereum hamartoma is not a true neoplasm. It can be sessile or pedunculated and is attached to the hypothalamus between the pituitary stalk and the mamillary bodies. It typically causes precocious puberty. On MRI, the hamartoma is isointense to gray matter on all pulse sequences (Fig. 13.53). It does not enhance because it contains an intact BBB.

An *aneurysm* of the cavernous segment of ICA (extradural portion) must not be missed and should not be mistaken for a solid tumor. Cavernous sinus aneurysm may cause progressive visual impairment and cavernous sinus syndrome (trigeminal nerve pain and oculomotor nerve paralysis). MRI is helpful in showing

flow artifacts along the phase-encoding direction. The aneurysm is often of mixed SI and contains different stages of hemorrhage, thrombus, and calcifications.

An infrequent parasellar tumor is *trigeminal schwannoma*, arising from the Gasserian ganglion, in Meckel's cave. It is located in the middle cranial fossa, posterior cranial fossa, or both. On MRI, a dumbbell- or saddle-shaped mass of variable SI is seen. Enhancement is inhomogeneous due to necrosis and cyst formation in large tumors. The tumor may erode the petrous tip. Thin slices should be obtained to look for enlargement of contiguous fissures, foramina, and canals (extension into the infratemporal fossa through an enlarged foramen ovale).

2.7 Cerebrovascular Disease

2.7.1 Stroke

The term *stroke* refers to a sudden or rapid onset of a neurologic deficit (in a vascular territory) due to a cerebrovascular disease. If the neurologic dysfunction lasts for less than 24 h, the term *transient ischemic attack* (TIA) is used. A cerebral infarct that lasts longer than 24 h, but less than 72 h, is called a reversible ischemic neurologic deficit (RIND). Two major types of stroke can be discerned: ischemic and hemorrhagic stroke (Table 2.15). In this section, we shall focus on the role of MRI in ischemic stroke. Hemorrhage is covered in Chap. 1.2.8 and shall not be discussed here.

Stroke is a medical emergency and can cause permanent neurological damage, complications, and even death. The arrival of promising new aggressive therapies aimed at reestablishing the blood flow, reducing the size of the infarction, and protecting the surrounding brain at risk (penumbra) has changed the traditional role of neuroimaging. CT and MRI play a crucial role in the diagnosis, clinical management, and treatment monitoring of stroke. The narrow time window for thrombolytic therapy (up to 6 h after the onset of symptoms) necessitates a rapid and accurate diagnosis.

In a patient with acute stroke, the imaging protocol should be able to (Table 2.16):

- Rule out intracranial hemorrhage. Traditionally, CT has been the gold standard for detecting intracranial blood, but there is growing evidence that MRI with susceptibility imaging (e.g., gradient-echo T2* or

Table 2.15 Classification of stroke types

1. Ischemic stroke
1.1 Thrombotic stroke
1.1.1 Internal carotid artery disease
1.1.2 Vertebrobasilar disease
1.1.3 Lacunar infarcts
1.2 Embolic stroke (from cardiac or arterial source)
1.2.1 Middle cerebral artery and branches
1.2.2 Anterior cerebral artery
1.2.3 Posterior cerebral artery
1.2.4 Vertebrobasilar distribution
1.3 Hypercoagulable states (including veno-occlusive disease)
1.3.1 Primary (e.g., protein S/protein C deficiency, antithrombin III deficiency)
1.3.2 Secondary (e.g., antiphospholipid antibody syndrome, paraneoplastic)
2. Hemorrhagic stroke
2.1 Intracerebral hemorrhage (e.g., due to hypertension or amyloid angiopathy)
2.2 Subarachnoid hemorrhage
2.2.1 Aneurysm rupture
2.2.2 Arteriovenous malformation

SWI) may be equally valid, for example, in ruling out hemorrhagic infarction. FLAIR sequences have been shown to be highly sensitive and specific for the detection of acute subarachnoid and intraventricular blood. The role of MRI as compared to CT remains a matter of discussion.

- Show parenchymal injury. DWI can reveal regions of acute cerebral infarction within minutes after onset of symptoms.
- Provide information on tissue blood flow. Perfusion-weighted imaging (PWI) can identify areas of brain with decreased perfusion.
- Indicate areas of potentially salvageable brain tissue. It is generally accepted that, if the PWI deficit is larger than the DWI abnormality (diffusion-perfusion mismatch), there is brain tissue to be saved (penumbra), though there are exceptions to this theory.
- Assess vessel patency. Magnetic resonance angiography (MRA) can reveal vessel occlusion, narrowing, or intracranial stenoses.

Table 2.16 Protocol for MRI of acute stroke

Sequence	Rationale
Axial DWI (trace images and ADC maps)	to detect foci of diffusion restriction (cytotoxic edema)
Axial turbo FLAIR	to detect other signs of recent stroke (e.g., hyperintense vessel sign, subarachnoid or intraventricular hemorrhage) and to detect signs of preexisting cerebrovascular disease
MRA 3D-TOF through base of skull and circle of Willis	to detect occlusion of a major blood vessel
Axial T2-W sequence (single echo)	to assess white-matter hyperintensities in the brain, including the posterior fossa (where FLAIR is less sensitive)
Axial gradient echo T2* or SWI	to look for hemorrhage and blood breakdown products
EPI MR perfusion with bolus injection of contrast	to reveal CBF and CBV, and mismatch with DWI
Contrast-enhanced MR angiography	to look for occlusion of a major blood vessel

The diffusion-weighted EPI sequences are motion sensitive; therefore the patient should be instructed to keep perfectly still. It is important to immobilize the patient's head as much as possible. Scan time for these sequences is <30 s. The sequence parameters depend on the equipment used. For MR perfusion imaging, contrast medium should be injected as a very tight bolus, about 10 s after the start of the EPI sequence. A MR-compatible power injector is useful. When evaluating for hemorrhagic stroke, add a partial flip angle spoiled GRE sequence, because of its increased sensitivity in detecting susceptibility artifacts. To evaluate internal carotid artery dissection, add an axial SE T1-W sequence which includes the upper neck and the skull base

2.7.1.1 Large Vessel Infarction

Imaging manifestations of cerebral infarction caused by large vessel occlusion vary over time. We can consider four stages: hyperacute (0–6 h after symptom onset), acute (first 4 days), subacute (between 4 days and 8 weeks), and chronic (after 8 weeks).

Hyperacute and Acute Infarction

The pathophysiological changes induced by acute stroke should be understood to interpret the MRI findings. In normal circumstances, cerebral blood flow

(CBF) is approximately 50 mL/100 g/min; blood flow is higher in gray matter than in white matter. When CBF starts to decrease, vasodilatation occurs, and the brain attempts to compensate for the diminished blood supply by increasing the oxygen and glucose extraction fractions. A mild decrease in CBF interferes with protein synthesis. A moderate decrease in CBF causes glycolysis, with lactate accumulation and acidosis. With a more severe decrease in CBF (10–20 mL/100 g/min), the metabolic pathway of oxydative phosphorylation becomes compromised and the cellular energy supply starts to fail. Brain cells are no longer able to produce sufficient quantities of ATP to fuel the Na^+/K^+ -ATPase sodium-potassium pump. Active membrane transport becomes impaired, and failure of the sodium-potassium pump causes irreversible ion fluxes across the cell membrane. The loss of membrane integrity, and the ensuing ion fluxes, causes rapid swelling of cells; this is known as *cytotoxic edema*. The process of cytotoxic edema, once started, is irreversible and ultimately leads to cell death. The cascade of events leading to cytotoxic edema starts within minutes after the onset of an arterial stroke, and causes neurological dysfunction.

Vasogenic edema starts to occur several hours (2–6 h) after the onset of ischemia and is caused by injury to endothelial cells and disruption of the capillary tight junctions, with the breakdown of BBB. This results in an accumulation of plasma proteins and water in the extracellular space from the intravascular space. Vasogenic edema usually peaks around 3–4 days after the onset of infarction.

Conventional MRI techniques are of limited use in demonstrating hyperacute stroke (<12 h). On the other hand, diffusion-weighted MRI and perfusion MRI are very useful, and compete with CT for a role in the management of the patient presenting with an acute stroke.

DWI is an echo-planar imaging (EPI)-based technique that measures the random motion of water molecules (i.e., diffusion) in biological tissues during the application of strong magnetic field gradients. The sensitivity to diffusion is expressed by the “*b* value” of the sequence (in s/mm^2). The higher the *b* value, the more dephasing occurs, and the more heavily the signal reflects areas of restricted diffusion. In clinical practice, *b* values around 1,000 s/mm^2 are most commonly used.

Diffusion gradients are applied in (at least) three orthogonal directions. These images can be combined in a so-called “trace” image, which represents the sum

of the elements along the main diagonal of the 3 by 3 matrix, which is formed by applying individual diffusion gradients to the slice, read, and phase directions. In practice, the trace image represents a sort of mean of the individual images. In clinical practice, we obtain three images per anatomic slice position (Fig. 2.38):

- $b = 0$ image. This is merely a heavily T2-W EPI image, with the diffusion gradients switched off.
- $b = 1,000$ trace image. In regions of acute cerebral infarction (cytotoxic edema), diffusion of water is restricted, causing the lesion to appear bright on DWI.

- ADC maps. ADC maps are parametric images in which each pixel reflects the “ADC” at that location. Tissues in which water mobility is restricted appear dark on ADC maps (the ADC is lower in the infarcted lesion).

In case of a complete arterial occlusion, DWI can depict the lesion within minutes, due to the rapid onset of cytotoxic edema. The DWI lesion volume progressively increases up to day 3 or 4; this enlargement presumably reflects progressive infarction of the ischemic penumbra, as well as increasing edema. After 1 week, the volume of

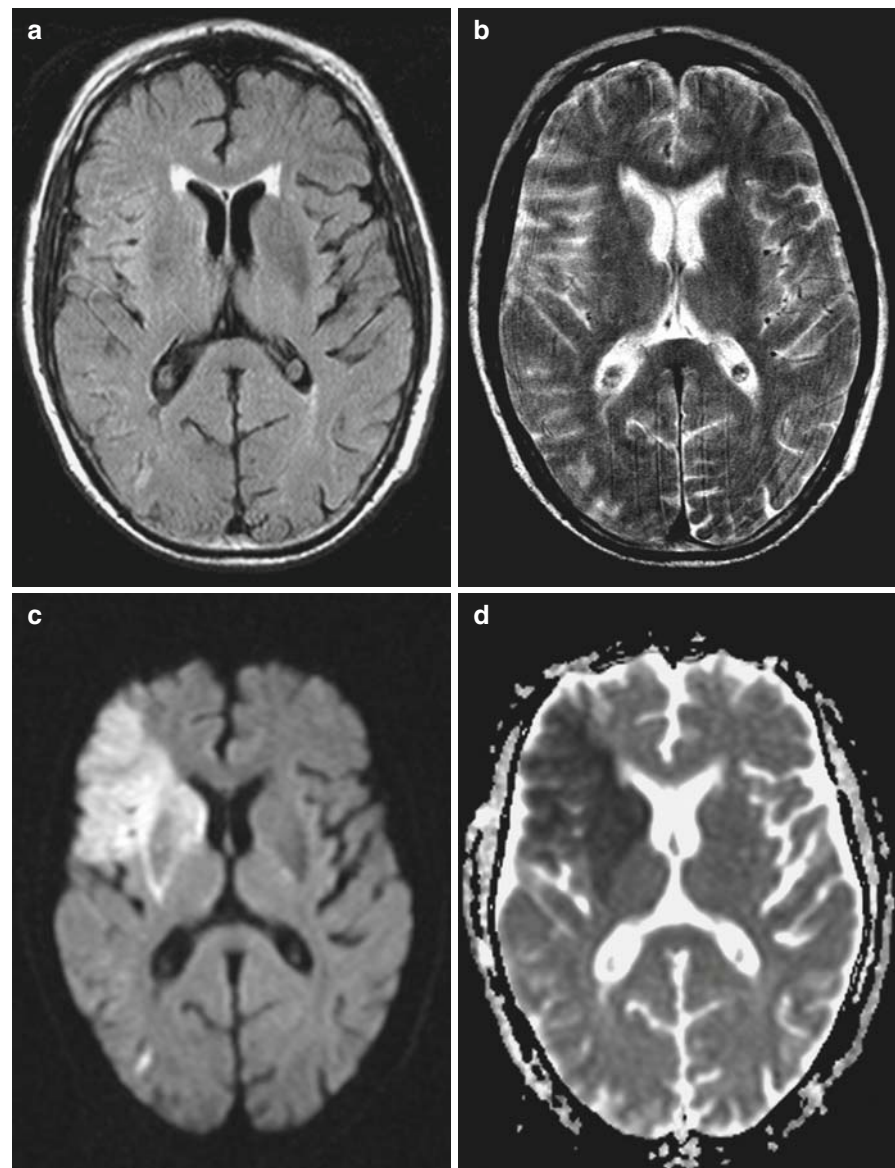


Fig. 2.38 Diffusion-weighted MRI in hyperacute infarction. The patient is a 71-year-old man examined within 2 h after acute onset of left hemiplegia and left facial nerve paralysis. **(a)** Axial turbo FLAIR image. **(b)** Axial TSE T2-WI. **(c)** Axial diffusion-weighted image (DWI), trace image. **(d)** Axial apparent diffusion coefficient map (ADC). The axial FLAIR and TSE T2-WI are within normal limits. Image quality is somewhat degraded by motion artifacts. The DWI shows a focal area of bright signal intensity in the right operculofrontal and sylvian region. On the ADC map, the area of restricted diffusion is confirmed as a hypointense lesion (decreased ADC). Signal abnormalities in the DWI and ADC maps indicate cytotoxic edema. The findings are consistent with hyperacute infarction of the right middle cerebral artery.

the DWI abnormality starts to decrease to a level approaching the T2-defined lesion on day 30. This is explained by the fact that, as cells die, cell membranes and other microstructures restricting diffusion disappear.

PWI can be performed using two basic approaches. In arterial spin labeling (ASL), hydrogen protons are labeled outside the head, and the flow of this *endogenous* contrast agent (i.e., tagged spins) through the brain is observed. There are two main approaches: continuous ASL and pulsed ASL. Despite recent technical advances and promising results, ASL is not yet widely used in clinical practice, because it suffers from poor SNR, requires longer imaging times, and can only be

applied at higher field strengths (3 T or higher). The currently more widespread approach uses injection of an *exogenous* contrast agent (Gd-based chelate) to act as a T2* contrast agent during its first pass through the cerebral vasculature. The contrast agent causes a transient decrease in SI (T2*-shortening susceptibility effect), proportional to the concentration in a given region (Fig. 2.39). The technique is known as *dynamic susceptibility contrast (DSC) imaging*. Using a rapid imaging sequence (typically EPI), as many as 50 sequential images can be obtained during bolus injection of contrast, covering a time interval of roughly 70 s. Bolus injection of contrast is performed 5–10 s after

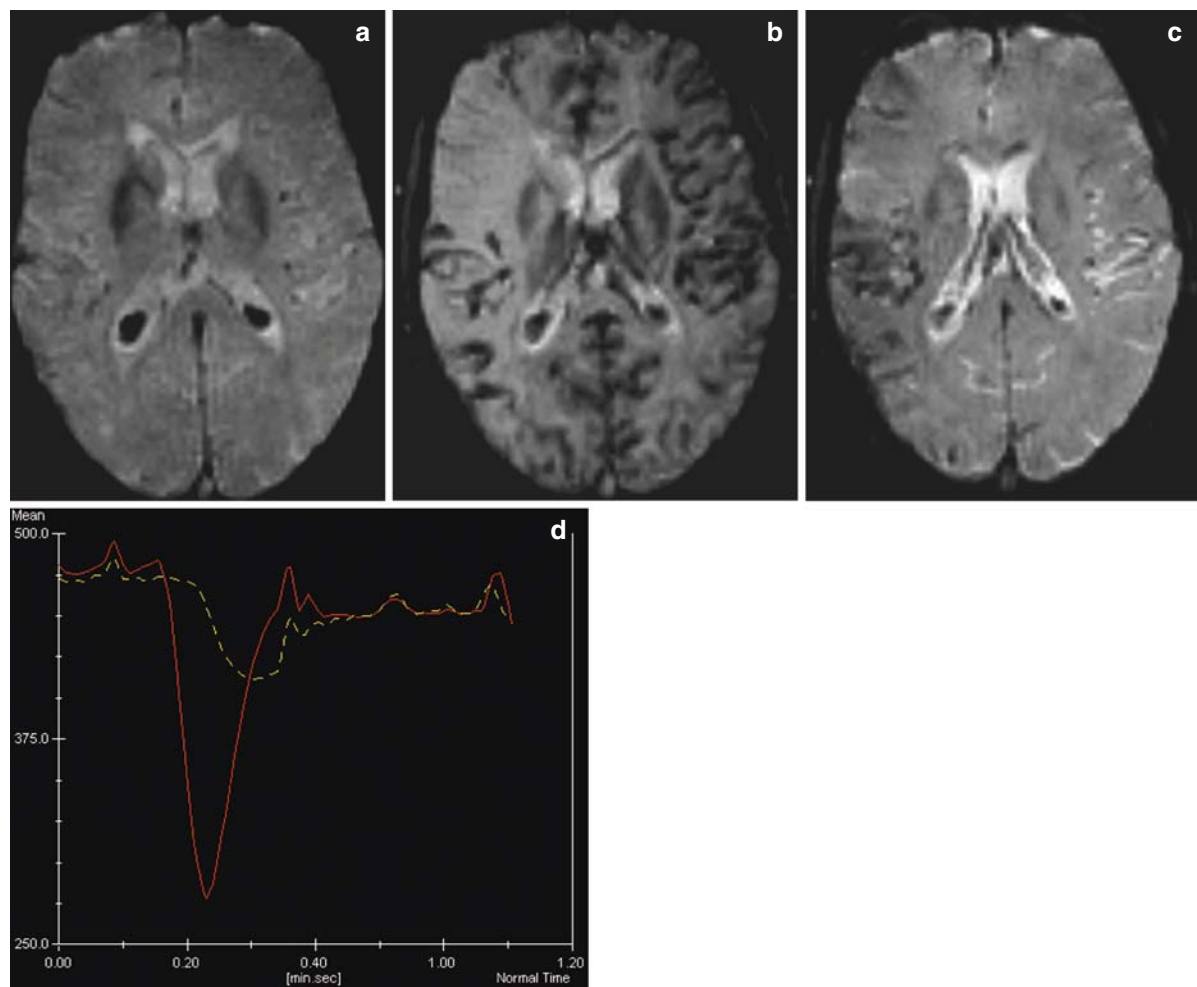


Fig. 2.39 Technique of perfusion-weighted imaging in a patient with hyperacute right middle cerebral artery stroke (same patient as Fig. 2.38). Fast EPI images are obtained during rapid intravenous injection of a contrast bolus (5 mL/s, antecubital vein, 18-gauge IV catheter). **(a)** Baseline image before arrival of the bolus. **(b)** Image during first pass of the contrast bolus. **(c)** Image

after passage of the bolus. **(d)** Time-intensity plot, covering 70 s. The first pass of the contrast agent through the cerebral vasculature causes a rapid and sharp decrease in signal intensity, which is due to a T2-shortening susceptibility effect. Specific regions-of-interest can be placed on the image to assess local differences in the bolus arrival time

the start of the imaging sequence, to ensure that an adequate number of baseline images are obtained. We inject a contrast volume of 0.2 mmol/kg body weight (i.e., 30 mL for a 75 kg person) at an injection rate of 5 mL/s (antecubital vein, 18-gauge i.v. catheter). This is followed by injection of 20–30 mL of saline, to flush the gadolinium out of the tubing, arm vein, and lung vasculature. When available, a power injector should be used, although with some experience, adequate results can be obtained also with hand injection (two syringes,

containing contrast and saline flush, connected to a bifurcated “Y” check valve system). Sequential images are acquired simultaneously in multiple slice positions. The EPI sequence that we currently use performs 50 chronological images in 12 slice positions, yielding to a total dataset of 600 images. If more slice positions are required, a slightly longer TR is needed, and this would negatively influence the quality of the sequence.

These images must then be processed in parameter maps such as Fig. 2.40:

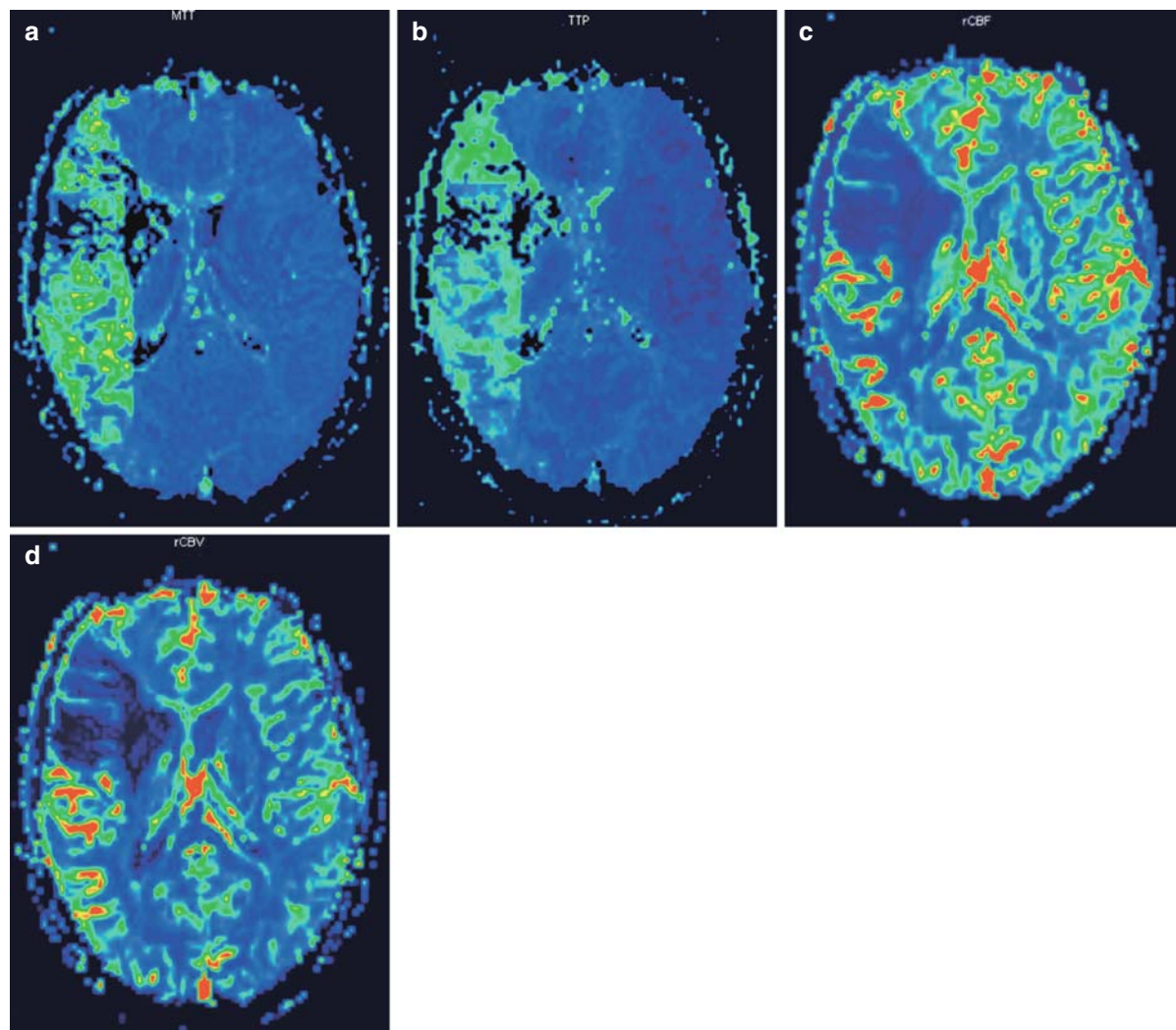


Fig. 2.40 Parametric maps generated by perfusion-weighted imaging (PWI) in a patient with hyperacute right middle cerebral artery stroke (same patient as Fig. 2.38 and 2.39). **(a)** Mean transit time (MTT) map. **(b)** Time to peak (TTP) map. **(c)** Regional cerebral blood flow (rCBF) map. **(d)** Regional cerebral blood volume (rCBV) map. The hypoperfused area corresponds

to the distribution territory of the right middle cerebral artery. The perfusion deficit is much larger than the diffusion abnormality (compare with Fig. 2.38c, d). This represents a diffusion-perfusion mismatch, and indicates potentially salvageable brain tissue (see text)

- Time to peak (TTP)
- Mean transit time (MTT)
- Cerebral blood volume (CBV)
- CBF, which can be calculated using the formula:

$$\text{CBF} = \text{CBV}/\text{MTT}$$

Perfusion MRI has been widely used in the setting of (hyper)acute (and subacute) stroke. However, with the arrival of multi-detector computed tomography (MDCT) scans, CT perfusion has become a valuable alternative to MR perfusion. In the diagnostic work-up of an acute stroke patient, many stroke centers start with a noncontrast CT (to rule out intracranial hemorrhage), followed by CT perfusion (to show the ischemic tissue and penumbra), and CT angiography (to reveal occlusion of a major blood vessel).

DWI/PWI Mismatch. In patients with (hyper)acute stroke, the volume of ischemic tissue documented by PWI is often greater than the region of parenchymal injury shown by DWI. In these patients, intravenous thrombolysis with recombinant tissue plasminogen activator (r-TPA) is of proven benefit within 3 h of symptom onset, and intra-arterial thrombolytic therapy shows promise within a 6-h window of therapeutic opportunity. The DWI/PWI mismatch has been considered as a possible correlate of the ischemic penumbra (i.e., tissue at greatest risk for infarct progression). The DWI abnormality reflects the area of brain tissue that is irretrievably lost (cytotoxic edema with cell death). The penumbra region indicates an area of decreased CBF, but the threshold for irreversible cell death has not yet been reached. Table 2.17 provides an overview of the theoretical possibilities and clinical implications of comparing PWI and DWI abnormalities.

Even without the use of such advanced techniques as diffusion and perfusion imaging, MRI is more sensitive than noncontrast CT in the detection of acute stroke. In the hyperacute and acute stages of a stroke, in addition to DWI, FLAIR is the most sensitive “conventional” imaging sequence. MRI findings of acute ischemic infarction include:

- Blurring of the gray–white matter interface on long TR images.
- Hyperintense swollen cortical gyri. These gyral areas of increased SI on FLAIR images indicate cytotoxic edema of brain parenchyma, which occurs more rapidly in gray matter than in white matter, due to its higher metabolic activity.

Table 2.17 Clinical implications of comparing perfusion-weighted imaging (PWI) and diffusion-weighted imaging (DWI) abnormalities

PWI and DWI findings	Clinical implication
Normal PWI and normal DWI	No stroke
Normal PWI and abnormal DWI	Early reperfusion (the DWI abnormality indicates some cytotoxic edema, but vessel patency has been restored, and PWI is normal)
Abnormal PWI and normal DWI	This situation can be found in chronic vessel stenosis. Alternatively, this could reflect a false-negative DWI
Abnormal DWI = abnormal PWI	Constituted stroke. The nonperfused brain has evolved to infarction with cytotoxic edema. The involved brain tissue is irretrievably lost, and there is no indication for thrombolysis
Abnormal PWI > abnormal DWI	Mismatch. The DWI abnormality (core infarct) surrounds the PWI deficit, reflecting the penumbra. In this case, there is a potential role for thrombolytic therapy to prevent the penumbra region from evolving to infarction

- Low-SI on T1-WI and high-SI on FLAIR images. The cortical hyperintensity of gyral infarcts may be masked on T2-WI due to the high signal of CSF in the cortical sulci.
- Hyperintense vessel sign. Arterial hyperintensity, most commonly observed in the middle cerebral artery on FLAIR, may reflect slow moving or stationary blood or intraluminal thrombus. The presence of the hyperintense vessel sign, together with abnormal findings on DWI, should prompt consideration of revascularization and flow augmentation strategies.
- Absence of normal signal void. MRI can detect the alteration in blood flow during acute ischemia immediately. High velocity blood flow is normally seen on MRI as an absence of signal. Absence of flow void indicates a significant compromise of arterial blood flow.
- Intravascular contrast enhancement. Enhancement of cortical arteries is often observed 1 or 3 days after the infarct, and most likely represents slow blood flow in collateral arteries, via leptomeningeal anastomoses.

- Meningeal enhancement, adjacent to the infarcted brain tissue, is a sign of meningeal inflammation. It usually appears in the subacute stage, after 1 to 7 days.
- Hyperintense intracranial hemorrhage or hemorrhagic transformation of an infarct (Fig. 2.41). FLAIR images are also useful in detecting hyperacute hemorrhagic lesions, including subarachnoid and intraventricular hemorrhage.
- MRA shows an occluded vessel.

Other later acute (1–3 days) findings include (Fig. 2.42):

- Sulcal effacement, gyral swelling, insular ribbon sign.
- Loss of gray-white matter distinction. The SI changes in infarction involve both white and gray matter. This is an important element in differentiating

infarct from tumor. The vasogenic edema associated with a brain tumor involves the white matter and tends to spare the gray matter.

- Increased SI of the brain parenchyma on FLAIR and T2-WI (due to increased water content), in a typical vascular distribution pattern.
- Mass effect (maximal 1–5 days after the event).
- Meningeal enhancement adjacent to the infarct.

In addition to the diffusion (and perfusion)-weighted sequences, the MRI protocol for a stroke patient should include a T1-WI sequence, a FLAIR sequence and/or a dual echo TSE sequence with PD-W and T2-W images, as well as an MRA sequence. Pay particular attention to the presence of normal signal void in all the *major* arteries, especially at the skull base. Use of i.v. contrast

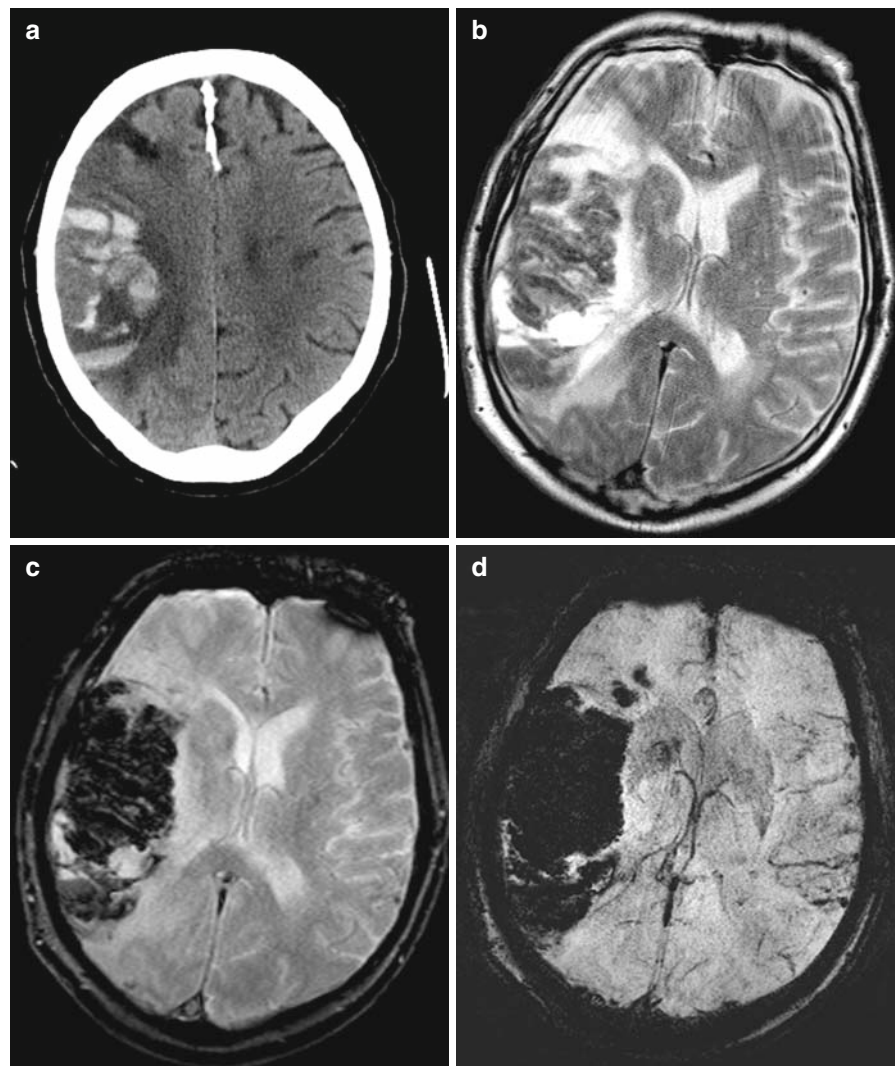
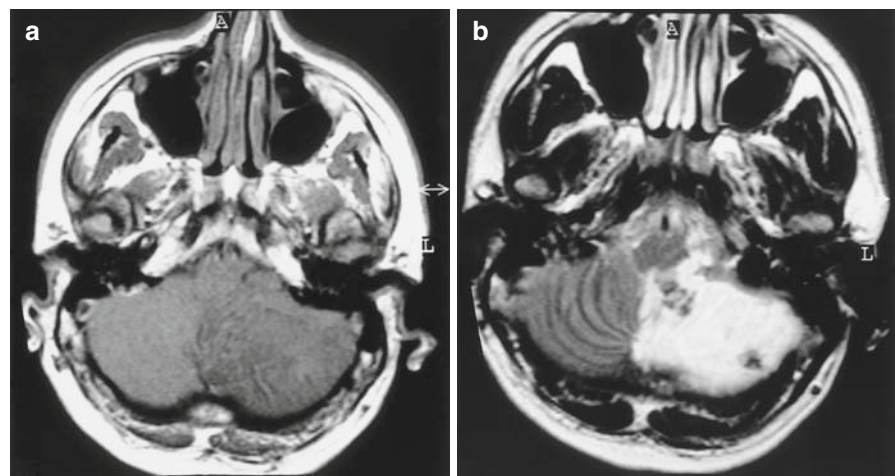


Fig. 2.41 Hemorrhagic transformation of right middle cerebral artery infarct. (a) Axial noncontrast CT scan. (b) Axial TSE T2-WI. (c) Axial gradient echo FLASH T2*-weighted image. (d) Axial susceptibility-weighted image (SWI). This 65-year-old man suffered a stroke involving the right middle cerebral artery distribution 4 days before. Noncontrast CT shows hemorrhagic transformation of the infarct (a). On T2-WI, the hemorrhagic infarct is hypointense, surrounded by a hyperintense halo of nonhemorrhagic infarction and edema (b). On T2* (c) and SWI (d), the involved area is markedly hypointense, due to susceptibility effects caused by blood breakdown products

Fig. 2.42 Cerebellar infarct in the distribution of the posterior inferior cerebellar artery (PICA). (a) Axial SE T1-WI. (b) Axial TSE T2-WI. The signal abnormality involves both gray and white matter in the distribution of the left PICA. The mass effect is limited compared with the size of the lesion. There are a few hemorrhagic components, which are isointense on T1-WI and hypointense on T2-WI (deoxyhemoglobin)



allows identification of the abnormal intravascular enhancement. Use of two different imaging planes facilitates identification of other acute findings. The sagittal plane is more useful as a second plane than the coronal plane for vertebrobasilar stroke. An MRI protocol for acute stroke is given in Table 2.16.

Accurate determination of the patency of the internal carotid artery can be difficult with conventional MRI. The presence of normal signal void in the carotid siphon does not exclude significant stenosis in the extracranial carotid artery. Isointense signal in the lumen may be due to either occlusion or high-grade stenosis with slow flow. With MRA, we can investigate both the carotid bifurcation and the intracranial circulation. This topic is covered elsewhere.

Subacute Infarction (Days to Weeks)

In the early subacute stage, the vasogenic edema becomes more prominent. The infarct is hyperintense on T2-WI and FLAIR, and hypointense on T1-WI. The high SI on diffusion-weighted “trace” images remains for 10–14 days, but the ADC values start to normalize a few days earlier (Fig. 2.43). The mass effect initially increases and then gradually diminishes. Although experimentally disruption of the BBB occurs 6 h after the onset of ischemia, parenchymal enhancement becomes visible only in subacute infarctions, because it requires reestablishment of a certain amount of blood supply. The parenchymal enhancement tends to follow a gyriform pattern (Fig. 2.44). Hemorrhagic changes are more frequently

observed (25%) than with CT. Therefore, it is useful to add a partial flip-angle gradient echo T2* or a SWI sequence, in order to detect hemorrhagic changes.

Chronic Infarction (Months to Years)

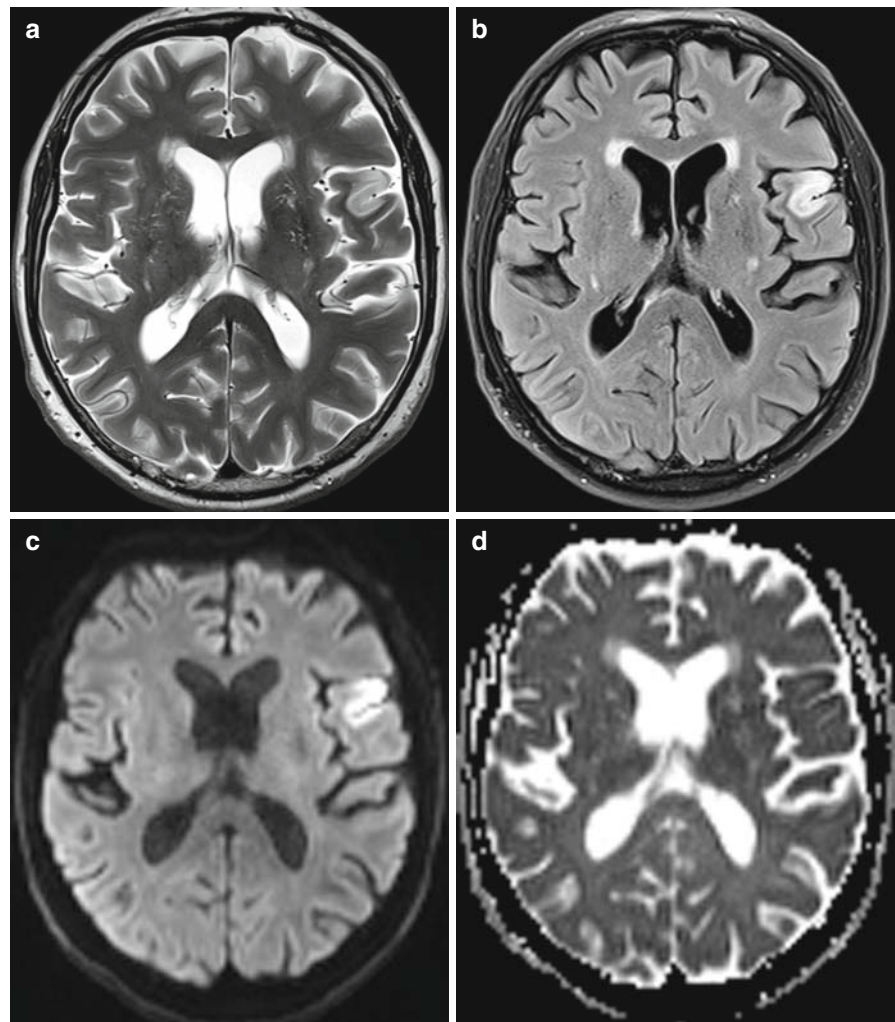
Prolonged ischemia causes irreversible brain damage. Tissue loss (negative mass effect), encephalomalacia, and replacement of tissue by CSF and/or gliosis are the causes of the SI abnormalities in this stage. Dilatation of the ipsilateral ventricle is common. The encephalomalacic area is sharply demarcated. Absence of normal flow void in major vessels in this stage indicates permanent vascular thrombosis. Wallerian degeneration of the corticospinal tracts can lead to volume loss of the ipsilateral cerebral peduncle and pons, and is due to antegrade degeneration of axons secondary to neural injury. Wallerian degeneration usually occurs as a late finding in old, large infarcts that involve the motor cortex (e.g., middle cerebral artery infarctions).

2.7.1.2 Small-Vessel Disease

Lacunar Infarct

The occlusion of small, penetrating end arteries arising from major cerebral arteries causes deep cerebral “lacunar” infarcts. The term “lacune” refers to a small area of cystic encephalomalacia. Lacunar infarcts account for 15–25% of all strokes, are most frequently

Fig. 2.43 Subacute infarction. **(a)** Axial TSE T2-WI. **(b)** Axial fat-sat turbo FLAIR. **(c)** Axial EPI diffusion-weighted “trace” image. **(d)** Apparent diffusion coefficient (ADC) map. This 70-year-old man presented 9 days before with acute motor aphasia. There is a cortical infarct involving the left inferior frontal gyrus, pars opercularis (Broca’s area). The infarction of the cortical gray matter is hyperintense on T2-WI **(a)** and FLAIR images **(b)**. There is marked hyperintensity on the diffusion-weighted scan **(c)** but ADC values have started to normalize, a normal finding after 9 days



associated with hypertension, and usually occur in late middle-aged or elderly individuals (>55 years of age). The most commonly involved locations are the basal ganglia (putamen, caudate), thalamus, internal capsule, and pons. This is because lacunar infarcts occur in the distal distribution of small penetrating vessels, such as the lenticulostriate arteries, recurrent artery of Heubner, thalamoperforating arteries, and pontine perforating arteries. If multiple lacunes are present, which is often the case, this is referred to as a lacunar state or “état lacunaire.”

In the acute stage, lacunar infarcts may be difficult to detect on standard MRI sequences, although DWI may show focal areas of diffusion restriction. Later, when they become associated with edema, they may be seen as hyperintense, small, rounded lesions on FLAIR and T2-WI. In the acute and

subacute phase, they may enhance following Gd-chelate administration, indicating disruption of the BBB. Older lacunar infarcts are isointense to CSF on all sequences, but they may be surrounded by hyperintense rim due to marginal gliosis (formation of scar tissue).

Subcortical Arteriosclerotic Leukoencephalopathy

Subcortical arteriosclerotic (leuko) encephalopathy (SAE) (also known as “leukoaraiosis” or “Binswanger’s disease”) is characterized by ischemia in the distribution territories of the poorly collateralized distal penetrating arteries. Hyperintense lesions are found on PD-WI, T2-WI, and FLAIR (Fig. 2.45). These signal

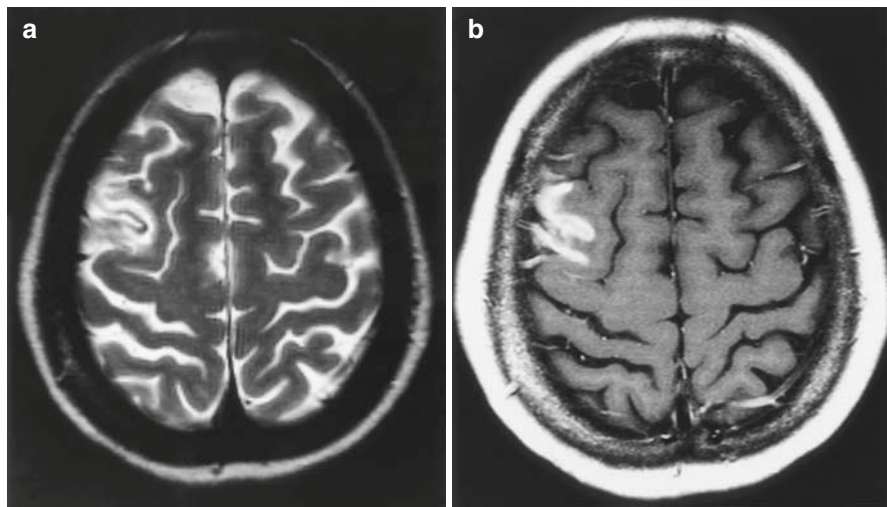


Fig. 2.44 Gyral enhancement in subacute right middle cerebral artery infarction. (a) Axial TSE T2-WI. (b) Gd-enhanced axial SE T1-WI. Two weeks prior to the present MRI examination, this 49-year-old woman suffered a stroke in the anterior part of the right middle cerebral artery distribution. The T2-WI shows

mildly increased signal intensity in the cortical-subcortical region of the right frontal lobe. After Gd injection, the typical gyriform enhancement is seen. This parenchymal enhancement denotes breakdown of the BBB

abnormalities occur in the periventricular white matter, centrum semiovale, basal ganglia, and subcortical “U”-fibers. The lesions may be focal, multifocal, or confluent and extend from the periventricular white matter to the subcortical region. The corpus callosum is usually spared (in contradistinction to MS, which typically involves the corpus callosum). The signal abnormalities of SAE reflect focal areas of demyelination and infarcts, as a result of microvascular arteriolar disease. SAE is a frequent finding in routine MRI, particularly in elderly people. There is a strong association with hypertension. No mass effect is present, and little or no abnormality is seen in the T1-WI. On the Fazekas Scale for scoring periventricular and deep white matter hyperintensities, SAE corresponds to grade 3 lesions: large confluent hyperintense areas in the deep white matter and irregular hyperintensities in the periventricular region.

In patients with chronic cerebrovascular disease, it is useful to add a T2*-WI and/or susceptibility-weighted sequence to the imaging protocol to look for punctuate hemosiderin deposits or so-called “micro-bleeds.” They are commonly found in patients with hypertension or amyloid angiopathy. SWI is the preferred technique for the detection of micro-bleeds, since it shows more lesions than T2*-WI (Fig. 2.46).

Normal Hyperintense Areas in the T2-WI

Lacunar infarcts and SAE must be distinguished from normal and age-related areas of hyperintense signal on FLAIR and T2-WI. They include:

- Areas of late myelination in the deep parieto-occipital white matter, adjacent to the ventricular trigone
- Focal breakdown of the ependymal lining with periventricular hyperintense signal anterolateral to the frontal horns (“ependymitis granularis”)
- Decreased myelination in posterior internal capsule
- Perivascular spaces of Virchow-Robin

2.7.1.3 Acute Hypertensive Encephalopathy

Acute hypertensive encephalopathy, perhaps more commonly known as posterior reversible encephalopathy syndrome (PRES) is a disorder of cerebrovascular autoregulation associated with hypertension. Patients usually present with headache, seizures, visual field deficits, and altered mental status. There are many precipitating factors including, abrupt elevation of blood pressure, (pre)eclampsia, renal decompensation, fluid retention, and immunosuppressive drug toxicity

Fig. 2.45 Subcortical arteriosclerotic leukoencephalopathy and micro-bleeds. (a, b) Axial TSE T2-WI. (c, d) Axial fat-sat turbo FLAIR. (e) Axial gradient-echo FLASH T2*-WI. (f) Axial susceptibility-weighted image (SWI). The patient is a 76-year-old man with hypertension. In both cerebral hemispheres, there are confluent hyperintense areas in the deep white matter and centrum semiovale and irregular multifocal hyperintensities in the basal ganglia. These signal abnormalities reflect focal areas of demyelination and infarcts, as a result of microvascular arteriolar disease. The T2* and SWI images show micro-bleeds, which are not visible on the other sequences

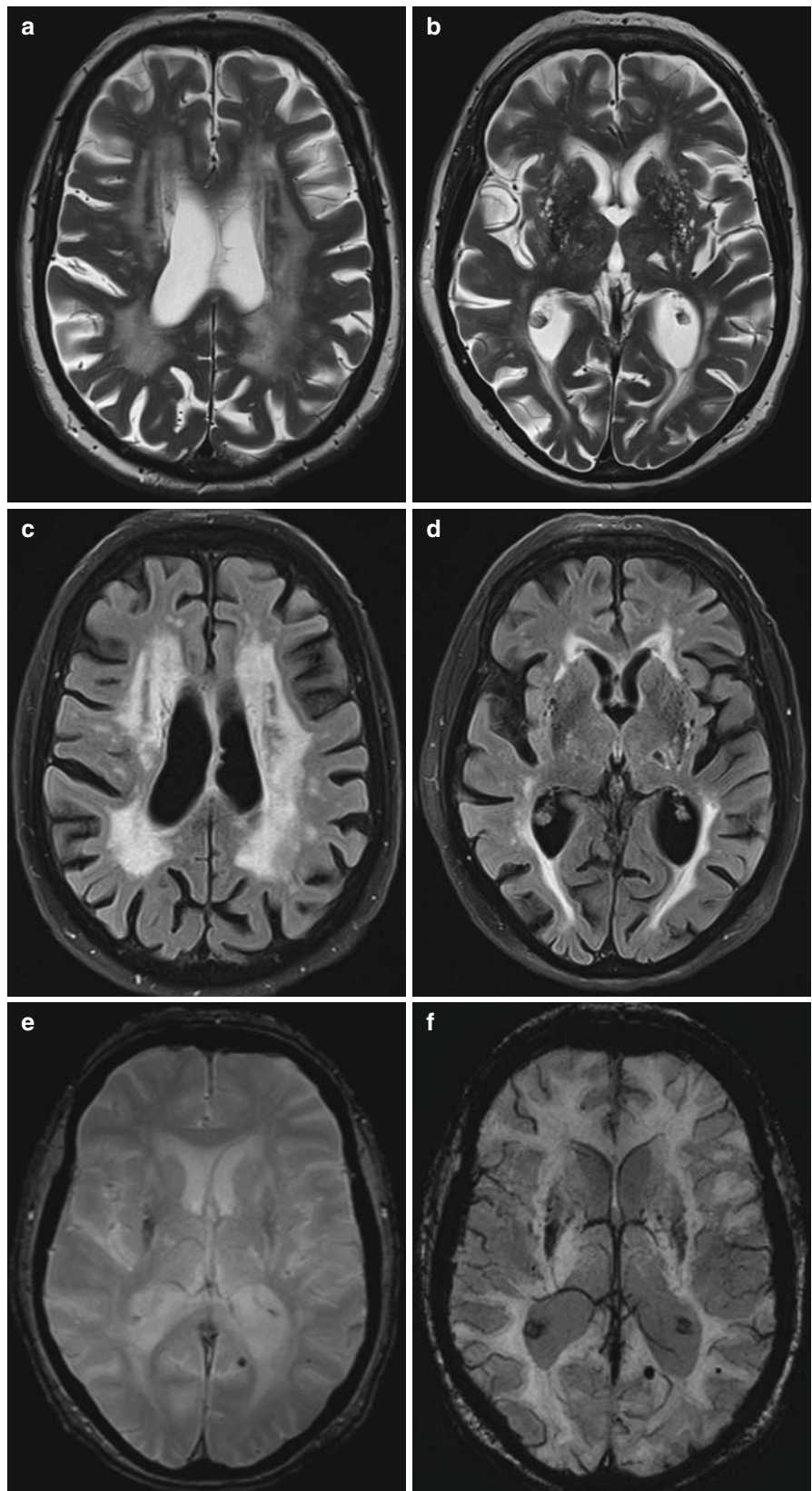
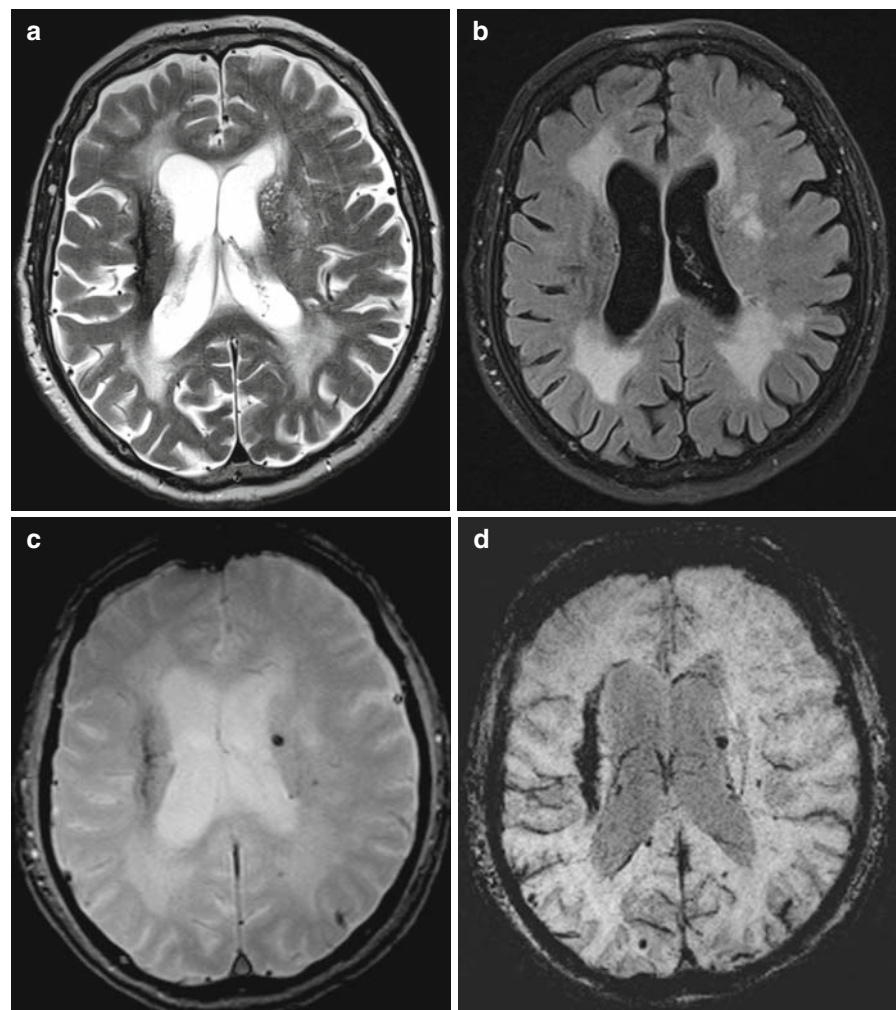


Fig. 2.46 SWI is superior to T2* in the detection of microbleeds. (a) Axial TSE T2-WI. (b) Axial fat-sat turbo FLAIR. (c) Axial gradient-echo FLASH T2*-WI. (d) Axial susceptibility-weighted image (SWI). This 73-year-old man has a history of long-standing arterial hypertension. Axial TSE-T2 (a) and FLAIR (b) show patchy hyperintensities involving the deep white matter in a pattern consistent with subcortical arteriosclerotic leukoencephalopathy. On T2*-WI (C) and SWI, multiple punctate hyperintensities are seen, consistent with microbleeds in the setting of amyloid angiopathy, as well as a large area of hemosiderin deposition in the right putamen (the patient had suffered a putaminal hemorrhage several years earlier). SWI shows more microbleeds than T2*-WI



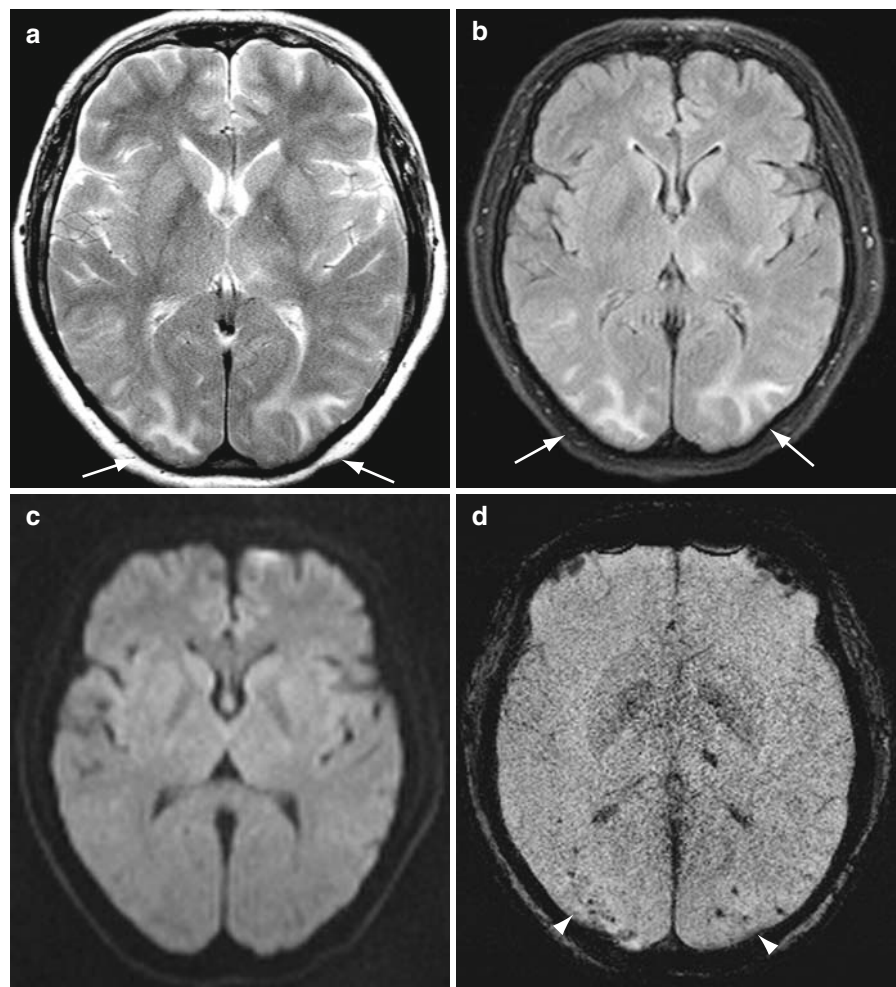
(especially cyclosporin). Hypertension is a common component and causes disruption of the BBB in the posterior circulation.

On MRI, the most typical findings are patchy, cortical and subcortical hyperintensities on T2 and FLAIR images in the posterior cerebral artery distribution territory (Fig. 2.47). The cerebellum may also be involved. There is no diffusion restriction, because the hyperintense signal abnormalities in PRES are caused by vasogenic (not cytotoxic) edema (due to damage of the vascular endothelium by hypertension) and are not due to cytotoxic edema (as in acute arterial infarction). PRES is a “must-not-miss” diagnosis because the condition is potentially life threatening; most cases resolve with aggressive therapy to normalize blood pressure and withdrawal of the drug producing the symptoms.

2.7.2 Subarachnoid Hemorrhage

CT remains the preferred imaging method for the detection of acute subarachnoid hemorrhage (SAH). On MRI, the diagnosis of subarachnoid and intraventricular hemorrhage relies on FLAIR imaging; in FLAIR, the SI of CSF is suppressed, and blood is seen as hyperintense. There is good evidence that FLAIR imaging is equally sensitive as CT for detection of SAH; other reports indicate that small amounts of SAH may be missed on MRI. The higher oxygen tension of the CSF in the subarachnoid space slows the transformation of oxyhemoglobin to paramagnetic breakdown products such as deoxyhemoglobin and methemoglobin. Additionally, pulsatile CSF flow tends to dilute and disperse the red blood cells.

Fig. 2.47 Posterior reversible encephalopathy syndrome (PRES) (arrows). (a) Axial TSE T2-WI. (b) Axial fat-sat turbo FLAIR. (c) Axial EPI diffusion-weighted “trace” image (DWI). (d) Axial susceptibility-weighted image (SWI). This 62-year-old woman was admitted with headache, vomiting, and visual field disturbances, associated with an acute hypertensive attack. Axial T2 (a) and FLAIR (b) images show foci of high signal intensity involving the cortex and subcortical white matter of both occipital lobes. There is no diffusion restriction (c), since PRES is associated with vasogenic edema and not cytotoxic edema. The SWI (d) shows hypointense punctate hemorrhagic foci. The patient recovered after aggressive antihypertensive therapy (arrowheads)



Repeated episodes of SAH may cause ferritin and hemosiderin deposition on the leptomeninges covering the brain. This condition is known as superficial siderosis. On T2-WI or T2*-WI MRI, superficial siderosis is seen as a hypointense line along the surface of the brain, especially the pons, mesencephalon, and cerebellar vermis.

In the postoperative follow-up of a patient after aneurysm clipping or after endovascular coiling, MRI is useful because the clip/coil causes fewer artifacts on MRI than on CT. Most aneurysm clips currently used are composed of nonferromagnetic material. However, in the past, many patients have undergone aneurysm clipping with ferromagnetic clips. There is a danger of fatal intracranial hemorrhage after movement of a ferromagnetic aneurysm clip in a MRI unit. Never scan a patient with an aneurysm clip without identifying the exact type of the clip! Contrast-enhanced MRA is the

preferred imaging technique in the follow-up of patients after endovascular coiling or clipping of aneurysms.

2.7.3 Dural Sinus and Cerebral Vein Thrombosis

Thrombosis of a dural sinus (or cerebral vein) is a serious, and in some cases, potentially lethal condition. The clinical presentation is often confusing and non-specific, and the radiologist may be the first to suggest the diagnosis to the clinicians. The goal of neuroradiologic examination is twofold: (1) to prove the existence of a thrombosis and (2) to evaluate the intracranial damage caused by the thrombosis. MRI is the method of choice for both of these tasks.

2.7.3.1 Identification of a Thrombosed Sinus or Vein by MRI

The superior sagittal sinus is the most common site of dural sinus thrombosis, followed by the transverse sinus, sigmoid sinus, and cavernous sinus. Deep cerebral vein thrombosis is less common, but even more dangerous. Cortical vein occlusion usually occurs in association with dural sinus thrombosis, though it can occur as an isolated finding.

There are several methods of identifying an occlusion of a dural sinus by MRI:

1. Conventional MRI: careful interpretation of the SI within the lumen of the venous sinus may indicate whether it corresponds to flow or thrombosis. Thrombosis of a dural venous sinus can be detected as an intravascular area of high SI on T1-WI (Fig. 2.48) or FLAIR.

2. MR venography which can either be performed with a phase-contrast technique (Fig. 2.49) or time-of-flight (TOF) MRA (“slow flow” technique or magnetic resonance “venography”).

Conventional MRI is unreliable. In practice, it is sometimes difficult to decide whether the intraluminal signal within a dural sinus or cerebral vein corresponds to flow or to thrombosis. The SI of a clot varies with its age. An acute clot is isointense to gray matter on T1-WI (and therefore easily missed) and hypointense on T2-WI. A subacute clot becomes hyperintense on both T1-WI and T2-WI; this corresponds to the formation of extracellular methemoglobin. However, in the intermediate stage, the clot can be hypointense on T2-WI (due to intracellular methemoglobin) and thus mimic normal flow void in a patent dural sinus. The SI of normal flow in a sinus is also variable. Instead of flow void, a high signal may be observed on T1-WI because of an entry

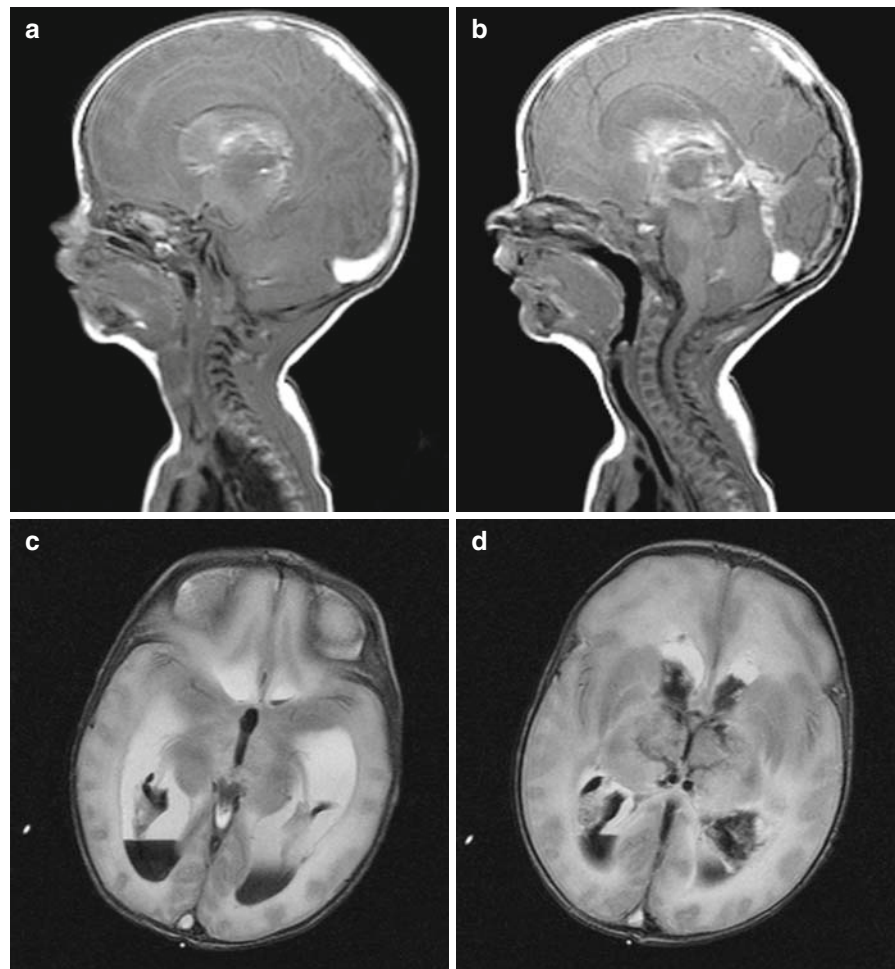


Fig. 2.48 Thrombosis of the cerebral veins and sinuses. (a, b) Sagittal TSE T1-WI. (c, d) Axial TSE T2-WI. This newborn baby boy presented with seizures and neurologic deficits. Sagittal T1-WI show complete sinovenous thrombosis involving the dural sinuses (superior sagittal sinus, torcular, transverse, and sigmoid sinus), but also the deep venous system (sinus rectus, great cerebral vein, internal cerebral veins). Axial T2-WI reveal venous infarctions in the thalamus and diencephalic structures. There is intraventricular blood (with hemorrhagic sedimentation layers). The child expired after a few days

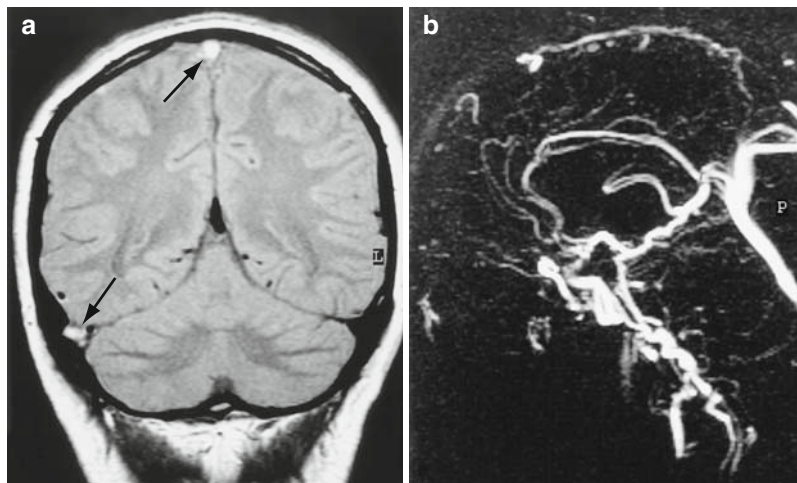


Fig. 2.49 Thrombosis of the superior sagittal and right transverse sinus. (a) Coronal SE PD-WI. (b) MIP reconstruction of a phase-contrast MR angiography (MRA) (sagittal view). On the coronal PD-WI, the signal within the lumen of the superior sagittal and right transverse sinus is hyperintense (*arrows*). The intraluminal

signal intensity was also high on the T1-WI and T2-WI (not shown). This signal-intensity behavior is consistent with a blood clot (extracellular methemoglobin). The phase-contrast MRA image reveals an absence of flow within the superior sagittal sinus, thereby confirming the diagnosis of thrombosis

slice phenomenon, in-plane flow, or slow flow. In T2-WI, the luminal signal can be high because of even-echo rephasing or slow in-plane flow, accentuated by flow compensation techniques. Wall enhancement of the thrombosed sinus or enhancement of the intraluminal thrombus may further confound the issue.

MR venography is the preferred technique for the detection of dural sinus or cerebral vein thrombosis. MR venography can be performed with slow flow TOF MRA, (e.g., oblique coronal 2D TOF (2D FLASH) with saturation of arterial inflow) or with phase-contrast MRA (e.g., single-slab phase-contrast angiography). A more detailed discussion of MRA techniques can be found in Chap. 1. Yet, even these techniques are not fool-proof, since a hyperintense thrombus on T1-WI can simulate flow-related enhancement on a slow-flow TOF (due to the T1-shortening effect).

2.7.3.2 Evaluation of the Intracranial Damage

Dural sinus and cerebral vein thrombosis can cause intracranial hypertension, hydrocephalus, venous infarction, and hemorrhage. MRI may show swelling of the brain with mass effect and sulcal effacement. On T2-WI, hyperintense lesions, not corresponding to an arterial territory may be found; they are frequently bilateral or involve more than one vascular distribution. Hemorrhagic

transformation of these venous infarcts is common. Parasagittal hemorrhages are highly specific for superior sinus thrombosis, and are secondary to cortical venous infarction. As a general rule, venous infarctions do not exhibit diffusion restriction; this is because, in the early phase, venous occlusion causes vasogenic edema unlike an arterial infarction which causes cytotoxic edema. After contrast injection, prominent venous enhancement in dilated cortical veins and collaterals is observed.

2.7.4 Vascular Malformations

2.7.4.1 Classification

The four archetypal vascular malformations are (1) AVM, (2) capillary telangiectasia, (3) cavernous angioma, and (4) developmental venous anomaly (venous angioma). The latter is considered an anatomic variant and not a true malformation.

2.7.4.2 Arteriovenous Malformation

AVMs are congenital disorders. The angioarchitecture of an AVM consists of one or more enlarged feeding arteries, a tangled collection of blood vessels (the nidus), and

a tortuous assortment of dilated draining veins. AVMs are a cause of intracerebral hemorrhage; they are also associated with headaches, ischemic or hemorrhagic infarctions, or SAH. The MRI examination is complementary to cerebral angiography for treatment planning. It must identify:

- Number, location, and course of the feeding arteries
- Exact delineation of the nidus
- Location of the draining veins
- Aneurysms or dilated blood vessels
- Parenchymal damage, atrophy
- Presence of hemorrhage and its relationship to the nidus

An important target of the MRI protocol is the accurate anatomic definition of the nidus and its relationship to vital cerebral structures. Therefore, the MRI examination has to include images in three imaging planes (axial, coronal, and sagittal), eventually supplemented by MRA. In at least one imaging plane, T1-WI and T2-WI should be performed. MRI findings in the typical case are:

- Multiple round, linear, or serpiginous areas of signal void (Fig. 2.50)
- Little or no mass effect in the absence of recent bleeding
- Atrophy of the surrounding brain, gliosis
- Absence of brain tissue inside the nidus

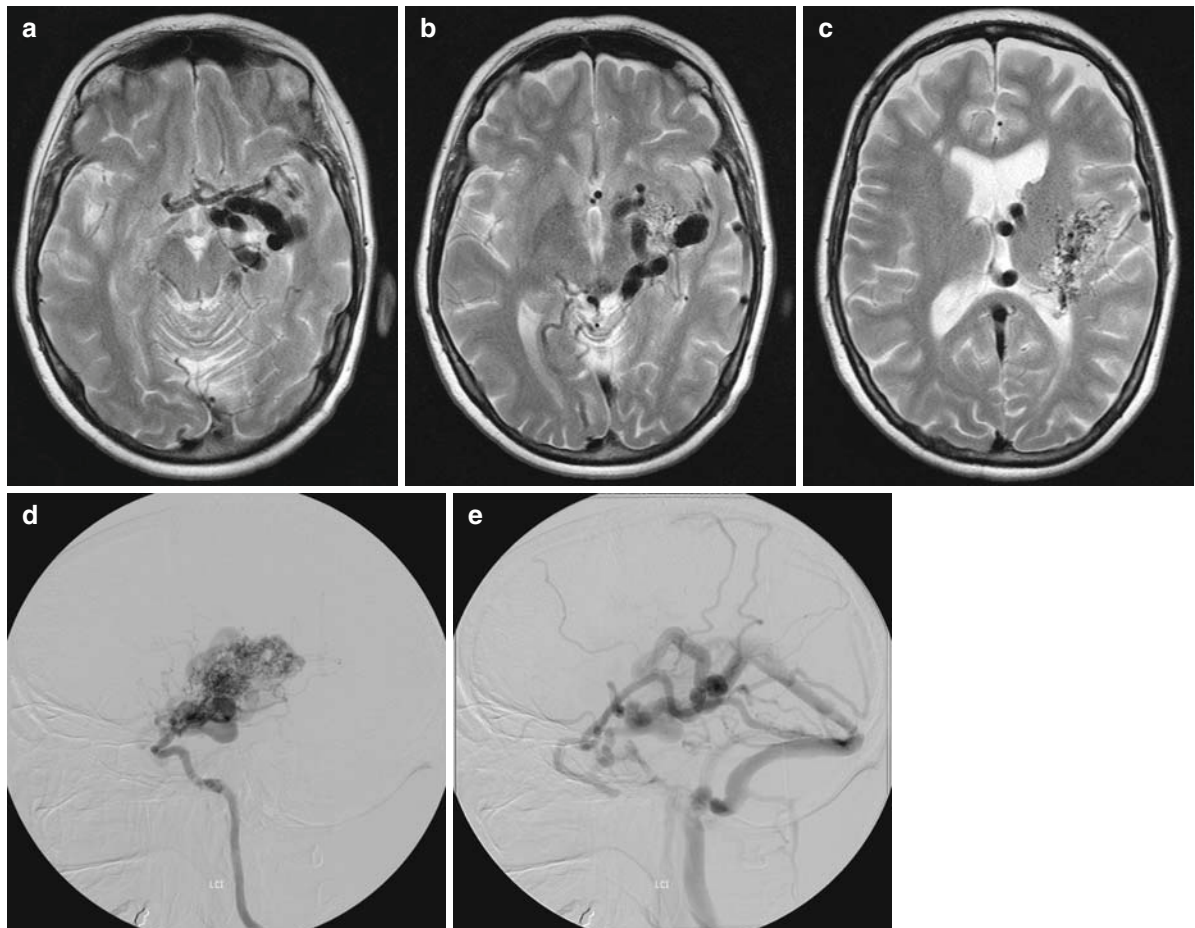


Fig. 2.50 Arterio-venous malformation. (a–c) Axial TSE T2-WI. (c, d) Cerebral angiography, left internal carotid artery injection, lateral view, late arterial phase (d) and venous phase (e). This 50-year-old woman has a high-flow arteriovenous malformation in the left subinsular/basal ganglia region. The drain-

ing veins are hypointense on the axial T2-WI (a–c), reflecting their high flow speed. Despite the size of the malformation and the large caliber of the draining veins, there is no mass effect, nor perilesional edema (and this is a typical feature of AVMs, unless there has been a hemorrhagic episode)

2.7.4.3 Capillary Telangiectasia

Capillary telangiectasias are vascular malformations which are composed of dilated capillaries with interposed normal brain parenchyma. They are the second most common vascular malformation (second only to venous developmental anomalies). At autopsy, they are frequently found as multiple lesions. The brainstem, especially the pons, is the most typical location, but capillary telangiectasias can also be found in the cerebellum, spinal cord, and supratentorially. Most of these lesions are clinically silent and are incidentally discovered on imaging studies. Capillary telangiectasias are invisible on cerebral angiography. On Gd-enhanced MR images, the so-called “racemose” type of capillary telangiectasia may be seen as a region of mild, stippled contrast enhancement. The “cavernous” type presents as hypointense lesions on SWI or T2*-WI, indicating evidence of old hemorrhage with hemosiderin deposition.

2.7.4.4 Cavernous Malformation (*Syn. Cavernous Hemangioma*)

Cavernous malformations occur in the brain and the spinal cord. The most frequent location is in the cerebral hemispheres, though they also occur in the brainstem. Sporadic and familial forms are possible. Lesions are frequently multiple (20–30%), with a familial pattern in 10–15% of the patients. Cavernous malformations may be asymptomatic. When symptomatic, their clinical presentation consists of seizures, headache, hemorrhage, and progressive neurological deficit.

Histopathologically, a cavernous malformation has three components: sinusoidal vascular spaces lined by a single layer of endothelial cells, fibrous septa with calcifications, and a peripheral component of gliotic hemosiderin-laden tissue. There is no brain parenchyma within the lesion. The flow is very slow or absent, with frequent intravascular thrombosis.

Noncontrast CT demonstrates cavernous angiomas as small, rounded, dense foci, often with associated calcification. However, MRI is more sensitive and more specific, due to its sensitivity to old blood-breakdown products.

In a typical cavernous angioma, MRI findings are:

- A well-delineated lesion, often with a high SI on T1-W images
- Reticulated “pop-corn” appearance; heterogeneous SI represents blood products of different age; hypointense signal areas (due to blood-breakdown products such as hemosiderin) are more prominent on T2-W and GRE images (Fig. 2.2)
- Peripheral closed rim of hemosiderin
- No flow; no arterial feeders, no draining veins
- No mass effect and no perifocal edema, unless a recent episode of bleeding has occurred

The MRI protocol should contain pulse sequences sensitive for old blood products (hemosiderin). The TSE sequence is insensitive and may miss the lesions. Susceptibility-weighted imaging (SWI) is the most sensitive sequence for detection of small, punctate cavernous malformations. The second choice is a spoiled partial flip-angle T2*-weighted GRE (Fig. 2.51).

2.7.4.5 Developmental Venous Anomaly

Developmental venous anomalies (DVAs; also known as “venous malformation” or “venous angioma”) are believed to represent an anatomic variant of the normal venous drainage pattern, and not a true malformation. Most often, they are discovered as an incidental finding. DVAs do not contain an arterial or capillary component. They consist of small tributary veins that drain into an enlarged venous channel. On T1-WI, they are seen as linear or curvilinear flow voids, often perpendicular to the cortex or the ventricular wall. On T2-WI, their SI is variable, depending on the direction and speed of flow, as well as technical factors, such as the entry phenomenon. After Gd injection, the small tributary veins enhance in a stellate fashion, often presenting the shape of a caput medusae (Fig. 2.52). Developmental venous anomalies are difficult to detect on precontrast images, and up to one-third are discovered only after an injection of Gd. Alternatively, susceptibility-weighted images (SWI) can be used to detect abnormalities of venous drainage, for example in Sturge–Weber syndrome (Fig. 2.53). The SWI sequence is very sensitive to veins because they contain paramagnetic deoxyhemoglobin. Therefore, SWI should constitute an important part of any neuroimaging protocol to reveal microarchitecture of neurovascular diseases.

Fig. 2.51 Multiple cavernous hemangiomas. (a) Axial TSE T2-WI. (b) Axial GRE image. In this patient with multiple cavernous malformations, note the striking difference in the number of lesions detected by the partial flip-angle T2*-weighted GRE compared with the TSE T2-WI sequence. This is due to the insensitivity of the TSE sequence for blood degradation products, such as hemosiderin

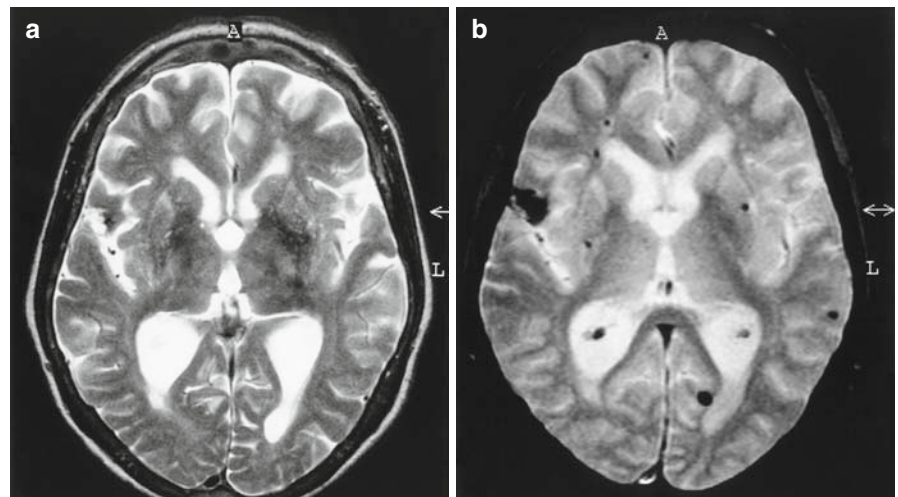


Fig. 2.52 Developmental venous anomaly (“venous angioma”). (a) Axial TSE T1-WI. (b) Axial susceptibility-weighted image (SWI). Gd-enhanced axial (c) and coronal (d) TSE T1-WI. The tubular structure in the left frontal lobe represents a large draining vein. Since this vein contains deoxygenated blood, it appears dark on the SWI (as all venous structures). After Gd injection, a cluster of small tributary veins enhance in a stellate fashion, (the so-called “caput medusae”), and they converge toward the large draining vein

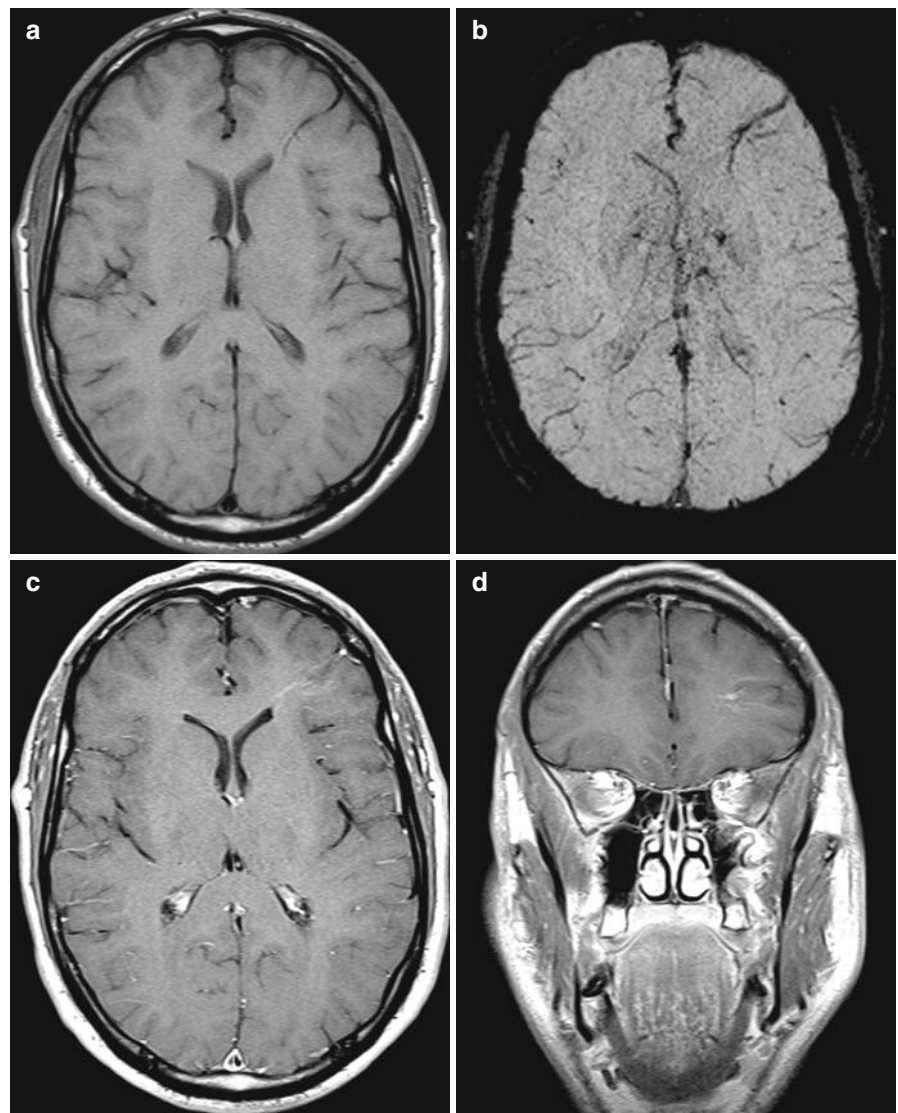
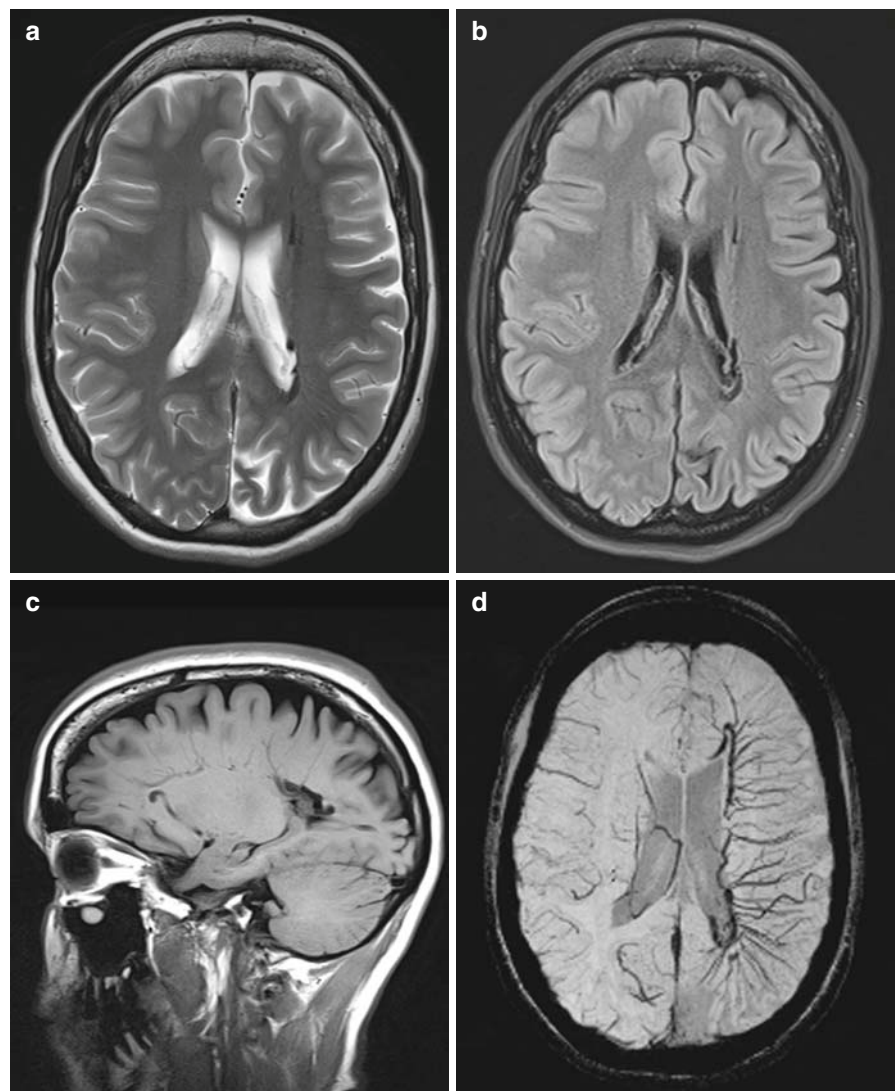


Fig. 2.53 Sturge-Weber syndrome with complex collateral venous drainage. (a) Axial TSE T2-WI. (b) Axial fat-sat turbo FLAIR. (c) Sagittal TSE T1-WI. (d), Axial susceptibility-weighted image (SWI). The axial T2 and FLAIR images show mild cortical atrophy of the left cerebral hemisphere (a, b). There are prominent vascular structures along the left lateral ventricle (a–c). The SWI shows extensive medullary collateral venous drainage (d). SWI is very sensitive to veins because of their deoxyhemoglobin content, and SWI should constitute an important part of any neuroimaging protocol to reveal micro-architecture of neurovascular diseases



2.8 White Matter Lesions

2.8.1 Introduction

In the neuroradiological assessment of white-matter disease, it is important to consider both the patient's age and the clinical presentation. Most white-matter diseases present with similar findings on MRI, with hyperintense lesions on T2-WI and hypointense lesions on T1-WI. Contrast enhancement occasionally occurs, and indicates breakdown of the BBB. Subtle differences in the pattern of white matter changes may direct us to the correct diagnosis.

Imaging strategy should be directed by the expected pathology, which depends on the age of the patient. In

the first year of life, periventricular leucomalacia and delayed myelination are frequent findings. In the first decade, the leukodystrophies can be the cause of white matter changes. In the adult population, MS is the most common white-matter disease, with an increasing incidence of nonspecific and vascular-related white matter changes with aging. Within certain patient groups, other diseases are more frequent (toxic demyelination, radiation necrosis).

2.8.2 Normal Development

Myelination of the CNS starts in the fifth fetal month. At the age of 2 years, 90% of myelination is complete. The

remainder of the process continues to early adulthood. The progression of myelination can be studied with MRI, and the visualization of this process depends on the pulse sequence and field strength. T2 Early changes ($\leq 6-8$ months) are best studied with a T1-W sequence; at a later age (6–18 months), changes are best depicted on T2-WI. The process of myelination follows a distinct pattern. In broad terms, myelination progresses from caudad to craniad, and from posterior to anterior. The myelination process is discussed in greater depth in Chap. 13.2.3.

The posterior limb of the internal capsule contains an area with different SI than the anterior limb. On T2-WI, this is seen as a focal symmetric area of high SI. Proton density and T1-WI show no difference between the anterior and posterior limb of the internal capsule. These regions probably represent a portion of the pyramid tract (parieto-pontine bundles). This normal finding should not be mistaken for lesions in the internal capsule.

2.8.3 T2-W and FLAIR

Myelinated structures are hypointense on T2- and FLAIR images. At birth, the dorsal white-matter tracts of the brainstem, the superior and inferior cerebellar peduncles, and the medio-dorsal tracts in the diencephalon are myelinated. Supratentorially, only the posterior limb of the internal capsule and the white matter in the postcentral gyrus are myelinated. As the process continues, more cerebral structures become myelinated. At the age of 6 months, the brainstem presents a mature myelination pattern, and the cerebellar hemispheres show central myelination. The optic radiation is fully myelinated, while the internal capsule and the corpus callosum are partially myelinated. The occipital and parietal lobes and the motor areas myelinate earlier than the frontal and temporal lobes. This is also reflected in the myelination of the internal capsule and the corpus callosum. The anterior limb of the internal capsule and the genu of the corpus callosum myelinate 4 months later than the posterior limb and the splenium. The occipital and parietal lobes reach a mature myelination between 6 and 18 months; the frontal and temporal lobes reach this point between 21 and 27 months.

2.8.4 T1-W Sequence

Myelinated structures are hyperintense on T1-WI. The myelination process as seen on IR T1-WI proceeds

parallel to that seen on T2-and FLAIR. However, myelination is seen earlier on T1-WI than on T2-WI. At birth, all three cerebellar peduncles are myelinated, and the optic pathways also show a high SI due to myelination. Not only the postcentral, but also the precentral gyrus is myelinated at birth on IR-SE T1-WI. At the age of 6 months, most of the brain reaches a mature myelination on the IR-SE T1-WI, and the frontal and temporal poles are fully myelinated on IR-SE T1-WI after 10 months.

2.8.5 Delayed Myelination

There is a close correlation between myelination and psychomotor development, both in normal and delayed myelination. In infants with a developmental delay of unknown cause, delayed myelination is present in 10% of cases. The most common causes of delayed myelination are malnutrition, hypoxia-ischemia, infections, congenital heart failure, hydrocephalus, and chromosomal abnormalities (Down's syndrome).

2.8.6 Leukodystrophy

Leukodystrophies constitute a group of disorders that are characterized by abnormal formation, turnover, or destruction of myelin. The underlying cause is an enzyme deficiency. Most of these disorders are encountered in the pediatric population. White matter changes on MRI are often nonspecific, though some are suggestive of certain diseases.

Canavan disease (see Chap. 13.2.4.8, Fig. 13.31) is rare and results in a diffuse, symmetric, low SI of the white matter on T1-WI. On T2-WI, the supratentorial white matter has a uniformly high SI. In *Alexander disease* (see Chap. 13.2.4.9, Fig. 13.32), the abnormal SI is initially located in the frontal lobes. Enhancement after contrast-medium administration of the basal ganglia and periventricular white matter has been reported. *Adrenoleukodystrophy* (see Chap. 13.2.4.3, Fig. 13.27) affects only boys and results in high SI in the occipital lobes on T2-WI; in due course, these abnormalities advance anteriorly. The anterior rim of the lesion may enhance after contrast-medium administration. An almost complete lack of myelination is seen in the *Pelizaeus-Merzbacher disease* (Fig. 2.54). Hyperintense lesions on T2-WI are found in the basal ganglia or

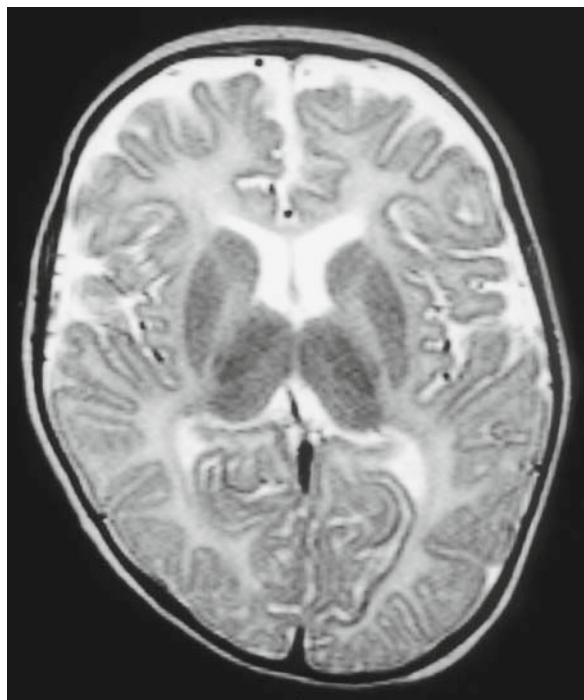


Fig. 2.54 Pelizaeus-Merzbacher disease. This axial TSE T2-WI shows abnormally high signal intensities throughout the white matter in both hemispheres. This finding is consistent with an almost complete lack of normal myelination

thalamus in *Krabbe disease*, *Leigh disease* (see Chap. 13.2.4.4, Fig. 13.28), and *methylmalonic aciduria*. A more exhaustive discussion of leukodystrophies is presented.

2.8.7 Multiple Sclerosis

MS is an inflammatory demyelinating disease of the CNS. It is the most common demyelinating disease after vascular- and age-related demyelination. MS is characterized by multiple “plaques” of demyelination in the white matter of the brain and spinal cord. The primary lesions are found in the perivascular spaces along penetrating veins. Though the etiology of MS is not fully understood, the destruction of myelin is most likely caused by an autoimmune process. Initial symptoms can sometimes be triggered by trauma or a viral infection, but a convincing link to the disease has not been made.

The clinical course of MS is highly variable. The age of symptom onset in MS is usually between 18 and 40 years; onset is uncommon in childhood and after the age of 50 years. Initial symptoms may include numbness, dysesthesia, double vision, or problems with

balance and coordination. Loss of motor function is also a frequent initial presentation. Less commonly, spinal-cord-related symptoms constitute the initial presentation of MS. There is a female:male ratio of 3:2.

The most common clinical presentation is “*relapsing-remitting*” MS (70% of cases). Patients experience symptomatic episodes (known as “attack” or “Schub” in German), which can last from 24 h to several weeks, followed by complete or partial disappearance of symptoms (remission). The interval between relapses may be weeks to years (and even decades). As white-matter lesions increase over time, and neurologic disabilities increase, the disease frequently becomes “*secondary progressive*.” Accumulating neurological deficits eventually lead to permanent disability. The evolution from relapsing-remitting to secondary-progressive MS occurs in approximately half of patients within 10 years after onset. Alternatively, in 10–20% of cases, MS can follow a “*primary progressive*” course; in this type of disease, there is a continuous, gradual evolution from the beginning, rather than relapses.

2.8.7.1 Diagnostic Criteria

No single clinical or laboratory test is pathognomonic for MS. For this reason, diagnostic criteria have been developed to assess the relative probability of MS. In 2001, an international panel convened by the National Multiple Sclerosis Society of North America and chaired by Ian McDonald recommended revised diagnostic criteria for MS. They replace the older Poser Criteria and have become known as the “McDonald criteria,” after their lead author (Table 2.18). These new criteria integrate MRI image assessment with clinical and other paraclinical methods in drawing diagnostic conclusions. The McDonald criteria take into account the high sensitivity of MRI in detecting lesions. In 2005, a revision to the “McDonald criteria” was proposed to clarify the exact definition of terms such as “attack,” “dissemination,” a “positive MRI” etc. It is now widely accepted that MRI plays an important role as a noninvasive diagnostic test to establish the diagnosis of MS lesions, showing demyelinating lesions in the brain and spinal cord. Because of its greater sensitivity, compared with clinical measures, MRI can be used to measure subclinical disease. Moreover, MRI outcome measures are routinely used in clinical trials of MS patients, and MRI has become the method of choice for patient follow-up and treatment monitoring.

Table 2.18 McDonald criteria for the diagnosis of Multiple Sclerosis

Clinical presentation	Additional data needed
Two or more attacks (relapses) Two or more objective clinical lesions	None; clinical evidence will suffice (additional evidence desirable but must be consistent with MS)
Two or more attacks One objective clinical lesion	Dissemination in space, demonstrated by: MRI A positive CSF and two or more MRI lesions consistent with MS Further clinical attack involving different site
One attack Two or more objective clinical lesions	Dissemination in time, demonstrated by: MRI Or second clinical attack
One attack One objective clinical lesion (monosymptomatic presentation)	Dissemination in space demonstrated by: MRI Or positive CSF and two or more MRI lesions consistent with MS and Dissemination in time demonstrated by: MRI Or second clinical attack
Insidious neurological progression suggestive of MS (primary progressive MS)	One year of disease progression (retrospectively or prospectively determined) and Two of the following: Positive brain MRI (nine T2 lesions or four or more T2 lesions with positive VEP) Positive spinal cord MRI (two focal T2 lesions) Positive CSF

2.8.7.2 MRI Appearance of MS

The characteristic abnormalities of MS in the brain consist of multiple white-matter lesions with a high SI on FLAIR, PD-WI, and T2-WI and low SI on T1-WI. Lesions are found predominantly in a periventricular distribution, centrum semiovale, and the callososeptal interface (Fig. 2.55). Additional sites of involvement include other parts of the cerebral white matter such as the subcortical

white matter, optic nerves, corpus callosum, internal capsule, cerebellar peduncles, brainstem, and spinal cord.

Demyelinating lesions appear smaller on T1-WI than on T2-WI. Occasionally, they show a hyperintense border on T1-WI. Lesions in MS can be small, large, or confluent. The typical configuration is that of an ovoid lesion extending perpendicularly from the ventricular surface (Dawson's finger) (Fig. 2.55). This probably reflects the perivascular inflammation along

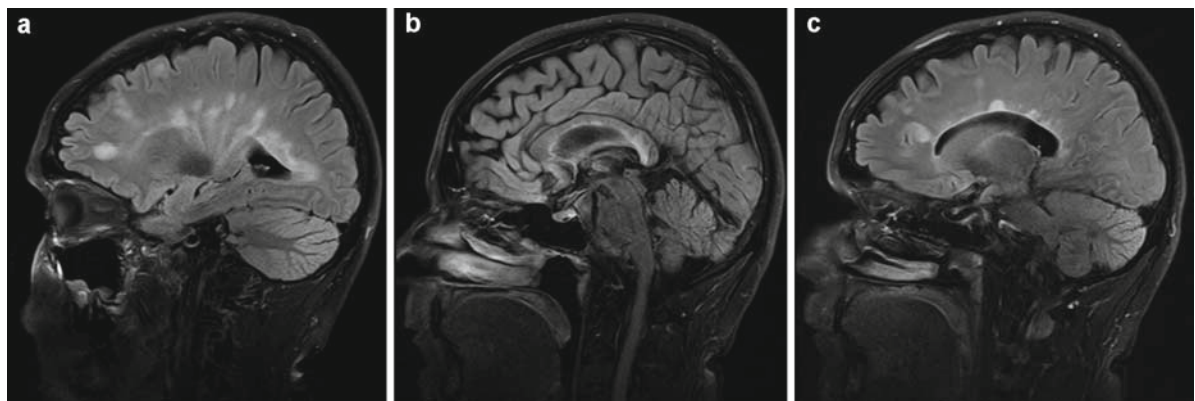


Fig. 2.55 Multiple sclerosis: value of sagittal FLAIR images. (a–c) Sagittal fat-sat turbo FLAIR images. These images, obtained in a 27-year-old woman with multiple sclerosis, show multiple demyelinating lesions in the periventricular white mat-

ter and corpus callosum. The periventricular lesions characteristically extend perpendicularly from the ventricular surface (Dawson's finger). There is extensive involvement of the corpus callosum, which is a hallmark of MS

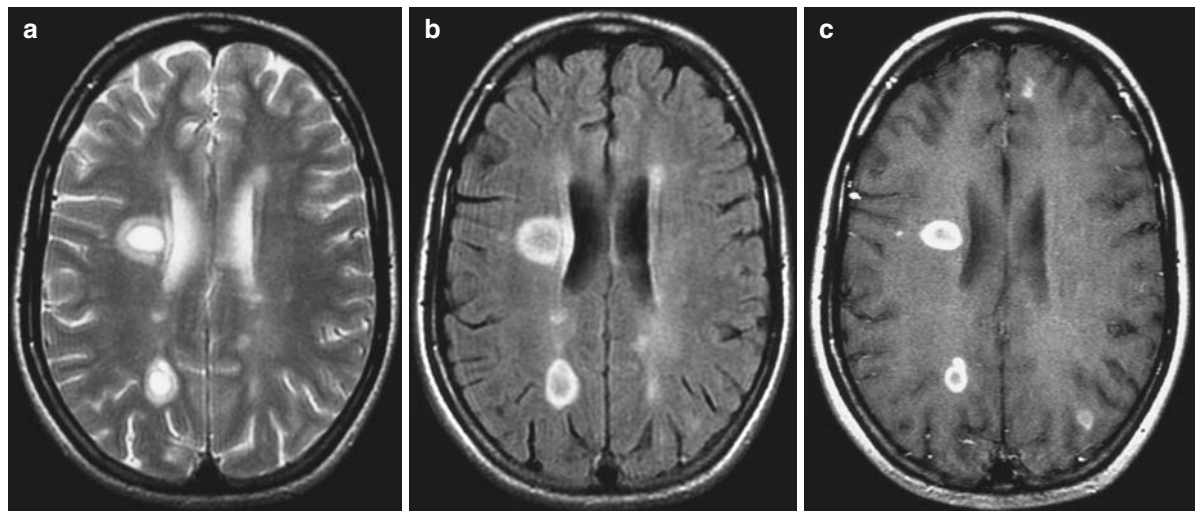


Fig. 2.56 Multiple sclerosis: role of gadolinium. (a) Axial TSE T2-WI and (b) axial TSE Flair through the centrum semiovale. (c) Gd-enhanced axial SE T1-WI through the centrum semiovale. On the T2-WI, all white-matter lesions are hyperintense. Active lesions have basically the same imaging appearance as

older lesions. After Gd injection, only a few lesions enhance, indicating disruption of the BBB. The pattern of enhancement can be solid (presumably indicating a fresh lesion) or ring-like (believed to represent an older or reactivated lesion)

a penetrating medullary vein. Atypical lesions and mass-like lesions occur with sufficient frequency to cause diagnostic errors.

MS lesions may enhance after contrast administration on T1-WI, depending on the age and activity of the lesion. New and active lesions commonly show contrast enhancement, due to BBB breakdown. New lesions tend to show solid enhancement, whereas reactivated lesions enhance in a ring-like fashion (Fig. 2.56). After 2 months, the integrity of the BBB is restored, and the majority of lesions no longer show contrast enhancement.

As with unenhanced lesions, the contrast-enhancing lesions are smaller than the corresponding lesions on the T2-WI scan. The discrepancy between the size of the lesion on T1-WI and T2-WI reflects the different components of the local process: edema, inflammation, and demyelination.

The poor correlation between the MRI findings and the clinical events is demonstrated by the frequent finding of enhancing lesions in clinically stable patients.

2.8.7.3 Lesion Distribution

White-matter lesions are abundant in the centrum semiovale, corpus callosum, optic chiasm, and optic nerves. Hyperintense lesions on T2-WI are commonly

found in the corpus callosum. Typically, these lesions occur along the inner callosal-ventricular margin, creating an irregular ventricular surface of the corpus callosum. This aspect can be differentiated from callosal atrophy due to the lobar white-matter lesions. The existence of callosal lesions improves both the sensitivity and the specificity of MRI for the diagnosis of MS. The absence of callosal lesions renders the diagnosis of MS less likely, but does not exclude it.

A frequent initial presentation of MS is optic neuritis, although there is controversy regarding the likelihood of definitive MS developing in patients who have had an optic neuritis. Brainstem lesions are common, and a lesion in the medial longitudinal bundle affects approximately one-third of MS patients. In patients with clinically possible MS and a normal MRI study of the brain, a spinal MRI study should be performed.

2.8.7.4 Imaging Strategies in MS

Initial and Baseline MRI Evaluation

Many patients are referred for an “initial evaluation” standardized MRI scan of the brain after an episode of neurological symptoms which is known as a “clinically isolated syndrome” or a “monosymptomatic

Table 2.19 Brain imaging protocols in multiple sclerosis in patients presenting with a clinically isolated syndrome and as a baseline or follow-up scan

Sequence	Diagnostic scan in a patient presenting with a clinically isolated syndrome	MS baseline or follow-up scan	Remarks
Scout (three-plane or other)	Yes	Yes	Use scouts to align axial scans according to protocol (e.g., parallel with the subcallosal or intercommissural line)
Sagittal Turbo FLAIR	Yes	Optional	Sensitive to show early MS lesions within the corpus callosum and at the callososeptal interface, as well as lesions perpendicular to the ventricular surface
Axial TSE PD/T2	Yes	Yes	TE1≤30 ms and TE2≥80 ms
Axial Turbo FLAIR	Yes	Yes	Sensitive to white-matter lesions including subcortical and cortical lesions
Axial T1 pregadolinium	Optional	Optional	Routine part of most neuroimaging protocols
3D T1	Optional	Optional	Can be used for volumetric assessment (e.g., atrophy measures)
Coronal fat-sat T2 or STIR	Optional	Optional	Indicated in cases of optic neuritis; slices to be positioned from the eye globe to the optic chiasm
Intravenous contrast injection (0.1 mmol/kg body weight)			
Five minutes delay		This delay can be filled by performing the axial turbo FLAIR after injection of contrast medium	
Axial and/or T1 postgadolinium	Yes	Optional	It is advised to perform more than one postgadolinium T1-W sequence, because enhancement tends to increase with time after injection

attack,” or with a past history that is suspicious for MS. Alternatively, for patients with an established diagnosis of MS, it is recommended that the “baseline evaluation” should include an MRI of the brain that meets the standardized protocol (in addition to a complete neurologic history and examination). Imaging protocols for the initial and baseline MRI evaluation are based on the consensus statement representing the consortium of MS centers consensus guidelines, published in 2006 by Simon et al. (Table 2.19).

In order to detect demyelinating lesions in white matter, the optimal MRI sequence should provide: (1) high contrast between lesions and CSF and (2) high contrast between lesions and normal white matter.

Traditionally, these dual goals have been achieved by a double-echo SE sequence, which provides PD-WI (first echo, TE ≤ 30 ms) and T2-WI (second echo, TE ≥ 80 ms). On PD-WI, the SI of CSF is almost equal to that of periventricular white matter; this allows excellent detection of periventricular lesions which stand out

as high-signal areas. On T2-WI, lesions are markedly hyperintense relative to the cerebral white matter. However, small periventricular lesions may be difficult to separate from the high SI CSF in the ventricles.

The combination of high-lesion CSF and high-lesion white-matter contrast can also be achieved by the turbo FLAIR sequence. FLAIR is an IR technique and typically uses a long inversion time of ±2,000 ms (2 s) to suppress the signal of CSF in combination with a long TR/long TE sequence. Turbo FLAIR possesses a superior sensitivity for focal white matter changes in the supratentorial brain, but lesions can be missed in the posterior fossa (Fig. 2.57).

Sagittal turbo FLAIR images are particularly useful for the detection of MS plaques in the corpus callosum and at the callosal-septal interface. Moreover, sagittal images demonstrate the radial orientation of plaques, perpendicular to the ventricular margins (Dawson’s fingers). This characteristic finding reflects the periventricular inflammation of MS.

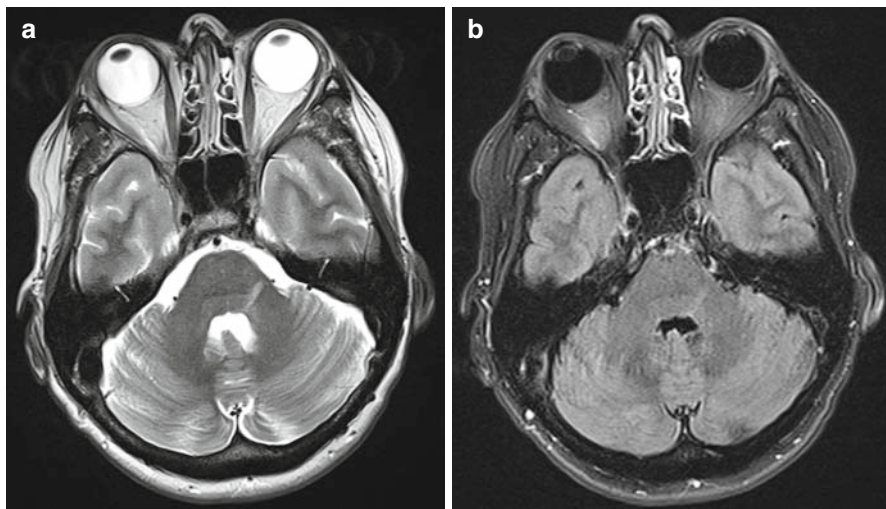


Fig. 2.57 T2-WI are superior to FLAIR images for the detection of posterior fossa lesions. **(a)** Axial TSE T2-WI. **(b)** Axial fat-sat turbo FLAIR. The demyelinating lesion in the left brachium pontis (middle cerebellar peduncle) is better seen on T2-WI than on FLAIR. In the posterior fossa, T2-WI provide

better lesion-to-background contrast; FLAIR images are less sensitive in the depiction of demyelinating lesions involving the brainstem and cerebellum. In patients with multiple sclerosis, on FLAIR images, the lesion load in the posterior fossa may be underestimated

Follow-Up MRI Scans

Follow-up MRI scans of the brain (and/or spine) are indicated if a patient's clinical condition is worsening unexpectedly, to reassess the disease burden for patients enrolled in therapeutic trials, or to rule out a secondary diagnosis. However, in the absence of these conditions, routine follow-up MRI scans are generally not recommended.

When follow-up MRI scans are obtained in MS patients, they should be performed in accordance with the standardized imaging protocol. The follow-up scans must be compared with previous studies. The radiologist should pay attention to the appearance of new lesions or enlarging T2-hyperintense lesions as well as to the number of contrast-enhancing lesions. Follow-up scans should also report on the presence or appearance of so-called "black holes." These are lesions that are markedly hypointense on T1-WI, indicating severe tissue injury (including axonal damage, matrix destruction, and myelin loss). Black holes cannot be ascertained on a single MRI scan, since, by definition, these chronic T1 hypointensities should persist for at least 6 months. Black holes should be differentiated from acute MS lesions, which may also appear hypointense on T1-WI due to transient vasogenic edema, which usually disappears

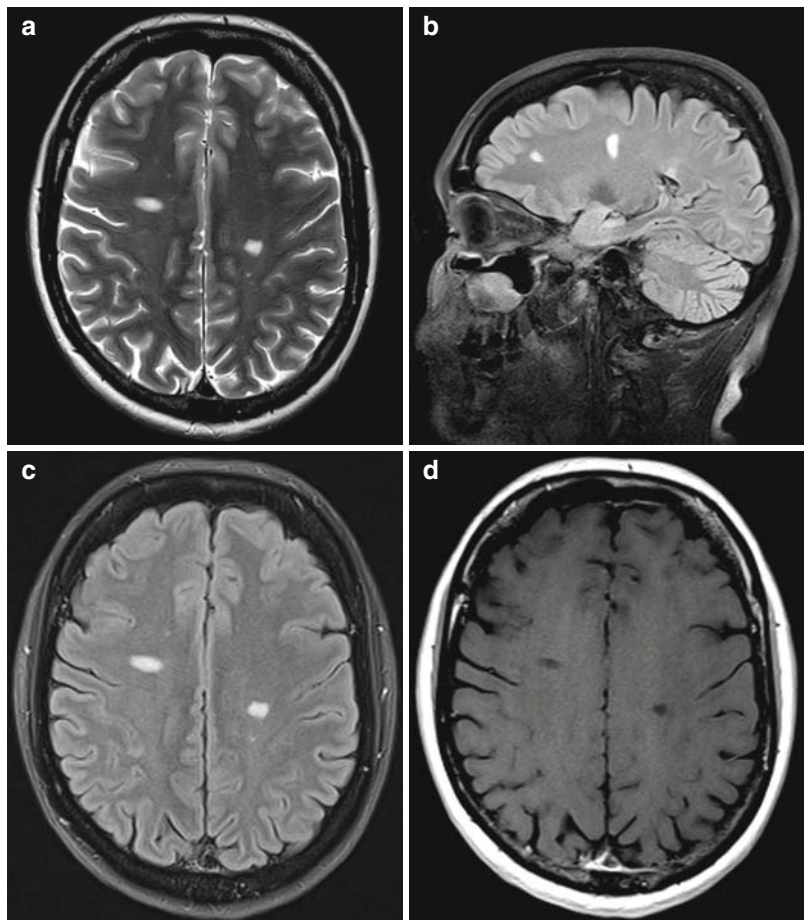
after a few weeks. In clinical practice, T1 black holes are lesions that remain hypointense on postgadolinium T1-WI scans, indicating a focal area of tissue loss (Fig. 2.58).

Follow-up MRI scans are of great value to count new or enlarging lesions over time, to register changes in enhancement, and to perform quantitative analysis of the T2-lesion volume (the so-called "burden of disease"). Standardized MRI protocols have proven to be useful to correlate imaging findings with clinical outcomes for patients enrolled in therapeutic trials. Cerebral atrophy, which can be assessed from the size of the ventricles and width of the cortical sulci, indicates overall volume loss of brain tissue and is mildly correlated with disability in MS patients. The use of 3D scans allows volumetric measurements of white-matter lesions and brain tissue.

Gd-Enhanced MRI in Patients with MS

Gd-enhanced MRI of the brain is recommended in patients with (suspected) MS for diagnosis and initial diagnostic evaluation. New and active demyelinating lesions are associated with BBB breakdown and may therefore enhance after contrast administration. The identification of enhancing white-matter lesions is an important component of the

Fig. 2.58 Black holes in multiple sclerosis. (a) Axial TSE T2-WI. (b) Sagittal fat-sat turbo FLAIR. (c) Axial fat-sat turbo FLAIR. (d) Gd-enhanced axial TSE T1-WI after a 5-min delay. There are several demyelinating plaques in the subependymal white matter and centrum semiovale; they are hyperintense on FLAIR and T2-WI. On contrast-enhanced T1-WI, the lesions remain hypointense and there is no enhancement. Black holes are defined as lesions that remain hypointense on postgadolinium T1-W scans, indicating a focal area of neural tissue loss



criteria providing evidence for dissemination in time and space. Enhancing white-matter plaques, at the time of the initial diagnostic evaluation, is a strong predictor of future clinical attacks and a diagnosis of MS. Enhancement tends to be solid with fresh lesions and becomes ring-like when the lesion is several weeks old (Fig. 2.56). In addition to showing enhancing MS lesions, the use of gadolinium-enhanced sequences is also very useful to rule out confounding diagnoses, which could otherwise be missed (e.g., leptomeningeal disease, meningioma, tumors, vascular malformations, etc.).

A 5-min delay is suggested between the start of the contrast injection and the postcontrast T1-W sequence. This delay is necessary to provide sufficient time for Gd to leak through the BBB. Some authors have suggested filling up the delay by obtaining the axial turbo FLAIR sequence postgadolinium. Although it is not

recommended in the consensus guidelines (Table 2.19), we routinely obtain at least axial and coronal postgadolinium T1-WI. The conspicuity and number of enhancing white-matter lesions can be increased by use of double-dose contrast or by increasing the delay after injection. However, there is no convincing evidence that supports higher doses at this time. We routinely use a standard dose of gadolinium-chelate (0.1 mmol/kg body weight, 20 mL maximum) with a 5-min delay. Application of a MTC (magnetization transfer contrast) prepulse renders the T1-W sequence more sensitive for contrast enhancement (Fig. 2.59). To avoid confusion between enhancement and an MTC effect, the precontrast T1-W sequence should also be performed with a MTC prepulse.

It is well-known that anti-inflammatory medications (e.g., corticosteroids) restore the BBB. Therefore, it is important to perform the MRI examination before

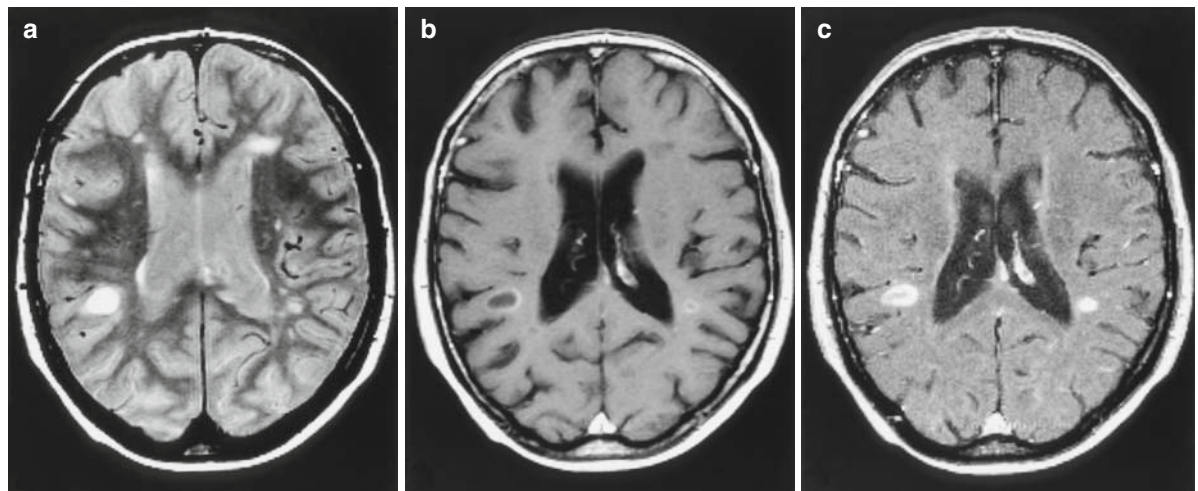


Fig. 2.59 Multiple sclerosis: value of magnetization transfer contrast. (a) Axial TSE PD-WI through the lateral ventricles. (b) Gd-enhanced axial SE T1-WI (same level). (c) Gd-enhanced axial SE T1-WI with MTC (same level). PD-WI shows multiple white-matter lesions in both hemispheres. The distribution pat-

tern is consistent with MS. After Gd injection, ring-like enhancement is observed in two lesions. The Gd-enhanced image with MTC shows more intense enhancement. The signal-to-noise ratio is poorer due to background suppression

medical treatment is instituted. If not, the activity of the disease may be underestimated.

Patients Presenting with Optic Neuritis

In patients presenting with a clinically isolated syndrome with visual disturbances, e.g., optic neuritis, the

imaging protocol should include sequences that depict the optic nerve, optic chiasm, and visual pathways. Imaging of the optic nerve is best performed with thin coronal images with fat-suppression (STIR or T2-WI with spectral fat saturation) (Fig. 2.60). Coronal images should cover the orbit and include the optic chiasm and optic tracts. On T2-WI, high SI indicating edema of the optic nerve can be seen. Due to the swelling of the nerve, the CSF-filled perioptic sheath is compressed, and the normal “target” configuration of the optic nerve surrounded by CSF disappears. T1-W sequences after contrast administration may show enhancement of the optic nerve.

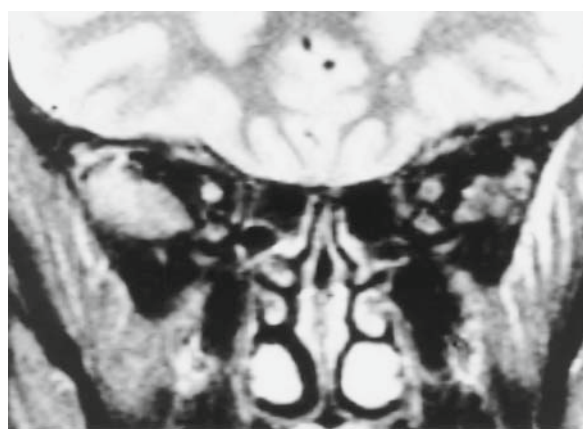


Fig. 2.60 Optic neuritis. This coronal STIR image with fat suppression shows abnormally high signal intensity in the right optic nerve. Note normal “target” appearance of the left optic nerve, which is outlined by the CSF space surrounding it

2.8.7.5 Differential Diagnosis

A diagnosis of MS should not only be made on the basis of MRI findings, but should take into account the patient's history, clinical signs and symptoms, as well as the appropriate laboratory tests. Because of improved MRI techniques, it is relatively easy to rule out obvious MS mimickers such as tumors or vascular malformations. However, it remains difficult to differentiate MS lesions from other diseases involving white matter such as: neurosarcoidosis, Sjögren syndrome,

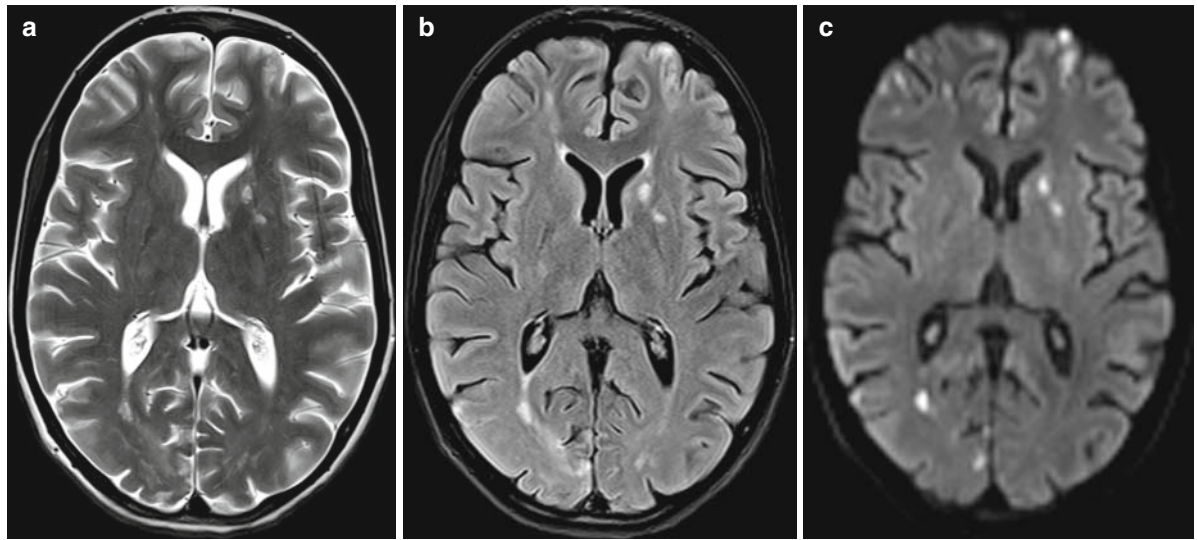


Fig. 2.61 Vasculitis. (a) Axial TSE T2-WI. (b) Axial fat-sat turbo FLAIR. (c) Axial EPI diffusion-weighted “trace” image (DWI). This 22-year-old woman with neuropsychiatric systemic lupus erythematosus and antiphospholipid syndrome was admitted with coordination difficulties, drowsiness, and confusion. T2 (a) and FLAIR (b) images show scattered, punctate hyperinten-

sities throughout both hemispheres. These lesions exhibit restricted diffusion (c), indicating recent infarctions. Vasculitis should be considered in the differential diagnosis of multiple sclerosis, even though in this case, the topography and distribution pattern of the lesions is suggestive of vascular rather than demyelinating etiology

vasculitis (e.g., systemic lupus erythematosus, Behçet disease, ...), Lyme disease, acute disseminated encephalomyelitis (ADEM), etc. These conditions may present clinical and MRI findings remarkably similar to MS. Lyme disease can mimic MS on an MRI study, and in endemic regions, this treatable disease should be considered in the differential diagnosis. Vasculitis is associated with multifocal T2-hyperintense lesions, representing micro-infarctions, sometimes with diffusion restriction

(Fig. 2.61). Vasculitis preferentially involves the peripheral, subcortical white matter and gray matter, with focal gray matter atrophy. ADEM is a monophasic disease with an MRI appearance which is often indistinguishable from MS.

In the elderly population, the main differential diagnosis is with nonspecific ischemic white-matter lesions associated with microvascular disease or systemic hypertension (subcortical arteriosclerotic leukoencephalopathy).

On MRI studies, overdiagnosis of MS should be avoided and the radiologist should be aware of pitfalls and differential diagnoses. A short list of multifocal white-matter lesions is provided in Table 2.20.

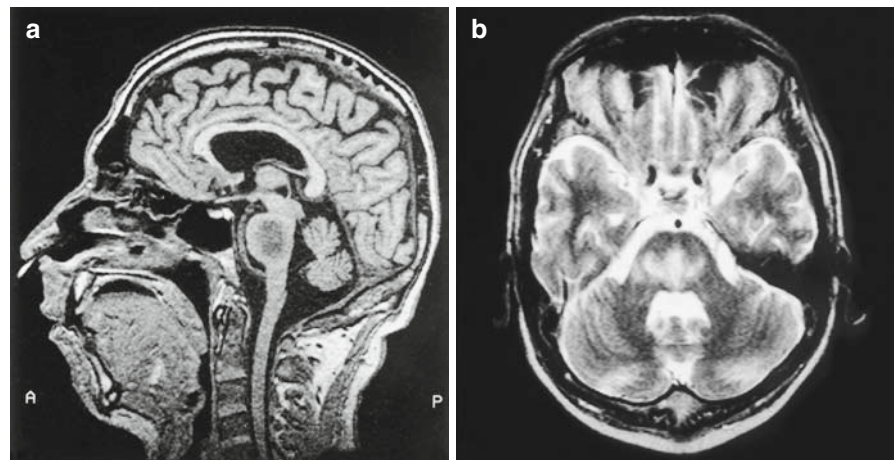
Table 2.20 Differential diagnosis of multifocal white-matter lesions

Aging
Multiple sclerosis
ADEM
Lyme disease
PML
Metastasis
Trauma
Vasculitis
Hypertension
Migraine

2.8.8 Toxic and Degenerative Demyelination

Radiation therapy and chemotherapy may lead to degeneration of cerebral white matter. T2-WI shows focal or diffusely confluent lesions in the lobar white matter. Local mass effect can be present due to focal necrosis. Peripheral enhancement is often seen after

Fig. 2.62 Central pontine myelinolysis. (a) Sagittal SE T1-WI. (b) Axial TSE T2-WI. Within the pons, there is a lesion which is hypointense on the T1-WI and hyperintense on the T2-WI. There is a surrounding rim of normal-appearing pontine parenchyma. On the axial image, the “trident” shape reflects the position of the corticospinal tracts in the anterior lateral part of the pons



contrast administration. Radiation-induced contrast-enhancing lesions may develop in patients after treatment for brain tumors, and these lesions can mimic recurrent or residual tumor. MRS can be used to differentiate recurrent tumor (increased choline/creatinine ratio and decreased *N*-acetylaspartate) from radiation necrosis (elevated lactate). Alternatively, dynamic susceptibility-weighted contrast-enhanced perfusion MRI can be used, since recurrent tumor shows elevated CBV (presumably reflecting tumor angiogenesis), whereas CBV is decreased in areas of radiation-induced necrosis (indicating that radiation necrosis is ischemic in nature and due to an insufficient blood supply).

Alcohol is another cause of toxic demyelination. Osmotic myelinolysis is an acute neurologic condition, which may occur as a complication of severe and prolonged hyponatremia, particularly when corrected too rapidly. This condition is most frequently found in alcoholics, but other risk factors include malnutrition, liver transplant surgery, burn patients, etc. The most common site of involvement is the central pons, and this condition is known as central pontine myelinolysis (Fig. 2.62). On MRI, an area of prolonged T1- and T2- relaxation times is observed in the pons. On axial T2-WI, the hyperintense signal abnormality presents a characteristic “trident”-shape in the central pons, with sparing of the pontine tegmentum and ventrolateral pons (corticospinal tracts). Extrapontine osmotic myelinolysis can also be found in the basal ganglia and the thalamus. Peripheral enhancement may be observed after contrast administration. Chronic alcoholism can also cause nonspecific deep white-matter lesions and periventricular demyelination.

2.9 Intracranial Infection

2.9.1 Imaging Strategy

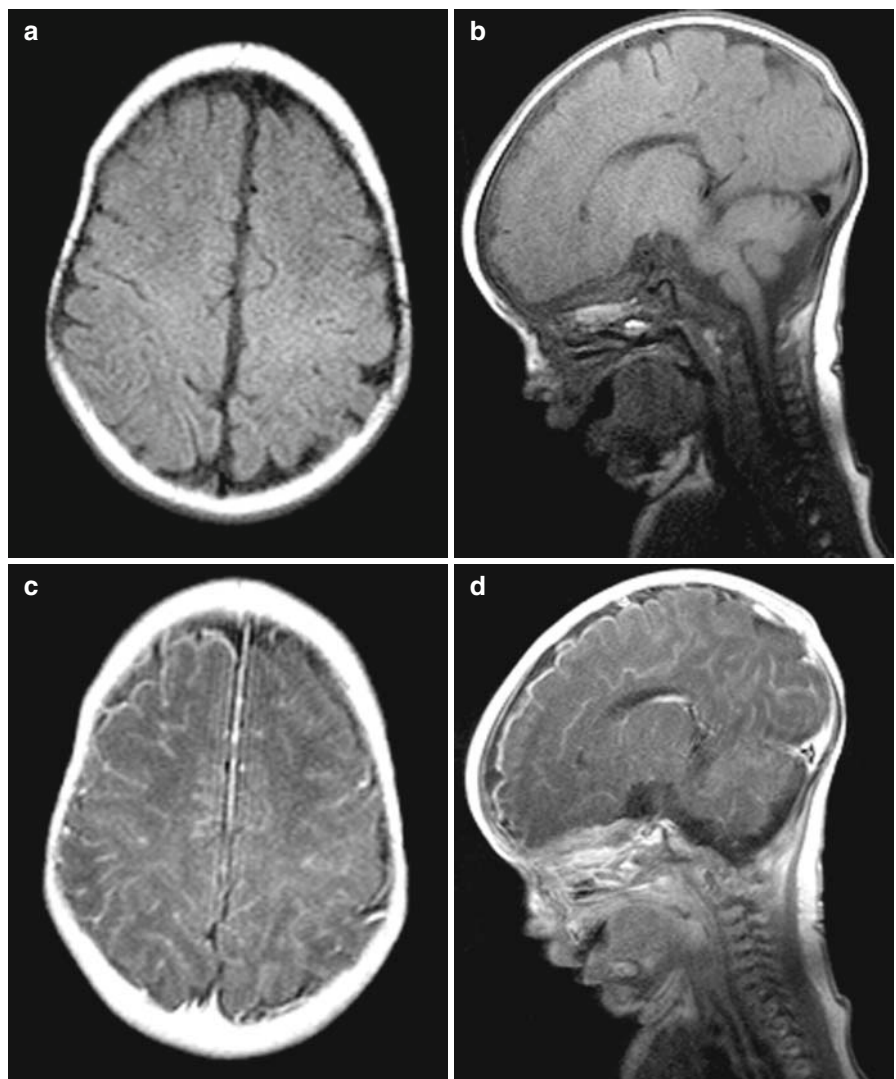
MRI is superior to CT for the detection of intracranial infections. The pulse-sequences used for the evaluation of intracranial infections are straightforward. Use of a paramagnetic contrast agent is crucial. In most cases, we use the same protocol as proposed for intracranial mass lesions.

2.9.2 Meningitis

Meningitis is the most common presentation of CNS infection. It can be caused by bacterial, viral, or fungal agents. Clinically, meningitis presents as an acute febrile illness with severe headache, stiffness of the neck, photophobia, and vomiting. Imaging does not contribute to the diagnosis, but can be used to exclude parenchymal abscess or localized empyema, to look for a source of infection (paranasal sinuses, petrous bones), to monitor the complications of meningeal infections (hydrocephalus, subdural effusion, infarction), and to rule out confounding diagnoses when the clinical presentation is atypical.

In most cases of meningitis, no abnormality is seen on unenhanced MRI scans; in some cases, obliteration of the basal cisterns is observed, with hyperintense signal on proton-density and FLAIR images. After contrast-medium administration, leptomeningeal

Fig. 2.63 Acute bacterial meningitis. (a, b) Precontrast axial and sagittal SE T1-WI. (c, d) Gd-enhanced axial and sagittal SE T1-WI (identical slice positions). Precontrast T1-WI is unremarkable because the thickened leptomeninges are isointense to CSF. T2-WI were normal (not shown). After Gd-administration, there is extensive enhancement of the leptomeningeal bacterial exudate involving the subarachnoid spaces and cortical sulci. Lumbar puncture confirmed meningococcal meningitis



thickening and enhancement is observed, especially in patients with chronic bacterial infection (Fig. 2.63).

In adults, 50% of patients with bacterial meningitis develop complications, which include:

- *Hydrocephalus*, due to fibropurulent infectious exudate and cellular debris, which obstructs the CSF flow at the foramina of Monro, aqueduct, fourth ventricle outlet foramina, and subarachnoid spaces.
- The infection can spread to the ventricular system, resulting in *ventriculitis* (also known as ependymitis) and *choroid plexitis*, both showing ependymal enhancement after contrast administration.
- *Subdural effusions* are a common complication of meningitis. They are seen as extra-axial fluid collec-

tions with smooth contours that displace the cortical veins medially and do not extend into the sulci. They should be differentiated from widened subarachnoidal spaces, where the extra-axial fluid extends into the sulci and does not displace the cortical veins.

- *Subdural empyema* (a collection of pus and fluid from infected tissue) can be caused by meningitis, but the most common cause is sinusitis. Empyema is recognized on MRI as a lentiform or crescentic extra-axial fluid collection, adjacent to the inner table, overlying the cerebral convexities, or extending into the interhemispheric fissure along the falx, or into the posterior fossa with strong enhancement of the surrounding pseudomembrane (Fig. 2.64). Most subdural empyemas are found in close proximity to the

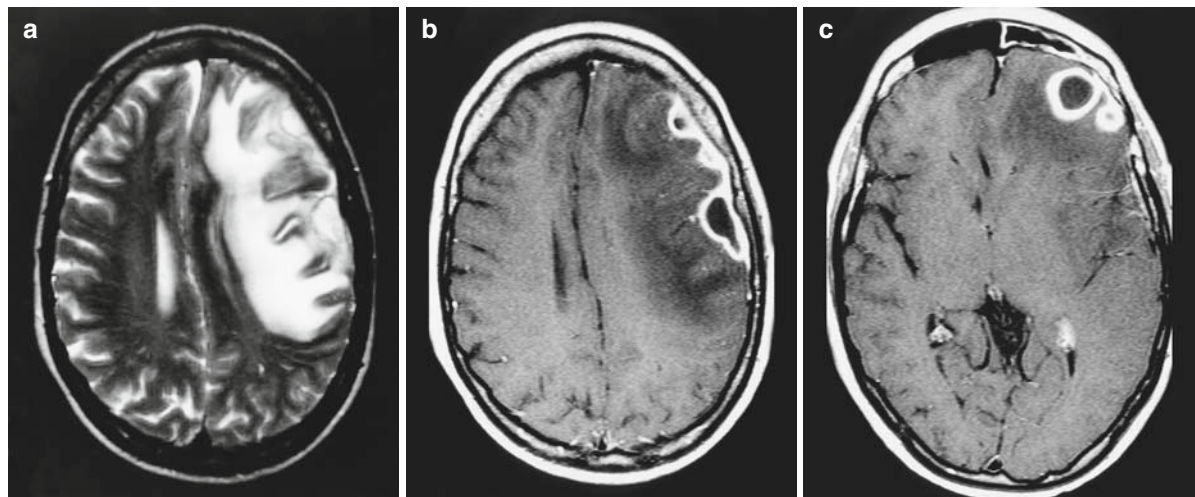


Fig. 2.64 Subdural empyema and intracerebral abscess. (a) Axial TSE T2-WI through the centrum semiovale. (b) Axial Gd-enhanced SE T1-WI (same level as a). (c) Axial Gd-enhanced SE T1-WI through the lower frontal lobes. The axial T2-WI shows nodular meningeal thickening over the left frontal convexity; there is extensive vasogenic edema in the white matter of

the left cerebral hemisphere. After Gd injection, extra-axial fluid collections are observed. There is strong enhancement of the meninges and surrounding pseudomembranes. In the lower frontal lobe, the pyogenic empyema has spread into the cerebral parenchyma with the formation of an intracerebral abscess, which enhances in a ring-like pattern

paranasal sinuses (anterior cranial fossa, frontal region) or the temporal bones (bases of the skull, middle and posterior cranial fossa).

- Pyogenic meningitis can spread into the cerebral parenchyma causing *cerebritis*. Hematogenous spread, however, is the most common cause of a cerebritis. MRI shows an ill-defined region of low signal on T1-WI and high signal on T2-WI. Patchy enhancement can be seen after contrast-medium administration.

The appearance of an intraparenchymal area of ring enhancement indicates formation of a *cerebral abscess* (Fig. 2.65). This process of encapsulation may take weeks depending on the organism, immune response, and therapy. An abscess has a thick enhancing wall and is surrounded by vasogenic white-matter edema. Because most abscesses result from hematogenous spread of microorganisms, the preferred location is the corticomedullary junction. On T2-WI, the wall of the abscess is hypointense (dark rim). After Gd-injection, there is thick-walled ring-enhancement. Characteristically, a bacterial abscess exhibits restricted diffusion on DWI trace images (hyperintense), and lowered ADC values (hypointense). This is due to the high cellular content and increased viscosity of the pus (decreased motion of water). This is a useful differentiating feature from a

necrotic tumor, which does not show diffusion restriction. However, some metastases, especially from mucinous primary tumors, may also exhibit diffusion restriction. Table 2.7 provides a differential diagnosis for ring-enhancing lesions in the brain.

Cranial nerve dysfunction is a common complication of bacterial or tuberculous meningitis.

Cerebral infarcts can occur as a complication of meningitis, due to arteritis, vascular compression, or dural sinus or cerebral vein thrombosis.

2.9.3 Encephalitis

The term encephalitis refers to a diffuse, nonfocal, inflammatory process of the brain parenchyma, usually of viral origin. The most common causative agents are: herpes simplex virus (HSV), cytomegalovirus, and, in patients with AIDS, the papovaviruses. Most of the encephalitides resemble each other and have few identifying imaging characteristics. Areas of involvement are characterized by mass effect, edema, hyperintensity on T2-WI, and, less frequently, small infarctions or petechial hemorrhages. A common nonviral cause of encephalitis is toxoplasmosis, especially in immunocompromised patients. ADEM is an autoimmune allergic encephalitis.

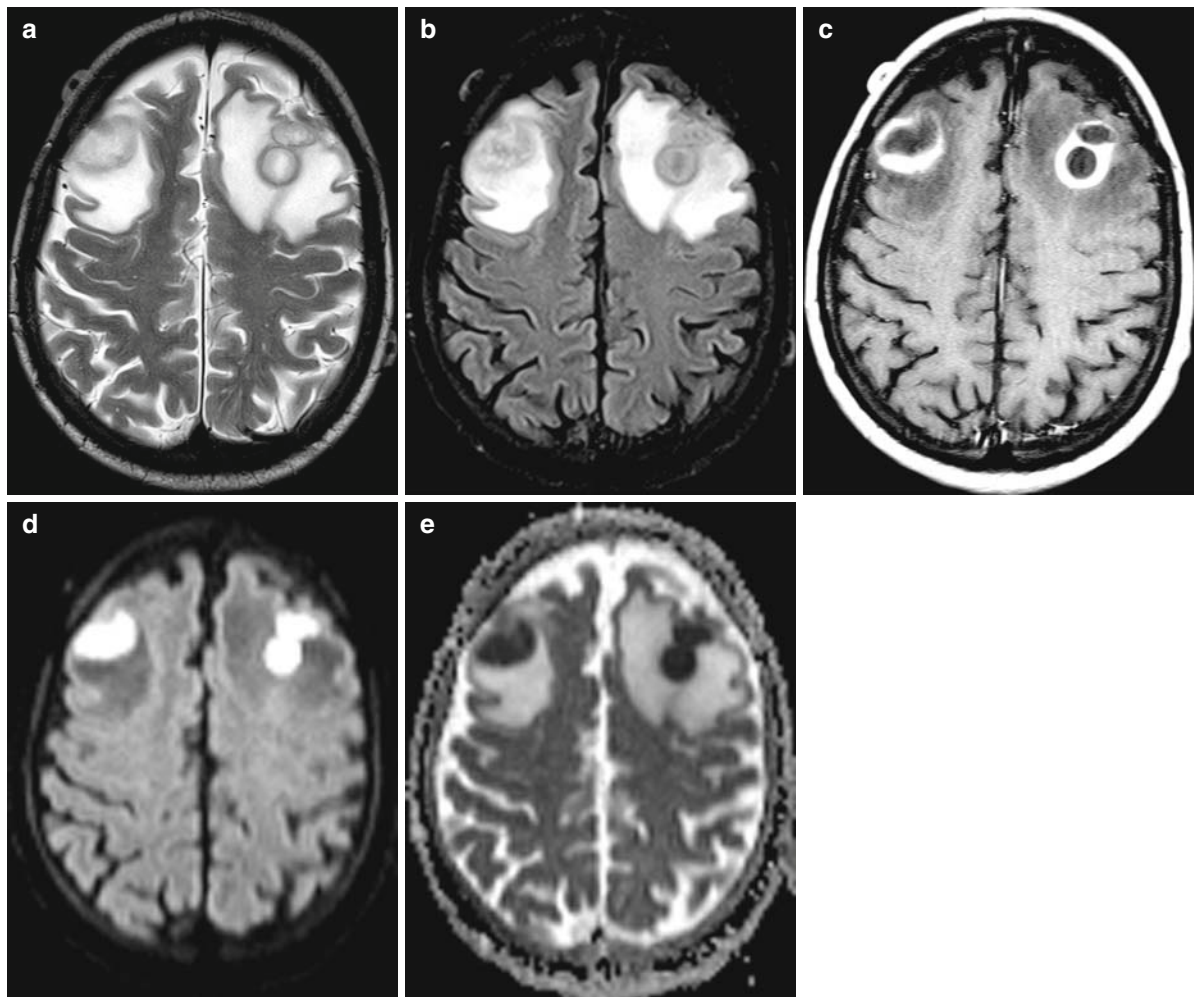


Fig. 2.65 Bacterial cerebral brain abscesses. (a) Axial TSE T2-WI. (b) Axial fat-sat turbo FLAIR. (c) Gd-enhanced axial T1-WI. (d) Axial EPI diffusion-weighted “trace” image. (e) Apparent diffusion coefficient (ADC) map. The patient is a 43-year-old man with alcoholic liver cirrhosis, chronic pancreatitis, portal vein thrombosis, and septicemia. There are pyogenic abscesses in both frontal lobes, surrounded by a large area of

vasogenic edema. On T2-WI the abscess capsule is hypointense (*dark rim*). After Gd-injection, there is bilateral ring-enhancement. The lesions show markedly restricted diffusion on the trace images (hyperintense), and lowered ADC values (hypointense). Diffusion restriction in pyogenic abscesses is due to the high cellular content and increased viscosity of the pus (decreased motion of water)

2.9.3.1 Herpes Encephalitis

There are two types of HSV encephalitis, type I (in adults) and type II (in neonates).

HSV type I (oral herpes) is the most common cause of sporadic viral encephalitis. It has a predilection for the subfrontal and medial temporal lobes. Although initially unilateral, most patients develop lesions in both hemispheres. The temporal lobe, insular cortex, subfrontal area, and cingulate gyrus are affected. Early MRI changes are: gyral effacement due to edema on

T1-WI and high signal of the temporal lobe and cingulate gyrus on T2-WI (Fig. 2.66). Bilateral temporal lobe involvement is considered nearly pathognomonic of HSV encephalitis. Later in the course of the disease, T1-WI may demonstrate gray matter hyperintensities in a gyral pattern (indicating petechial hemorrhages). After contrast administration, gyral enhancement may be observed. HSV encephalitis has a high mortality rate (50–70%), and those who survive show marked atrophy and encephalomalacia of the temporal and frontal lobes.

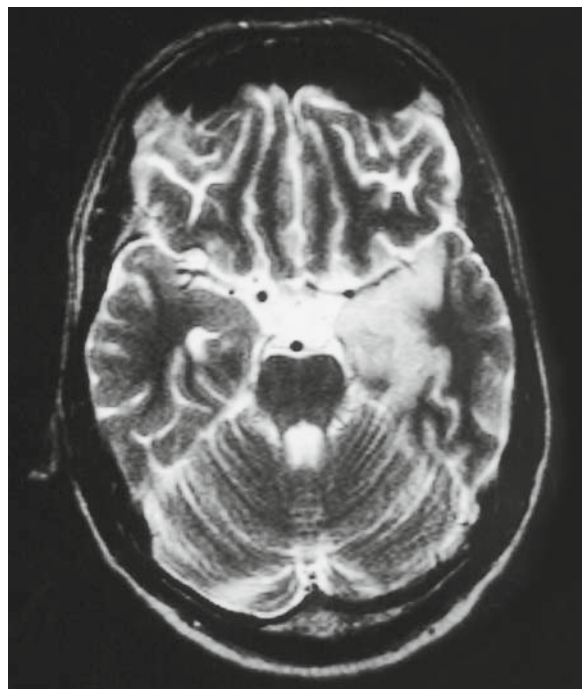


Fig. 2.66 Herpes simplex virus encephalitis. This axial TSE T2-WI was obtained in a patient with Herpes type 1 encephalitis. Note the increased signal intensity of the medial part of the left temporal lobe. There is some mass effect due to edema

The neonatal HSV type 2 (genital herpes) is a diffuse nonfocal encephalitis, known as panencephalitis. Because the neonatal brain is largely unmyelinated, diffuse edema is difficult to detect with MRI. Diffusion-weighted images may show increased signal

intensities, consistent with cytotoxic edema. Patchy meningeal or parenchymal enhancement can be seen.

2.9.3.2 HIV and AIDS-Related CNS Diseases

The retrovirus that causes AIDS is neurotropic and directly invades the peripheral nervous system and CNS. This virus is the most common pathogen in AIDS patients. Other AIDS-related CNS infections are opportunistic and are caused by *Toxoplasma gondii*, *Cryptococcus neoformans*, and papovaviruses.

HIV Encephalitis

The HIV virus causes a variety of neurological disorders, including encephalopathy (AIDS dementia complex), myelopathy, and peripheral neuropathy. HIV encephalitis is often found in combination with CMV encephalitis. The predominant imaging characteristic of HIV encephalitis is marked cerebral atrophy (Fig. 2.67). On T2-WI, confluent or patchy areas of increased signal are observed in the periventricular and deep white matter, most commonly in the frontal lobes. There is no enhancement after contrast injection.

Progressive Multifocal Leukoencephalopathy

Progressive multifocal leukoencephalopathy (PML) is a CNS infection caused by reactivation of the JC

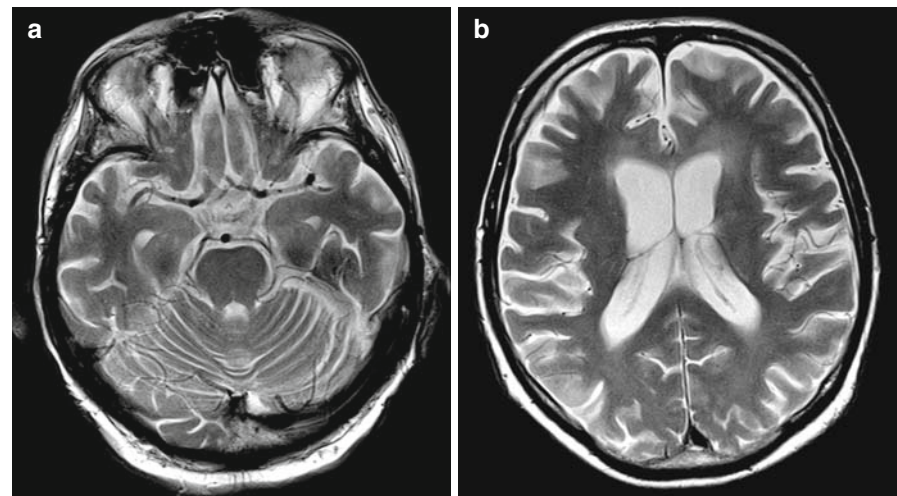


Fig. 2.67 HIV-encephalitis (AIDS dementia complex). (a, b) Axial TSE T2-WI. The patient is a 51-year-old man with AIDS, presenting with memory loss and confusion. The most striking finding of AIDS dementia complex is marked cerebral atrophy. In addition, there may be confluent areas of increased signal in the periventricular and deep white matter, most commonly in the frontal lobes

papovavirus. This viral infection causes destruction of oligodendrocytes, which results in extensive demyelination. Initial FLAIR and T2-WI show multifocal, subcortical, high-signal lesions, especially in the fronto-parietal and temporo-occipital white matter. In due course, these lesions become confluent and show central cavitation. Contrast enhancement is uncommon. Although PML can be unilateral, an asymmetric distribution in the white matter of both cerebral hemispheres is more common. Signal abnormalities can also be seen in the gray matter of the thalamus and basal ganglia (presumably secondary to involvement of traversing white-matter fibers). In many cases, the posterior fossa is also affected with areas of demyelination involving white-matter tracts in the brainstem and cerebellum.

Toxoplasmosis

Toxoplasmosis is the most common opportunistic CNS infection in AIDS patients. The infection is caused by *Toxoplasma gondii*. Cerebral toxoplasmosis causes multiple mass lesions in brain parenchyma, which are found near the corticomedullary junction and in the basal ganglia (Fig. 2.68). The lesions are difficult to see on unenhanced T1-WI; T2-WI are more sensitive in localizing multifocal lesions. After gadolinium-chelate administration, most lesions show ring-shaped or nodular enhancement. It is important to look for multiple lesions, because multifocality helps to differentiate a toxoplasmosis infection from a primary CNS lymphoma.

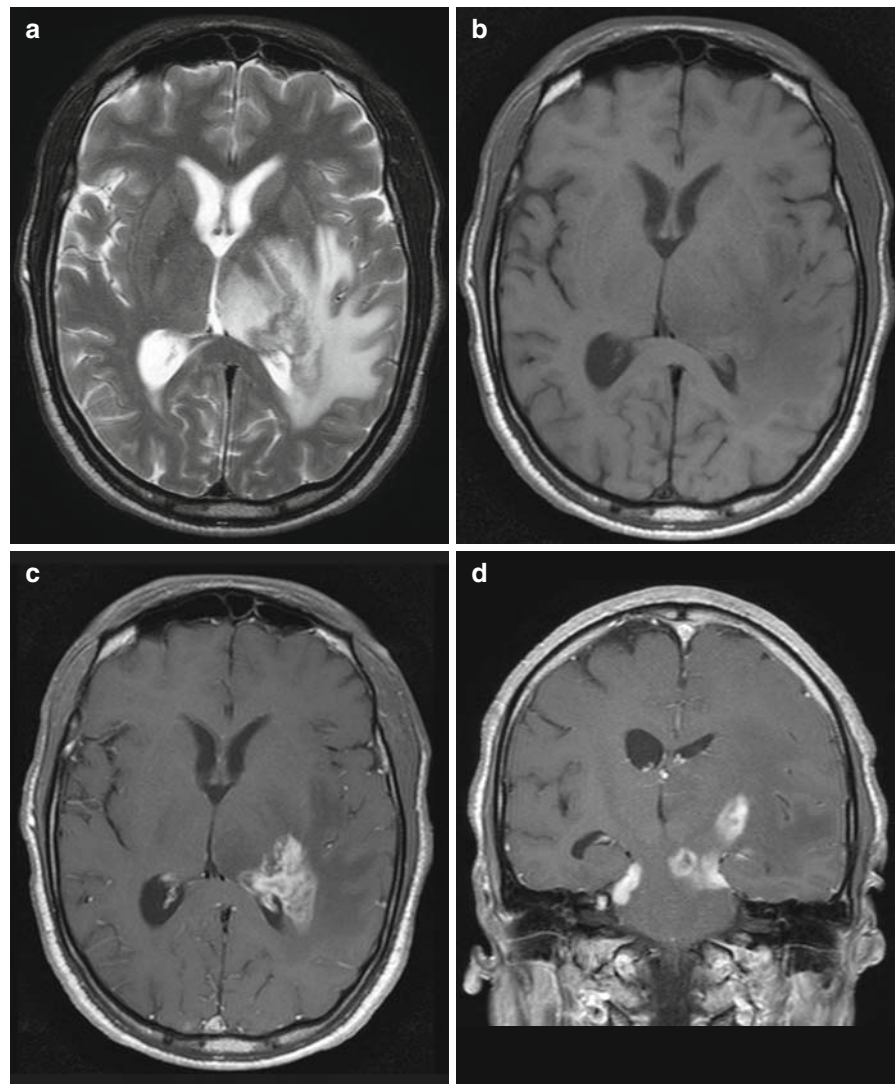


Fig. 2.68 Cerebral toxoplasmosis. (a) Axial TSE T2-WI. (b) Axial TSE T1-WI. (c) Gd-enhanced axial and coronal (d) TSE T1-WI. This 47-year-old man with AIDS developed cerebral toxoplasmosis. On TSE T2-WI, lesions present a mixed appearance with extensive white-matter edema. The abscesses are isointense with the surrounding edema on T1-WI. After Gd-injection, multiple enhancing lesions of varying size are seen; they represent parenchymal *Toxoplasma* abscesses with necrosis and surrounding inflammation. Differential diagnosis should include cerebral lymphoma and other infectious diseases

Primary CNS Lymphoma

Lymphoma is the second most common cause of a CNS mass lesion in AIDS patients (preceded only by toxoplasmosis). Primary CNS lymphoma in AIDS patients is typically a high-grade B-cell non-Hodgkin lymphoma, with strong association with the Epstein-Barr virus infection. Lymphomas can occur anywhere in the brain, but they are most commonly found in periventricular region and the corpus callosum. On T1-WI, lymphoma is iso-to hypointense to the surrounding brain tissue. The SI on FLAIR and T2-WI is variable, but frequently lymphoma is hypointense, reflecting its high-cell density. After gadolinium-chelate administration, primary CNS lymphoma enhances intensely and homogenously (Fig. 2.23). Ring enhancement is also a frequent finding and reflects central necrosis. It is important to remember that steroids may inhibit contrast enhancement, and may confound the diagnosis.

Cryptococcosis

Cryptococcosis is the most common cause of fungus infection in AIDS patients. Cryptococcus is a common soil fungus, which may infect the lungs and spread hematogenously to the CNS in patients with immunodeficiency. In the brain, cryptococcosis causes choroid plexitis, meningitis, and encephalitis. The fungus spreads along the perivascular Virchow–Robin spaces (VRS). It causes an enhancing granulomatous meningitis (if the immune response is still sufficient); otherwise, hydrocephalus and generalized brain atrophy are found (if the immune response is inadequate). On MRI, signal abnormalities (hypointense on T1-WI and hyperintense on FLAIR and T2-WI) can be observed in the lenticulostriate region; these lesions reflect gelatinous pseudocysts. After administration of gadolinium-chelates, leptomeningeal enhancement may be observed.

2.9.4 Acute Disseminated Encephalomyelitis

ADEM, also known as postviral leukoencephalopathy, is a type of postinfectious encephalomyelitis, following a viral illness (e.g., measles, chickenpox,

rubella, mumps, varicella, pertussis, Epstein-Barr, and viral upper airway infections). ADEM can also be triggered by a vaccination.

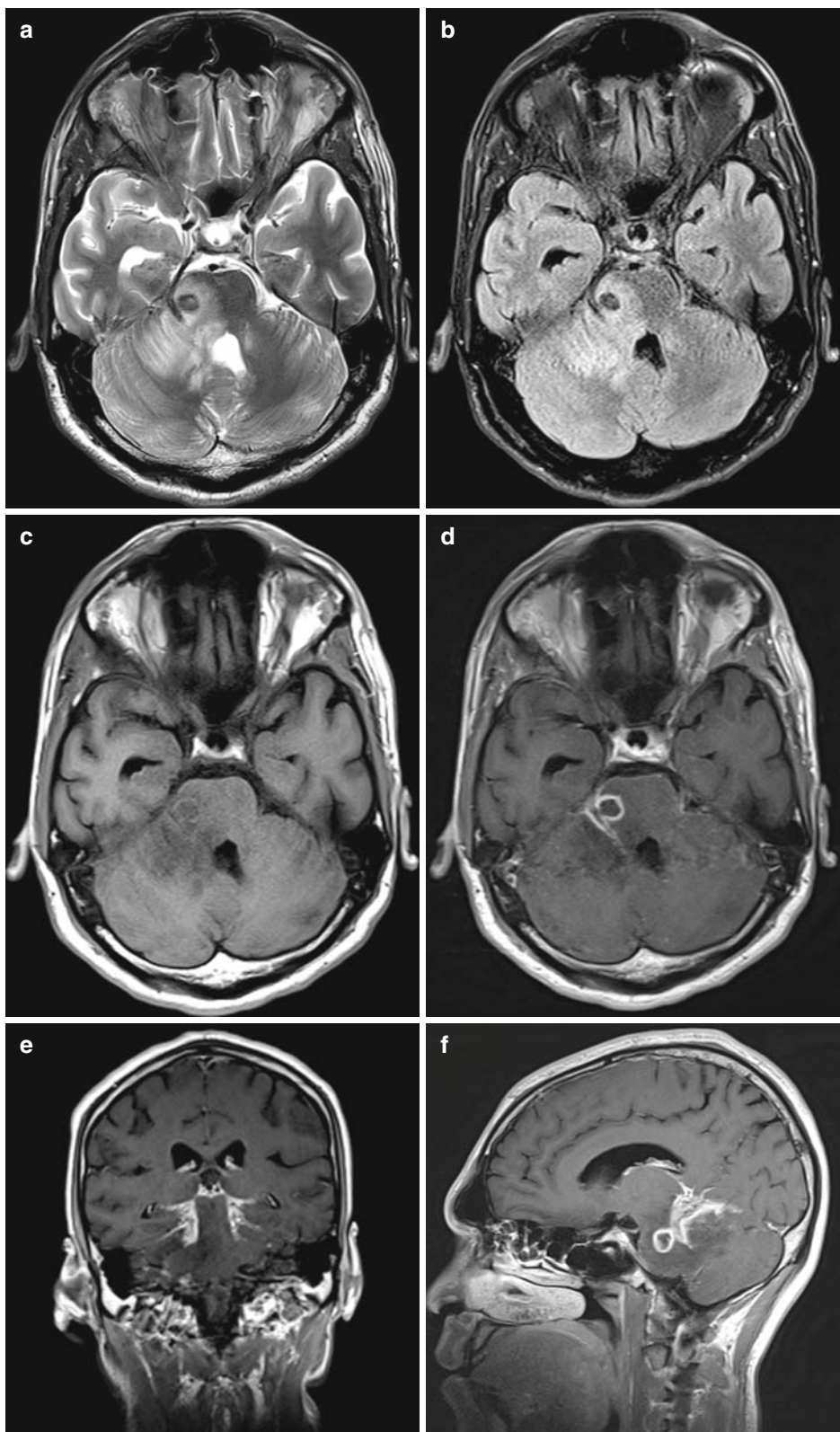
ADEM should be regarded as an autoimmune response against the patient's white matter resulting in demyelination. ADEM is usually a self-limiting disease, and as opposed to relapsing-remitting MS, is a monophasic disease. It is mostly found in children and young adults, but can be seen in all ages. FLAIR or T2-WI show multifocal subcortical areas of increased SI, with or without the involvement of posterior fossa. Lesions are widely distributed in both hemispheres, usually asymmetrically. After contrast injection, some lesions will enhance on a T1-W sequence. Although most patients recover completely without residual lesions, 10–20% of patients develop permanent sequelae. The main differential diagnosis is with MS (which usually occurs as a recurrent disease), autoimmune vasculitis, and even aging brain.

2.9.5 Tuberculosis

Tuberculosis remains a major public health problem, not only in developing countries, but also in industrialized nations. CNS tuberculosis results from hematogenous dissemination. Tuberculosis can affect the CNS in several ways (Fig. 2.69):

- *Tuberculous meningitis* is presumed to occur after rupture of an initial subependymal or subpial focus tuberculosis (a so-called Rich focus). Tuberculous meningitis in the brain typically involves the basal cisterns, interhemispheric fissure, Sylvian fissure, and the cerebral convexities. It causes meningeal thickening (“pachymeningitis”) and marked enhancement of the basal cisterns, corresponding on pathology to a gelatinous exudate. Hydrocephalus is a common complication, due to obstruction of the subarachnoid spaces and CSF drainage pathways. Ischemic infarctions of the basal ganglia, internal capsule, and thalamus occur due to vascular compression of the lenticulostriate and thalamoperforating arteries. T1-WI after contrast administration show thickening and intense enhancement of the meninges in the basal cisterns.
- *Tuberculomas* occur in the brain as a result of granuloma formation within the brain parenchyma. Tuberculomas are most commonly found in the posterior

Fig. 2.69 Tuberculous pachymeningitis and tuberculoma in the brainstem. **(a)** Axial TSE T2-WI. **(b)** Axial fat-sat turbo FLAIR. **(c)** Axial TSE T1-WI. **(d)** Gd-enhanced axial, **(e)** coronal and **(f)** sagittal TSE T1-WI. This 32-year-old man, with pulmonary tuberculosis was admitted with chronic bifrontal headaches, papilledema, nuchal rigidity, and worsening general condition. On the right side of the pons, there is a tuberculoma. This lesion is hypointense on T2-WI, is surrounded by vasogenic edema, and show rim enhancement. These characteristics indicate a caseating tuberculoma. In addition, there is severe pachymeningitis around the upper brainstem (pons and mesencephalon), with extension into the ambient and pontocerebellar cisterns. This combination of tuberculous pachymeningitis with (multiple) tuberculous brain abscesses has been compared to a “soap-bubble” appearance on gadolinium-enhanced MRI scans



fossa, and in the cortical and subcortical regions near the gray-white matter junction of the frontal and parietal lobes. More than two-third of tuberculomas are found as a solitary lesion, which poses a differential diagnostic problem. The MRI appearance depends on the maturity of the tuberculoma. A non-caseating tuberculoma is hypointense relative to brain tissue on T1-WI, hyperintense on T2-WI, and shows homogeneous, solid enhancement. A caseating tuberculoma with a solid center is isointense or even markedly hypointense on T2-WI, is surrounded by an area of vasogenic edema, and tends to show rim enhancement. When the caseating tuberculoma has developed a necrotic center, the core becomes hyperintense on T2-WI, the perilesional edema disappears, though ring enhancement may persist. Tuberculous meningitis with formation of multiple tuberculous brain abscesses can present a so-called “soap-bubble” appearance on gadolinium-enhanced MRI scans (Fig. 2.69).

the frontal horns of the lateral ventricles. They are usually small, although larger, often symmetric foci can also be found in normal individuals. High-signal rims (bands), contiguous with the margins of the lateral ventricles on FLAIR images, are also a frequent normal finding. These periventricular hyperintensities (PVH) correspond to areas of mild demyelination, associated with subependymal gliosis, discontinuity of the ependymal lining, and widening of the extracellular spaces (known as “ependymitis granularis”). The ependymal lining of the ventricles is regular and thin in the younger population, but becomes thicker and irregular, with extensions into the white matter, in the elderly population. Larger lesions cannot reliably be differentiated from demyelinating disease and infarcts; the MRI appearance can be indistinguishable. Extensive, confluent T2-hyperintense periventricular signal abnormalities are also found in hydrocephalus as a result of intraparenchymal leakage of CSF (“interstitial edema”).

2.10 Normal and Abnormal Aging of the Brain

The morphologic appearance of the brain changes with aging. These changes start to occur in adults, but become more pronounced in elderly individuals. In addition to an irreversible loss of brain substance (a process known as cerebral atrophy), specific age-related changes occur in the cerebral white matter, CSF spaces, and gray matter. These findings should be considered as normal aging phenomena, and should not be mistaken for disease.

2.10.1 White Matter Changes in Aging

2.10.1.1 Periventricular Hyperintensities: “Caps” and “Bands”

In almost all adult and elderly individuals, one finds so-called “caps” and “bands” around the lateral ventricles. The periventricular caps, which are hyperintense on FLAIR images, are found predominantly around

2.10.1.2 Deep White-Matter Hyperintensities

With increasing age, focal T2-hyperintense regions are found in the deep white matter of normal individuals. With the exception of the subcortical U-fibers, they can be located anywhere in the cerebral white matter. Minor perivascular damage (but not infarction) is the most likely substrate of punctate MR white-matter hyperintensities in elderly brains. These foci show high SI on both echoes of a long TR sequence, are best seen as hyperintense foci on FLAIR images, show low SI on T1-WI, and there is no contrast enhancement or mass effect. There is a correlation between the incidence of these nonspecific white-matter lesions and cerebrovascular disease and hypertension. On MRI alone, it is often impossible to distinguish these age-related lesions from multifocal disease, although the MRI characteristics together with the clinical data usually lead to correct interpretation.

In 1987, a scoring system was proposed, which subsequently became known as the “Fazekas scale,” after the first author. The Fazekas scale rates periventricular and deep white-matter hyperintensities (PVH and DWMH) on a four grade scale (Table 2.21).

Table 2.21 The Fazekas Scale for scoring periventricular and deep white-matter hyperintensities (1987)

Periventricular hyperintensities (PVH)	Deep white-matter hyperintensities (DWMH)
(0) Absence	(0) Absence
(1) "Caps" or pencil-thin lining	(1) Punctate foci
(2) Smooth "halo"	(2) Beginning confluence of foci
(3) Irregular PVH extending into the deep white matter	(3) Large confluent areas

2.10.1.3 Perivascular Hyperintensities

Perivascular spaces or VRS surround penetrating arteries for a short distance as they enter the cerebral parenchyma. They are lined by pia mater and contain interstitial fluid. They are in continuity with the subpial space, and are separated from the subarachnoid space by a single layer of pia mater. VRS are found predominantly in the basal ganglia (in the lower putamen, around the anterior commissure) and in the centrum semiovale (Fig. 2.70). However, VRS can also occur in other parts of the brain, such as the mesencephalon and cerebral peduncles. On T1-WI, they are hypointense, and on T2-WI they appear as punctate or linear hyperintensities. Since they are filled with interstitial fluid, their signal is suppressed on FLAIR images, unlike nonspecific age-related white-matter lesions which appear bright on FLAIR images. Most VRS are small and punctuate, or linear, larger, and more confluent perivascular spaces can occur in the basal ganglia. The occurrence

of VRS is age related. VRS are an almost constant finding in adults, and a frequent finding in children.

2.10.2 Age-Related Changes in the CSF Spaces and Cortical Gray Matter

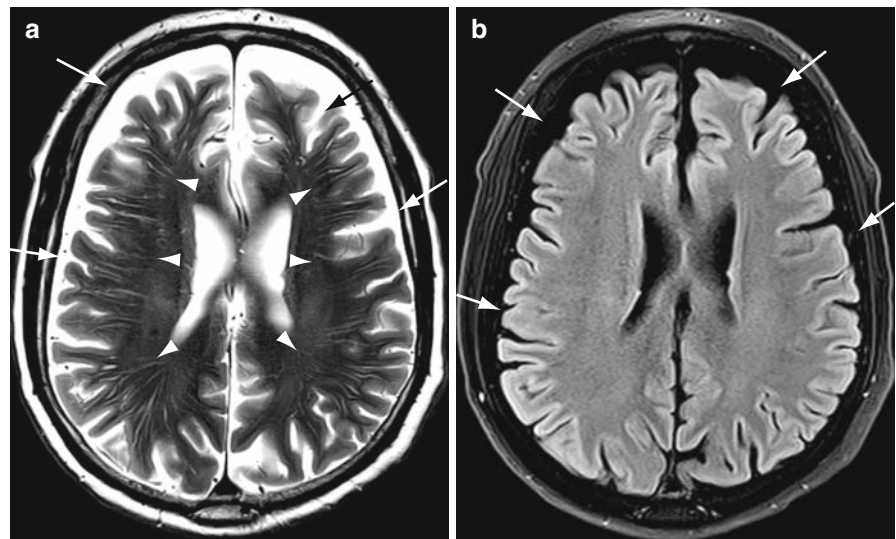
Volume loss of the cerebral parenchyma and subsequent widening of the CSF-containing spaces (ventricles, sulci, and cisterns) is a normal effect of aging. There is, however, a large overlap with neurodegenerative diseases such as Alzheimer's disease, frontotemporal dementia, or dementia with Lewy bodies. Prominent sulci are also seen in young children up to the age of 1 year. The interhemispheric distance can be as wide as 6 mm in normal neonates.

Widening of the ventricles in elderly patients can be due to atrophy, reflecting central volume loss of the brain; this is known as ventriculomegaly (we try to avoid the older term "hydrocephalus ex vacuo"). However, ventricular enlargement due to central atrophy may be impossible to differentiate from certain types of hydrocephalus, such as normal pressure hydrocephalus.

2.10.3 Age-Related Changes in Brain Iron

Iron metabolism in the brain is independent of the iron metabolism and storage in the rest of the body. It is an

Fig. 2.70 Perivascular Virchow-Robin spaces. (a) Axial TSE T2-WI. (b) Axial fat-sat turbo FLAIR. The T2-WI (a) shows prominent perivascular Virchow-Robin (VRS) spaces throughout the white matter of a 65-year-old man with diffuse atrophy (arrows) and widening of the extracerebral CSF spaces. The VRS, which contain interstitial fluid, are seen as linear hyperintensities. On the FLAIR image, the VRS spaces are not visible, because the fluid signal is suppressed (arrowheads).



essential element for the maturation and function of the brain. Iron depositions can be detected on MRI because of the susceptibility effect. On T2*-W scans, or susceptibility-weighted imaging (SWI), foci of iron deposition are seen as hypointense areas. In the first year of life, iron deposition becomes visible in the basal ganglia, substantia nigra red nucleus. In childhood, the dentate nucleus also becomes hypointense on T2-WI and T2*-WI. The iron content of the basal ganglia increases with age; the globus pallidus becomes hypointense on T2-WI in the middle-aged and elderly population, and the putamen is hypointense only in the elderly population.

2.10.4 MRI in Abnormal Aging and Dementia

The boundary between “normal” and “abnormal” aging is not clearly defined. In patients with clinical signs and symptoms of dementia, MRI is useful, though imaging findings are often nonspecific and there is considerable overlap with physiologic changes of the brain of the aging patient.

Alzheimer's disease is the most common of all dementing disorders in the elderly. It is a disease of gray matter, with loss of cells from the cerebral cortex. On MRI, the brain presents a “cracked walnut” appearance, with symmetrical enlargement of the sulci in the high-convexity regions. Focal atrophy is most obvious in the medial temporal lobes, with volume loss of the hippocampus and parahippocampal gyrus. Frequently, a smooth periventricular halo of T2-hyperintensity is also present.

Other types of dementia include frontotemporal lobar degeneration, dementia with Lewy bodies, Vascular dementia, Creutzfeld-Jacob disease or variant Creutzfeld-Jacob disease, and HIV-related dementia.

As a general rule, in patients with dementia, MRI is preferred over CT. Common imaging findings include atrophy of the medial temporal lobes and white matter damage. The imaging protocol to evaluate patients with dementia should include a FLAIR sequence, because of its high sensitivity to periventricular and DWMH, and its ability to differentiate lacunes (hypointense) from areas of demyelination or gliosis (hyperintense). As an alternative, a long TR dual-echo TSE (providing proton-density and T2-WI) sequence can be employed; this sequence is not as good as FLAIR to characterize ischemic lesions, but has the advantage of a higher

sensitivity for posterior fossa lesions. The MRI protocol should also include at least one sequence to detect intracerebral deposits of iron, calcium, and hemosiderin. This can be achieved either with a gradient echo T2*-W sequence or with a susceptibility-weighted sequence (SWI). It is important to look for “microbleeds” (punctate hemosiderin deposits), which have a much higher prevalence in subjects with dementia than those without dementia (Fig. 2.46). Microbleeds occur in patients with amyloid angiopathy, and it has been shown that SWI is more sensitive than gradient echo T2*-imaging in the detection of these small hemosiderin deposits. Finally, it is recommended that the imaging protocol for patients with dementia should also include a 3D volumetric sequence, e.g., a 3D MP-RAGE.

2.11 Craniocerebral Trauma

Traumatic injury of the brain and spinal cord is a leading cause of death and permanent disability. Clinical management of patients with craniocerebral trauma requires an assessment of the degree of patient risk according to the symptoms of intracranial injury. However, the severity of brain injury cannot be evaluated exclusively by the extent of impairment as determined by clinical examination. Modern imaging techniques play an important role in the management of the patient with craniocerebral trauma, and should be used to detect anatomic and physiologic abnormalities.

Multidetector computed tomography (MDCT) is the initial imaging modality of choice in severe acute craniocerebral trauma. MDCT is used for the detection of intracranial hemorrhage, mass effect and edema (including brain herniation), skull fractures, displaced bone fragments, foreign bodies, intracranial air, etc. New generation MDCT scanners (with 64, 128 or more detector rows) provide isotropic data sets, which can be used for high-resolution three-dimensional postprocessing, to show fractures of the skull vault, maxillofacial region, and even the petrous bones and skull base.

2.11.1 MRI in Acute and Subacute Trauma

MRI is generally not the preferred technique in acute trauma. There are significant logistic difficulties in

installing a traumatized patient in the MR unit. Appropriate MRI-compatible monitoring and life-support equipment should be available. All staff involved in the procedure should be aware of the dangers and necessary precautions for working near an MRI scanner. MRI is contraindicated if there is any suspicion that the patient might harbor an intracranial or intraorbital metallic foreign object, implant or incompatible device (e.g., penetrating injury, bullet fragment, shrapnel, stainless steel aneurysm clip, etc.). MRI is relatively insensitive for the detection of skull fractures and small bone fragments. Long acquisition times cause problems with regard to patient motion. The availability of the MR scanner on a stand-by basis may be problematic and interferes with normal patient flow. For all of these reasons, in most hospitals, MDCT scanning remains the preferred technique in acute trauma patients.

However, thanks to recent technological developments, the role of MRI is growing in the assessment of acute and subacute craniocerebral injury. MRI provides superior contrast resolution and has the highest sensitivity for parenchymal lesion detection. MRI has the potential to reveal nonhemorrhagic (and hemorrhagic) white-matter shearing injuries, even in patients with normal CT examinations.

Phased-array head coils, in combination with PAT such as SENSE and GRAPPA have significantly shortened MRI scan times. This has led to decreased motion artifacts and improved image quality, even in poorly cooperative head-injured patients. In the acute stage, FLAIR sequences are used for the detection of diffuse axonal injury (DAI), edema, and hemorrhage. Moreover, FLAIR has a high sensitivity for the detection of intracranial hemorrhage, including subarachnoid and intraventricular hemorrhage. Gradient echo T2* and SWI sequences are valuable for detection of intracranial hemorrhage and blood degradation products. DWI has been shown to be useful in the evaluation of craniocerebral trauma, and especially DAI (Fig. 2.71). Decreased ADC values can be demonstrated in patients with DAI in the acute setting and may persist into the subacute period (up to 18 days after the initial event), beyond that described for cytotoxic edema in ischemia. DWI is able to identify traumatic shearing injuries which are not visible on routine pulse sequences. Moreover, DWI can show hypoxic-ischemic brain damage, for example in cases of nonaccidental head injury (e.g., shaken baby syndrome) or vascular damage (e.g., carotid or vertebral artery dissection).

As a general rule, MRI is indicated in stable patients in whom there is a discrepancy between clinical symptoms and CT findings. Patients with DAI and nonaccidental head trauma (child abuse) should be examined with MRI. There is growing evidence that DWI serves as a valuable biomarker for the severity of tissue injury and as a predictor for outcome.

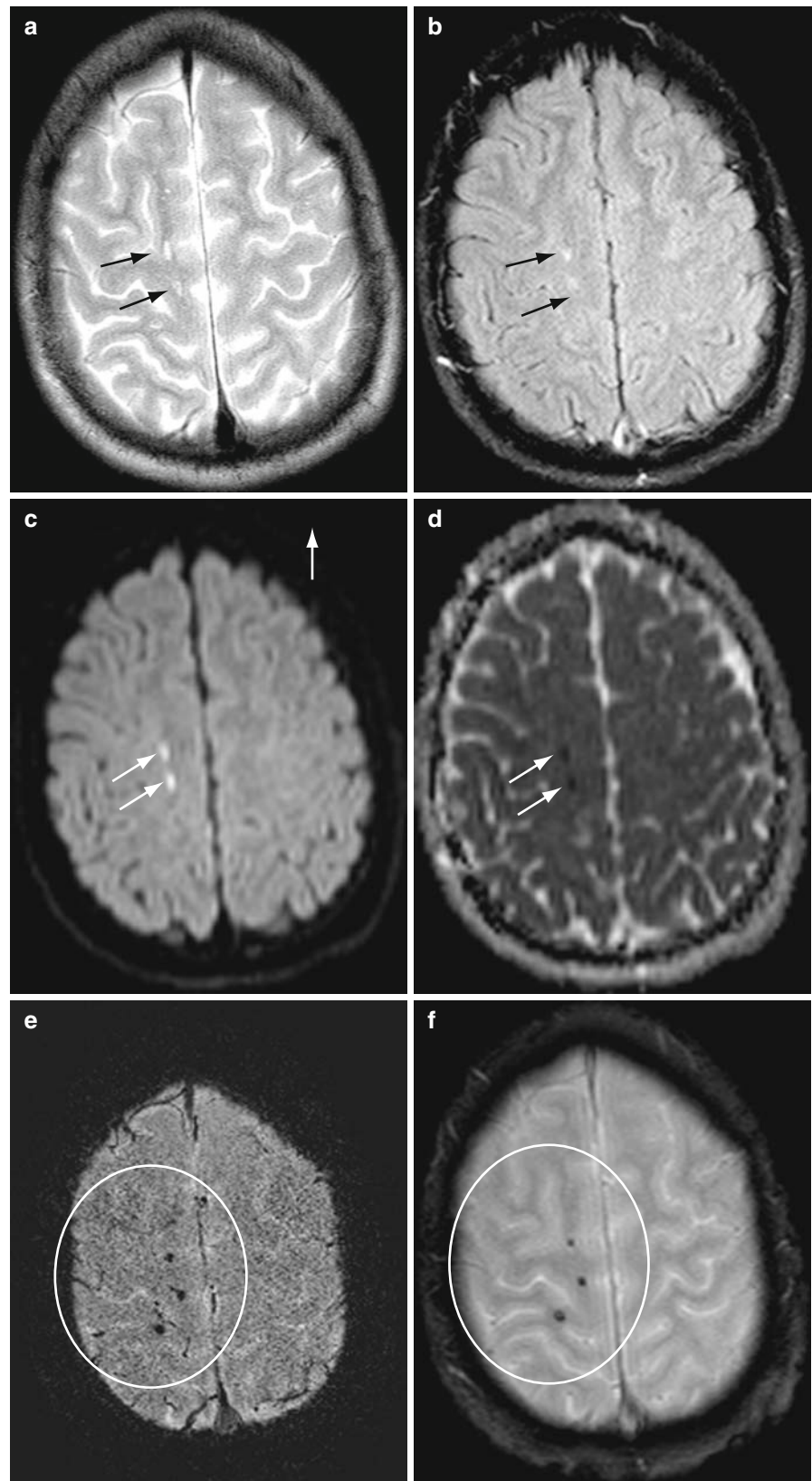
2.11.2 MRI in Chronic Trauma

MRI is of great use in the evaluation of trauma patients in the chronic phase, due to its superior contrast resolution. MRI is superior to CT for the detection of chronic subdural hematomas, which are often isodense to CSF on noncontrast CT scans, but can be seen on MRI, because they contain blood degradation products (methemoglobin) and high concentrations of protein. Fat-saturated FLAIR sequences are superior to T2-WI in the detection of small subdural hematomas (Fig. 2.72). When a subdural hematoma contains blood of varying ages, due to repeated episodes of bleeding, MRI may show layers of different SI, reflecting varying phases of the blood-breakdown process.

FLAIR sequences are used mainly for the detection of gliosis and cystic encephalomalacia. Gradient echo T2* or SWI sequences allow visualization of hypointense hemosiderin deposits after DAI. These punctate hemosiderin deposits are the result of shearing injuries due to rotational acceleration and deceleration forces, commonly encountered in motor vehicle accidents and blunt trauma to the head. DAI lesions occur in the cerebral hemispheres (subcortical brain parenchyma, gray-white matter junction, centrum semiovale), corpus callosum, basal ganglia, brainstem, and cerebellum. In every patient with a history of previous head trauma, a T2* or SWI sequence, which is highly sensitive to blood-breakdown products such as hemosiderin and ferritin, should be routinely added to the MRI scanning protocol. DAI lesions are seen as punctate hypointense foci; multiple lesions are frequent.

Posttraumatic encephalomalacia is much better appreciated with MRI than with CT, because of the absence of bone artifacts and the multiplanar imaging capabilities of MR. Foci of encephalomalacia often result from cortical contusions and should be looked

Fig. 2.71 Diffuse axonal injury (DAI). **(a)** Axial TSE T2-WI. **(b)** Axial fat-sat turbo FLAIR. **(c)** Axial EPI diffusion-weighted “trace” image. **(d)** Apparent diffusion coefficient (ADC) map (arrows). **(e)** Axial susceptibility-weighted image (SWI). Axial and coronal gradient echo FLASH T2*-WI. This 17-year-old boy suffered a high-velocity deceleration trauma when his motorcycle struck a parked truck at high-speed. Upon admission, GCS was 9/15. Noncontrast CT scan of the brain was unremarkable. Because of the discrepancy between the patient’s clinical status and the normal CT findings, MRI of the brain was performed on the same day. Diffuse axonal injuries (DAI) are scattered throughout both cerebral hemispheres, mainly involving the hemispheric gray-white matter interfaces, centrum semiovale, and corpus callosum. The DAI lesions are hyperintense on T2 (**a**) and FLAIR (**b**). They exhibit diffusion restriction (**c**) with lowered ADC values (**d**). On axial SWI (**e**) and axial (**f**) and coronal (**g**, **h**) gradient echo T2* images, multiple, punctate, hypointense lesions (*circles*) are seen in the centrum semiovale, at the corticomedullary junctions, and in the subcortical white matter (corresponding to areas of shearing stress). The pattern of distribution and signal intensity behavior is typical for DAI with petechial hemorrhages



(continued)

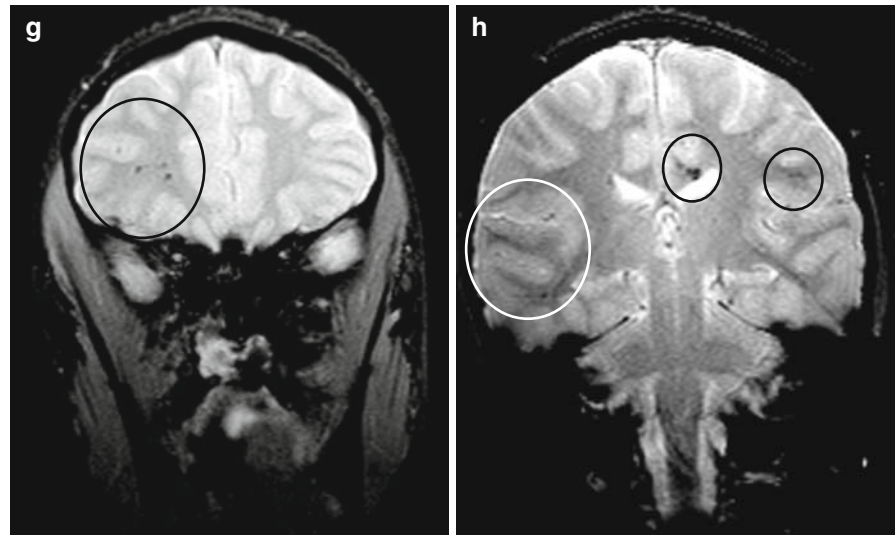
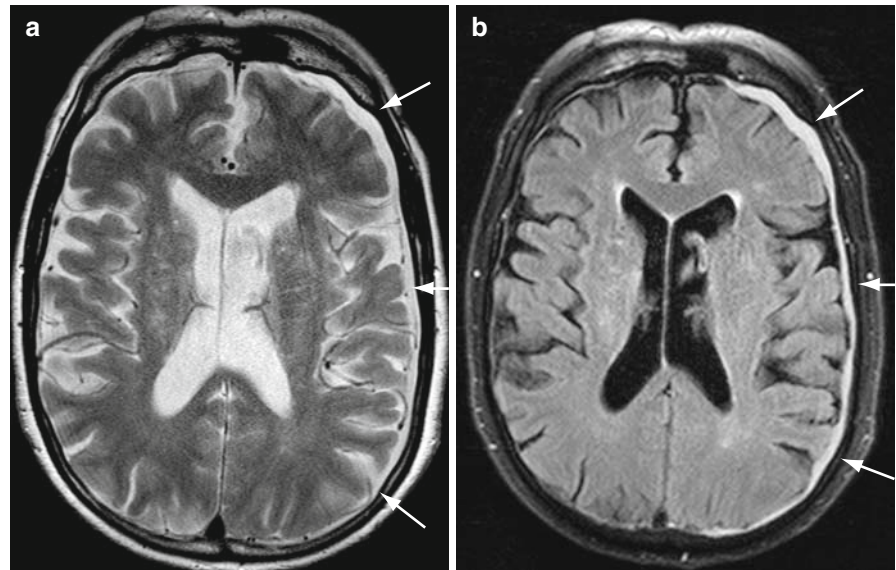
Fig. 2.71 (continued)

Fig. 2.72 Chronic subdural hematoma (arrows). (a) Axial TSE T2-WI. (b) Axial fat-saturated FLAIR. There is a thin subdural hematoma overlying the left cerebral hemisphere (missed on a noncontrast CT scan performed 2 days earlier). The hyperintense subdural hematoma is much better seen on the FLAIR image, due to the suppression of fluid and fat



for in the basal, frontal, and anterior temporal lobes. These regions are vulnerable to deceleration injury. They are seen as areas of tissue loss, which are hyperintense on T2-WI. On PD or FLAIR images, the area of tissue loss is isointense to CSF and is surrounded by a hyperintense rim of gliosis.

Diffusion tensor imaging (DTI) with fractional anisotropy (FA) maps is used to evaluate white-matter tracts, by measuring the degree and spatial distribution

of anisotropic diffusion within the brain. FA maps and DTI reveal changes in the white matter that are correlated with both acute Glasgow Coma Scale and Rankin scores at discharge. Because FA and DTI changes are present at both early and late time points following injury, they are valuable biomarkers and could be used as an early indicator for the severity of tissue injury and as a prognostic measure of subsequent brain damage.

2.12 Seizures

The primary goal of MRI in the evaluation of epilepsy is to identify and localize the neuropathologic substrate of a partial onset seizure. The diagnosis and localization of the lesion determines the therapeutic possibilities. Many different abnormalities can cause epilepsy (Table 2.22). Most of these abnormalities are dealt with in other sections; in this section, we will discuss mesial temporal sclerosis (MTS) and a general imaging strategy for epilepsy.

Table 2.22 Causes of partial-onset epileptic seizures

Tumors	Astrocytoma Oligodendrogioma Ganglioma DNET Metastasis
Migration disorders	Tuberous sclerosis Focal cortical dysplasia Schizencephaly Nodular heterotopia Laminar heterotopia Lissencephaly Hemimegalencephaly
Vascular malformations	Cavernous angioma AVM Sturge-Weber
Mesial temporal sclerosis	
Brain injury	Ischemia Trauma

2.12.1 Mesial Temporal Sclerosis

MTS is the most common cause of intractable temporal lobe epilepsy. The condition is characterized histopathologically by marked neuronal loss in the hippocampus (with relative sparing of the CA2 subfield), amygdala, parahippocampal gyrus, mesial temporal cortex, and entorhinal cortex. The terms MTS, hippocampal sclerosis, and Ammon's horn sclerosis are used interchangeably, but the extent of the lesion differs for each term.

On T2-WI and FLAIR images, the main MRI findings are increased SI and decreased volume of the hippocampus (Fig. 2.73), compared to the contralateral side. These abnormalities are best seen on coronal slices, preferably orientated perpendicular to the long axis of the temporal lobe. T1-WI shows hippocampal atrophy and dilatation of the temporal horn (Fig. 2.73). FLAIR sequences are more sensitive to the signal changes than (fast) SE sequences. There is no enhancement of the hippocampal sclerosis after contrast-medium administration. In the majority of cases, the abnormality is bilateral but asymmetric, and the most affected side is presumed to be the origin of the seizures.

MTS is frequently associated with abnormalities of the limbic system, including atrophy of the ipsilateral fornix and ipsilateral mammillary body. Patients with MTS may show hyperintensity of the cerebral cortex in the anterior temporal lobe; rarely cerebral hemiatrophy is found.

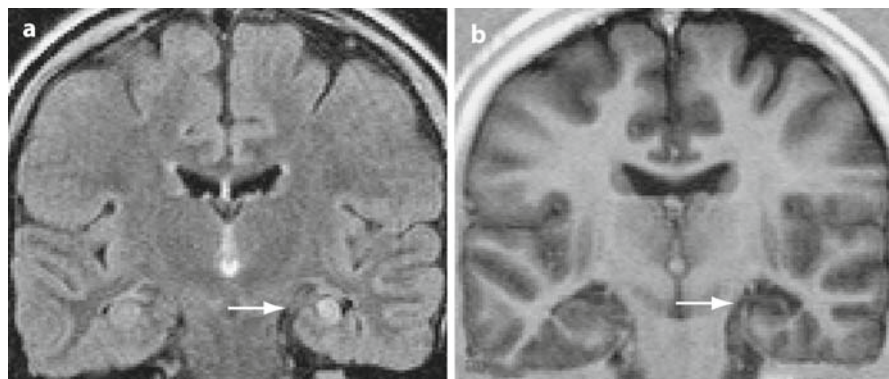


Fig. 2.73 Mesial temporal sclerosis (arrows). (a) Coronal FLAIR T2-WI through the hippocampus. (b) Coronal IR-T1-WI (same slice position). On the FLAIR T2-WI sequence, there is an area of abnormally increased signal intensity in the left hippocampus. IR

T1-WI shows focal tissue loss with widening of the left temporal horn. T1-WI shows hippocampal atrophy and dilatation of the temporal horn. T2-WI shows an increased signal intensity of the hippocampus

2.12.2 MRI Strategy for Epilepsy

Imaging protocols for the diagnosis of hippocampal sclerosis vary widely from center to center. An imaging protocol for epilepsy should be guided by the location of the epileptogenic focus as provided by the clinical presentation and the electroencephalogram (EEG). For general screening, one can substitute axial turbo FLAIR and TSE T2-W sequences for the traditional double-echo long TR sequence. The imaging protocol should include most cerebral pathologies associated with seizures, including cortical development disorders. Therefore, a coronal T1-W sequence with thin slices should be added, e.g., an MP-RAGE sequence. Cortical alterations, e.g., migration disorders, can be detected on this high-resolution scan, and side-to-side comparison of the hippocampus can be made. A coronal turbo-FLAIR sequence will show signal changes in the hippocampus more clearly than the conventional T2-WI. In patients with seizures, it is always wise to include a gradient echo T2*-sequence or a susceptibility-weighted imaging (SWI) sequence to detect old hemorrhagic foci or cavernous malformations. Finally, the imaging protocol must be adapted to the equipment that is available (field strength, gradient performance, available sequences, etc.).

Further Reading

- Armed Forces Institute of Pathology (1994) Tumors of the central nervous system. Armed Forces Institute of Pathology, Washington DC
- Atlas SW (1996) Magnetic resonance imaging of the brain and spine. Lippincott-Raven, Philadelphia
- Atlas SW (2002) Magnetic resonance imaging of the brain and spine, 3rd edn. Lippincott Williams & Wilkins, Philadelphia
- Barkovich JA (2000) Pediatric neuroimaging, 3rd edn. Lippincott Williams & Wilkins, Philadelphia
- Barkovich JA (2005) Pediatric neuroimaging, 4th edn. Lippincott Williams & Wilkins, Philadelphia
- Byrd SE, Darling CF, Wilczynski MA (1993) White matter of the brain: maturation and myelination magnetic resonance in infants and children. *Neuroimaging Clin North Am* 3: 247–266
- Castillo M (1997) Prethrombolytic brain imaging: trends and controversies. *AJNR Am J Neuroradiol* 18:1830–1833
- Castillo M (guest ed) (1998) New techniques in MR neuroimaging. *Magnetic resonance imaging clinics of North America* 1998, vol 6. Saunders, Philadelphia
- Castillo M (1998) New techniques in MR neuroimaging. In: Magnetic resonance imaging clinics of North America, vol 6. Saunders, Philadelphia
- Fazekas F, Ropele S, Enzinger C, Gorani F, Seewann A, Petrovic K, Schmidt R (2005) MTI of white matter hyperintensities. *Brain* 128:2926–2932
- Finelli DA, Hurst GC, Gullapalli RP (1998) T1-W three dimensional magnetisation transfer MR of the brain: improved lesion contrast enhancement. *AJNR Am J Neuroradiol* 19: 59–64
- Forsting M, Wanke I (2008) Intracranial vascular malformations and aneurysms, from diagnostic work-up to endovascular therapy (2nd revised edition). Springer, New York
- Gillard JH, Waldman AD, Barker PB (2005) Clinical MR neuroimaging. Cambridge University Press, New York
- Gilman S (1998) Imaging the brain (first of two parts). *N Engl J Med* 338:812–820
- Gilman S (1998) Imaging the brain (second of two parts). *N Engl J Med* 338:889–896
- Hergan K, Schaefer PW, Sorensen AG, Gonzalez RG, Huisman TA (2002) Diffusion-weighted MRI in diffuse axonal injury of the brain. *Eur Radiol* 12:2536–2541
- Hartmann M, Jansen O, Heiland S, Sommer C, Mükel K, Sartor K (2001) Restricted diffusion within ring enhancement is not pathognomonic for brain abscess. *AJNR Am J Neuroradiol* 22:1738–1742
- Hoang TA, Hasso AN (1994) Intracranial vascular malformations. *Neuroimaging Clin North Am* 4:823–847
- Jack CR (1995) Magnetic resonance imaging: neuroimaging and anatomy. *Neuroimaging Clin North Am* 5:597–622
- Lacerda S, Law M (2009) Magnetic resonance perfusion and permeability imaging in brain tumors. *Neuroimaging Clin N Am* 19:527–557
- Law M (2009) Advanced imaging techniques in brain tumors. *Cancer Imaging* 9(special issue A):S4–S9
- Law M, Young RJ, Babb JS, Peccerelli N, Chheang S, Gruber ML, Miller DC, Golfinos JG, Zagzag D, Johnson G (2008) Gliomas: predicting time to progression or survival with cerebral blood volume measurements at dynamic susceptibility-weighted contrast-enhanced perfusion MR imaging. *Radiology* 247:490–498
- Lee SH, Rao KCVG, Zimmerman RA (1992) Cranial MRI and CT, 3rd edn. McGraw-Hill, New York
- Lee SH, Rao KCVG, Zimmerman RA (2004) Cranial MRI and CT, 4th edn. McGraw-Hill, New York
- Louis DN, Ohgaki H, Wiestler OD, Cavenee WK (eds) (2007) WHO classification of tumours of the central nervous system. IARC, Lyon
- Louis DN, Ohgaki H, Wiestler OD et al (2007) The 2007 WHO classification of tumours of the central nervous system. *Acta Neuropathol* 114:97–109
- Lufkin RB (1998) The MRI manual, 2nd edn. Mosby-Year Book, St Louis
- McDonald WI, Compston A, Edan G et al (2001) Recommended diagnostic criteria for multiple sclerosis: guidelines from the International Panel on the diagnosis of multiple sclerosis. *Ann Neurol* 50:121–127
- Osborn AG (1994) Diagnostic neuroradiology. Mosby-Year Book, St Louis
- Osborn AG (2004) Diagnostic imaging – brain. Amirs, Salt Lake City

- Parizel PM, Van Goethem JW, Özsarlak Ö, Maes M, Philips CD (2005) New developments in the neuroradiological diagnosis of craniocerebral trauma. *Eur Radiol* 15:569–581
- Pierallini A, Caramia F, Falcone C, Tinelli E, Paonessa A, Ciddio AB, Fiorelli M, Bianco F, Natalizi S, Ferrante L, Bozzao L (2006) Pituitary macroadenomas: preoperative evaluation of consistency with diffusion-weighted MR imaging – initial experience. *Radiology* 239:223–231
- Polman CH, Reingold SC, Edan G (2005) Diagnostic criteria for multiple sclerosis: 2005 revisions to the “McDonald Criteria”. *Ann Neurol* 58:840–846
- Provenzale JM, Mukundan S, Barboriak DP (2006) Diffusion-weighted and perfusion MR imaging for brain tumor characterization and assessment of treatment response. *Radiology* 239:632–649
- Sahraian MA, Radue E-W (2007) MRI atlas of MS lesions. Springer, Berlin
- Simon JH, Li D, Traboulsee A, Coyle PK, Arnold DL, Barkhof F, Frank JA, Grossman R, Paty DW, Radue EW, Wolinsky JS (2006) Standardized MR imaging protocol for multiple sclerosis: Consortium of MS Centers consensus guidelines. *AJNR Am J Neuroradiol* 27:455–461
- Sorensen AG, Reimer P (2000) Cerebral MR perfusion imaging: principles and current applications. Thieme, Stuttgart
- van der Knaap MS, Valk J (1995) Magnetic resonance of myelin; myelination and myelin disorders. Springer, Berlin
- van der Knaap MS, Valk J (2005) Magnetic resonance of myelin; myelination and myelin disorders, 3rd edn. Springer, Berlin



<http://www.springer.com/978-3-540-74501-3>

Clinical MR Imaging

A Practical Approach

Reimer, P.; Parizel, P.M.; Meaney, J.F.M.; Stichnoth, F.-A.
(Eds.)

2010, XX, 820 p., Hardcover

ISBN: 978-3-540-74501-3